Natural Resources Canada | Ressources naturelles Canada

GEOLOGICAL SURVEY OF CANADA
OPEN FILE 7833

Crustal Structure of Eastern and Central Canada from a Neighborhood Algorithm Inversion

A.L. Bent and H. Kao

2015

Canada

GEOLOGICAL SURVEY OF CANADA
OPEN FILE 7833

Crustal Structure of Eastern and Central Canada from a Neighborhood Algorithm Inversion

A.L. Bent and H. Kao

2015

doi:10.4095/296797

This publication is available for free download through GEOSCAN (http://geoscan.nrcan.gc.ca/).

Recommended citation
Bent, A.L. and Kao, H., 2015. Crustal Structure of Eastern and Central Canada from a Neighborhood Algorithm Inversion; Geological Survey of Canada, Open File 7833, 68 p. doi:10.4095/296797

Publications in this series have not been edited; they are released as submitted by the author.

Abstract

Teleseismic receiver functions created from waveforms of large earthquakes recorded by twenty-one broadband stations of the Canadian National Seismograph Network in eastern and central Canada were analyzed to determine the shear wave velocity structure of the crust and uppermost mantle beneath these stations. Preliminary models were obtained from a simple, linear inversion and then an improved Neighborhood Algorithm was employed to enable a larger number of models to be tested and to provide robust uncertainty estimates of the models. Common features are observed at stations falling within the same geological provinces. While azimuthal variations in receiver functions may be an indication of dipping structure, most stations in this study showing an azimuthal dependence are located near the boundaries of two or more geological provinces. The receiver functions at some azimuths and the structure obtained by modeling them may more closely resemble that of a neighboring province through which the waves propagated for a significant portion of their path. The goal of structural modeling is to provide improved models for use in earthquake location and focal mechanism determination, which in turn should improve our understanding of regional seismotectonics and seismic hazard. A test case using the aftershock sequence of a moderate earthquake shows some clear advantages of using a local velocity model over a generic one.

Introduction

While limitations in computing power once necessitated the use of large scale regional models for earthquake locations and source studies, it is now possible to use site or path specific models leading to increased accuracy. In turn, the improved locations and source models may result in the identification of seismogenic faults as well as lead to better hazard estimates.

Teleseismic receiver functions are one method to determine the crustal velocity structure beneath three-component seismograph stations. With the increasing number of broadband three-component stations in eastern Canada the site specific models can be obtained and then compared to those for nearby stations allowing regional trends to be modeled. A simple, linear inversion is used to obtain a preliminary model for each station. These models are used as starting models for the Neighborhood Algorithm method which allows for the systematic testing of a large number of models and provides an objective measure of the relative fit of each.

Data recorded at twenty-one broadband stations operating in eastern and central Canada were analyzed to determine the structure of the crust and uppermost mantle. While eastern Canada is part of the stable North American craton and far from active plate boundaries, its geology, comprising several geological provinces (National Atlas of Canada, 2015), is considerably more complex than might be expected. When stations are grouped by geological province rather than merely geographic proximity, common features are noted. Among these are a “double” crust and ambiguous Moho in the Superior Province of northern Ontario and Quebec. Many stations, particularly in southern Ontario and Quebec, are located near the boundaries of two or more geological provinces. Upon further investigation, azimuthal dependencies observed in the receiver functions that were initially thought to be evidence for complex dipping structures appear to be path rather than site effects. That is, waves recorded at a station in one geological province may have traveled primarily through it at some azimuths but through a different one at other azimuths. Thus, the velocity structure determined from the receiver function at a particular azimuth may appear to more closely resemble that of the adjacent province. Stations located along the St. Lawrence River are particularly affected as there are three geological provinces in close proximity.

Data and Methods

For twenty-one three-component broadband stations (Figure 1; Table 1) of the Canadian National Seismograph Network (CNSN) waveforms from earthquakes of magnitude 6.5 or greater recorded at distances of 30°-90° were collected and processed to create receiver functions, which were then inverted for velocity structure. When appropriate, data were stacked over 10° windows in distance and azimuth to enhance the signal to noise ratio. Azimuthal coverage was generally good with the largest gaps occurring in the southeast quadrant. Figure 2 shows the earthquakes used in the study of station GAC, for which the distribution is typical of most of the other stations although, obviously, the distribution of

events for each station is dependent on the station and how long it has been operating. Note that stations of the southern Ontario Polaris network and the second Fednor deployment in northern Ontario were not included in this study as they were under investigation by others with a regional focus (Eaton et al, 2006; Darbyshire et al., 2007). Similarly, stations in northern and western Canada were not evaluated in this study as they have been previously modeled by others (Cassidy, 1995a and references therein; Darbyshire, 2003). While our work was in progress Postlewaite et al. (2014) used receiver functions to determine Moho depths beneath most seismograph stations in Canada but we note that their study was focused on Moho depth and bulk crustal properties whereas our study provides more detailed models of the crust and uppermost mantle. Studies involving surface wave dispersion (Motazedian et al., 2013) have also been used to evaluate crustal structure in some regions covered by our study. This method uses pairs of stations and thus produces broader, regional models rather than local-scale models.

Each receiver function was created using the method of Langston (1979) as modified by Ammon (1991). A receiver function can be defined as the response of the structure beneath a seismograph station to an incident P wave. P to SV conversions occur at structural interfaces and are recorded as part of the P wave coda with the P waves dominating the vertical component and the converted SV phases dominating the radial. By deconvolving the vertical component from the radial the information in the seismograms resulting from the source, near source effects and deep mantle propagation effects are removed. The deconvolved seismogram known as the receiver function can then be analyzed to determine the shear wave structure beneath the recording station. For flat layered structure the amplitude of the tangential component should be zero. As the dip of an interface increases some energy is deflected from the radial-vertical plane leading to non-zero amplitudes on the tangential component. Although we invert for structure using only the radial receiver functions, a visual inspection of the amplitudes and polarities of the tangential receiver functions provides an indication as to whether a flat-layered or 1-D model is appropriate for that station. Differences in the radial receiver functions as a function of azimuth may also indicate whether the structure is likely to be dipping. Good examples illustrating the difference in receiver functions from flat and dipping layers may be found in Cassidy (1992).

The receiver functions were smoothed using a Gaussian pulse of 1.5, which is the equivalent of a low-pass filter at approximately 0.7 Hz. Spectral holes were filled using the water-level method (Clayton and Wiggins, 1976; Helmberger and Wiggins, 1971). A range of water-level parameters was applied to the data with the best value selected on an individual receiver function basis. In almost every case the preferred water-level parameter was 0.0001. Any receiver functions for which the amplitudes of the pre-P wave arrivals were comparable to or larger than the post-P wave trace were rejected as it would be difficult to verify whether we were modeling signal or noise. Stacked data were compared to the individual receiver functions used to make them and whichever had the best signal to noise ratio was used in the modeling. Although in theory stacking improves the signal to noise ratio sometimes one very clear signal is preferable to a stack made from several noisy traces.

The shear wave velocity structure beneath each station was determined by inversion. Using the "CANSD" model of Brune and Dorman (1963) as the starting model, the linear inversion method of Ammon et al. (1990) was applied to determine a preliminary model for each station. Radial receiver functions from as wide a variety of azimuths and distances as possible were inverted to determine whether the structure was likely to be one-dimensional (i.e. consisting of flat layers) or more complex.

The models obtained by this procedure were then used as starting models in a Neighborhood Algorithm (NA) inversion (Sambridge, 1999), which allows for a much more thorough search of potential models and an objective ranking of them. This method is less dependent on the starting model than the linear inversion previously discussed (Ammon et al., 1990). However, it is computer intensive whereas the linear inversion allows us to model a larger number of receiver functions quickly and thus to determine how much variability there is among the receiver functions and velocity models, which provides us with a representative starting model and reasonable bounds for use in the NA inversion.

By the NA method (Sambridge, 1999) a suite of models, rather than a single model, is found. The inversion is initiated with a fixed number of randomly distributed points within a bounded parameter space. The model space is then divided into regions each of which is the nearest neighborhood about one of the points determined by a least squares norm. The misfit function is then calculated with the lowest misfits selected for use in the next iteration. In each subsequent iteration a new set of models is generated by performing a random walk in each of the selected cells. Typically 3000 iterations are performed. A curve showing the improvement in the misfit with successive iterations is generated, allowing the number to be modified if the fit is not converging.

Crustal Structure

In the discussion below we group the stations according to the geological provinces in which they are located based on the boundaries defined in the National Atlas of Canada (2015). The results are discussed progressing from west to east. We note that several stations occur near the boundaries of two or more geological provinces. These stations are included in the section covering whichever province they fall within but we comment on their proximity to adjacent provinces. For each group, the models and data shown in the Figures are presented in alphabetical order. For ease of comparison, when more than one station falls within a geological province we also provide a plot showing the preferred models for all stations in that province.

Interior Platform

The receiver functions for station ULM in southern Manitoba (Figure 3) were the simplest of any station and showed no variation with either distance or azimuth, providing strong evidence for laterally homogeneous, flat layers. The preferred model consists of a crustal layer with a positive velocity gradient from the surface to 5 km. Below that the crust appears to have a uniform velocity of approximately 3.6 km/s. There is weak evidence for

an additional higher velocity layer from 5-15 km depth. There is a sharp Moho transition at 35 km. In a recent study of bulk properties of the crust and Moho depths across Canada, Postlewaite et al. (2014) obtained a Moho depth of 34 km beneath ULM. Motazedian et al. (2013) have a similar Moho depth for the southern Manitoba-northwestern Ontario region.

Hudson Bay Platform

Three of the study stations (FCC, SILO and VIMO) are located in the Hudson Bay Platform. The velocity models for FCC and SILO are very similar in terms of the number of layers and depths of discontinuities although the two differ in detail (Figure 4a,b). The model for VIMO shares some characteristics with these two but overall is different (Figure 5).

Both FCC and SILO have a high velocity lid that extends to 12 km, although SILO may have a very thin (< 1 km thick) low velocity layer at the surface. This topmost crustal layer has a uniform velocity beneath SILO and a positive velocity gradient beneath FCC. At both stations this layer is underlain by a crustal layer with a positive velocity gradient that extends to 20 km. The primary difference between the two stations is in the absolute velocity with the top of this layer matching the bottom of the overlying layer at SILO and with a lower velocity than the base of the top layer at FCC. Both stations also have a third crustal layer and a sharp Moho at 40 km. This bottom crustal layer has a uniform velocity beneath FCC and a slight positive gradient beneath SILO. An early study by Cassidy (1995b) put the Moho at FCC at 43 km and a more recent one by Postlewaite et al (2014) obtained a Moho depth of 42 km. Studies by Darbyshire (2007) and Postlewaite et al. (2014) obtained a Moho depth of 38 km for SILO.

Like the other two stations VIMO (Figure 4c) shows evidence for crustal layering with the uppermost layer being 8 km thick and exhibiting a strong gradient from 2.5 km/s at the surface to 4.2 km/s at 8 km. This layer is underlain by a lower velocity layer which extends to 17 km. Below this is a third crustal layer with a negative velocity gradient to 30 km below which there is a sharp increase in velocity. Below this boundary there are several layers of internally uniform velocity with a step-like increase from each to the layer beneath. A study by Darbyshire et al (2007) concluded that the Moho depth at VIMO was 44 km while Postlewaite et al. (2014) had 46 km. The discontinuity at 45 km in our model would be consistent with their interpretations and with mantle velocities although a Moho at the layer above (37 km) cannot be completely ruled out. The shallower Moho would be more consistent with the shear wave dispersion results of Motazedian et al. (2013) for the region covered by the paths between FCC, SILO, VIMO and MALO.

We note that the overall misfit as well as the difference between the misfit of the best model and the average of the top 1% models is slightly higher for VIMO than for SILO and FCC suggesting that the structure is less well resolved. However the top 30% of the models for VIMO all exhibit the major features discussed here. We also note that VIMO is close to the boundary between the Hudson Bay Platform and the Superior Province. Thus the receiver functions from some azimuths (particularly from the south) may include

residual signals from propagation at depth through the Superior Province. VIMO does show more azimuthal variation than either FCC or SILO as well as a similar structure to the station OTRO, which is the nearest Superior Province station studied. The receiver functions from earthquakes to the northwest are very similar to those from the other two stations whereas those from earthquakes to the south show more subdued reflections, which would be consistent with that interpretation (Figure 6).

Superior Province

The majority of the stations in northern Ontario and adjacent Quebec (VLDQ, KAPO, MALO, MUMO, OTRO and KILO) lie within the Superior Province, which makes up a large portion of the Canadian Shield. While the models for these stations differ in detail there are two pervasive features (Figures 7a-f and 8). The first of these features consists of two crustal layers with steep negative velocity gradients. At KAPO and MUMO these layers are almost identical to each other and are each about 10 km thick. At OTRO and VLDQ there is one thick and one thinner layer. The negative gradient is not observed at KILO although this station has two discontinuities with a negative change in velocity. The layers are also not seen on the best models for MALO but we note that the fit for MALO was the poorest of any station modeled and these layers do appear in some of the best 1-10% models.

The second regional feature is an ambiguous Moho. By this we mean that either there is not a sharp discontinuity at the range of depths (roughly 35-50 km) expected for the Moho or that there is a discontinuity but the velocity is lower than what would be expected for the upper mantle. This may mean that the crust-mantle boundary is gradational rather than sharp or that the signal from the Moho is being masked by another structure, which must be large-scale as it affects stations over a wide geographic area.

Except for MALO all stations have a layer with a sharp increase in velocity at 33-36 km. However, the velocity at this depth is lower than what would be expected for the upper mantle. Below this layer at most stations there is a positive velocity gradient to depths of about 50 km. At all stations the best estimate for the Moho is in the 40-43 km range based on the velocity itself rather than the presence of a sharp discontinuity. We cannot, however, rule out the Moho boundary being at either the observed, shallower discontinuity or either above or below our preferred depth. MALO shows a strong increase in velocity at 44 km, which we interpret as the Moho.

The model for OTRO is somewhat unusual in that the velocities below 35 km are lower than would be expected for mantle material and increase very gradually to depths of 75 km. There is a boundary at about 45 km that would be consistent with the Moho depths at the other Superior Province stations but it is difficult to say from the model alone whether this truly represents the Moho.

Darbyshire et al (2007) in a study of the Superior Province determined the Moho depth beneath several of these stations: KAPO 48 km, KILO 35 km, MALO 37 km, MUMO 38

km and OTRO 41 km. Postlewaite et al. (2014) also evaluated some of these stations and obtained the following Moho depths: KAPO 43 km, KILO 40 km, MALO 39 km, MUMO 39 km and VLDQ 33 km. Except at the KAPO the Darbyshire et al. (2007) depths are very similar to ours. We note that our model for KAPO has a discontinuity at 50 km, which might correspond to their interpreted Moho at 48 km. Similarly we are in general agreement with the results of the Postlewaite et al. (2014) study except at VLDQ but we note that their Moho depth is in agreement with our observations of an increase in velocity at this depth.

Southern Province

Station SUNO is located in the Southern Province, a narrow mineral rich zone between the Superior Province and St. Lawrence Platform. The structure beneath SUNO can be modeled as two crustal layers (Figure 9): a layer from the surface to 13 km with a positive velocity gradient underlain by a layer with a uniform velocity or slightly negative gradient, which extends to 35 km. The Moho transition at 35 km is sharp. The Moho depth is consistent with and falls between the values of 34 km for Darbyshire et al (2007), 36 km of Eaton et al (2006) and 37 km of Postlewaite et al. (2014).

St. Lawrence Platform

Stations within the St. Lawrence Platform include three located in the seismically active West Quebec Seismic Zone (OTT, MNT and KGNO) and one (SADO) in the much less active southern Ontario region. The velocity structure for stations OTT and MNT, both of which are located near the St. Lawrence- Grenville boundary, is very similar (Figures 10b,c and 11). Both stations have a crustal layer with a positive velocity gradient extending from the surface to 15 km below which is a lower velocity layer with a negative velocity gradient which extends to 25 km. A third crustal layer with a more or less uniform velocity underlies these layers. The Moho is at 37 km for MNT and 38 km for OTT and in both cases there is a positive velocity gradient in the uppermost mantle. Postelwaite et al. (2014) had a Moho depth of 34 km for MNT but did not include OTT in their study.

The velocity structure for KGNO and SADO is somewhat different although the two share some features (Figures 10a,d and 11). Both have a crustal lid with a steep velocity gradient from the surface to 5 km. Below the lid KGNO has a uniform higher velocity layer to 11 km and SADO has a low velocity layer with a negative gradient (similar to the slightly deeper layer seen at MNT and OTT) to 12 km. At both stations these two layers are underlain by a thick layer with a positive gradient extending to 31 km at KGNO and 34 km at SADO. At SADO there is no sharp increase in velocity to denote the Moho but a change in the velocity gradient occurs at 31 km. At KGNO there is evidence for a fourth crustal layer with a uniform velocity to 45 km marked by a sharp increase in velocity, which presumably represents the Moho.

Eaton et al. (2006) and Postlewaite et al. (2014) also find that the Moho beneath KGNO is relatively deep and prefer depths of 40 km and 41 km, respectively and consistent with our

results. Both studies also looked at nearby POLARIS station PECO and obtained Moho depths in excess of 40 km- 44 km by Eaton et al. (2006) and 41 km by Postlewaite et al. (2014). Eaton et al. (2006) obtained a Moho depth of 38 km for station SADO while Postlewaite et al. (2014) had a slightly greater depth of 40 km.

Grenville Province

The stations GAC, LMQ and ICQ lie within the Grenville Province but very close to its boundary with the St. Lawrence Platform. At depth signals coming from the south also travel through the Appalachian Orogen. All three stations are located within active seismic zones: West Quebec (GAC), Charlevoix (LMQ) and Lower St. Lawrence (ICQ). The velocity structure for GAC (Figure 9a), which is near the Grenville-St. Lawrence boundary, is similar to that for OTT and MNT, which are located within the St. Lawrence platform discussed in the previous section and which are geographically close to GAC. GAC shows a steep velocity gradient to 4 km over a layer with a negative velocity gradient ending at 20 km. A strong Moho is not seen at GAC but rather the velocity continues to increase in step-like increments with depth. A discontinuity at 45 km is interpreted as the Moho but another at 38 km cannot be completely ruled out. Cassidy (1995b) put the Moho beneath GAC at 43 km while Postlewaite et al. (2014) have a shallower Moho depth of 39 km. Each of these corresponds roughly to a discontinuity seen in our model.

LMQ and ICQ are similar to each other in that the velocity structure consists primarily of a crustal layer with a steadily increasing velocity with a sharp Moho at 35 km for LMQ and 38 km for ICQ (Figures 12a,b and 13). LMQ shows changes in the crustal velocity gradient at 12 and 20 km (Figure 12c). We note that Cassidy (1995b) had difficulties modeling LMQ. Postlewaite et al.'s (2014) depth of 49 km for LMQ is significantly greater than ours. We do not have a good explanation for the difference and note that our model has no discontinuity at or near 49 km depth.

A thin low velocity layer occurs at ICQ from 15-18 km. We note that this layer appears in almost every model for ICQ from the best to worst fitting and thus appears to be real and not just an attempt to fit a spurious peak. The Postlewaite et al. (2014) Moho depth of 40 km for ICQ is consistent with our results.

An ongoing project using the more dense array in the Charlevoix seismic zone and temporary stations deployed in the less active regions between the Charlevoix and Western Quebec Seismic Zones (Bent and Kao, 2015a,b) will provide a much more detailed picture of the structure along the length of the St. Lawrence. Preliminary results from stations within the Charlevoix Seismic Zone on the north shore of the St. Lawrence River and in Quebec City area are indicative of structure similar to that of LMQ. The structure beneath the stations in the Charlevoix Seismic Zone on the south shore of the St. Lawrence River is different. However, these stations lie within the Appalachian Orogen and not the Grenville Province. They have lower upper crustal velocities than the

north shore stations. The models are fairly similar to the model for GGN (see Appalachian Orogen section) but with slightly higher crustal velocities. We note that the Postlewaite et al. (2014) study included Moho depths for other stations in the Charlevoix region in which LMQ is located and that their Moho depths are widely variable ranging from 27-43 km. No interpretation of the wide range of depths is provided.

Churchill Province

Station SCHQ is situated within the Churchill Province but very close to its boundaries with both the Hudson Bay Platform and the Superior Province. The velocity structure for this station (Figure 14) is a bit odd consisting of a low velocity lid with a positive gradient to 5 km below which there is a thick crustal layer with a relatively high (4.2 km/s) and uniform velocity to 50 km where there is a sharp transition at what appears to be the Moho. However, the Moho velocity of 5 km/s is relatively high and it is not entirely clear whether this really is the Moho or whether it represents a discontinuity within the upper mantle with the Moho reflection and another structural boundary masking each other. The results from the preliminary, linear inversion showed a similar lack of crustal structure and a strong velocity discontinuity at 50 km. Postlewaite et al. (2014) indicate a Moho depth of 50 km at SCHQ. We note that their depth is indicated as 50 with no digits after the decimal whereas they published additional significant digits for all other stations evaluated, suggesting that their model is also less well constrained. They obtain a Moho depth of 49 km at WBHL, which is closest station to SCHQ but was not included in our study as it is not a CNSN station.

Appalachian Orogen

Both New Brunswick stations (LMN and GGN) are located in the Appalachian Orogen. The structure at LMN (Figure 15b) consists of 2 almost identical layers with a slight positive velocity gradient- the first from the surface to 12 km and the second from 12 to 22 km- over a third crustal layer with a negative gradient that ends at the Moho, which appears as a sharp discontinuity at 38 km. The upper mantle shows increasing velocity with depth. An earlier paper by Cassidy (1995b) had put the Moho at 43 km.

The model for GGN (Figures 15a and 16) shares some features with LMN but overall looks more similar to the Grenville province stations and could be described as a hybrid of ICQ and LMQ. It consists of a low velocity lid to 15 km which overlies a higher velocity mid-crustal layer with a negative gradient extending to 22 km. Below this the velocity steadily increases to 36 km where there is a slight increase in velocity and a sharp decrease in the velocity gradient, which presumably represents the Moho. The results of Postlewaite et al (2014) for this region are similar to ours with a Moho depth of 35 km at GGN and 38 km at LMN.

Discussion

One potential, practical use of the receiver function derived velocity models is improved earthquake locations. A rich aftershock sequence associated with the March 1999 Côte-Nord earthquake in the Lower St. Lawrence seismic zone, discussed in more detail by Lamontagne et al. (2004) provided an opportunity to compare locations made using a generic eastern Canada velocity model (Brune and Dorman, 1963) to a regional model. In this case, the model for station ICQ, the closest broadband station, was selected. The aftershocks were relocated using the joint hypocenter determination method. The epicentral locations were not strongly dependent on which of the two velocity models (shown in Figure 13) was used but the differences in depths were quite pronounced. With the generic model the aftershocks span the full range of depths from the surface to 20 km with one outlier at 40 km. When the local velocity model is used the aftershocks fall mostly in the 10-20 km range and the average uncertainties, particularly for the shallower events, are noticeably decreased (Figure 17). The mainshock occurred at a depth of 20 km and narrower range of depths seems more probable given the mainshock depth and magnitude (M_N 5.1).

The regional centroid moment tensor (RCMT) inversion method used in Canada (Kao et al., 2012) allows for multiple velocity models to be used in the same inversion. This feature is used for western Canadian earthquakes. That is the most appropriate of seven regional models for the source-station path may be used for each station used in the inversion. At the present time a single model is used for all earthquakes in southeastern Canada. The same model with a slight modification made to the Moho depth is used for the eastern Arctic. Better models of the structure in eastern Canada will help us evaluate whether there would be any advantage to using a suite of models in the RCMT inversion.

As was commented upon throughout the text, many stations are located near the boundaries of two or more geological provinces and signals arriving from some azimuths may have traveled predominantly through a geological province other than the one in which the station is located. We intend to explore these azimuthal variations more thoroughly as a future research project and there are alternative explanations, such as dipping structure or anisotropy that must also be considered. However, we provide one example here to illustrate the observed azimuthal variations (Figure 18). Station LMQ is located within the Grenville Province but near the Appalachian Orogen where the two are separated by a narrow strip of the St. Lawrence Platform (Figure 1). Figure x shows the radial and tangential receiver functions for station LMQ plotted in order of increasing back azimuth. The direct P wave is noted. The marker T1 is aligned with a particularly strong, presumably Moho, reflection for an event with a back azimuth of 134°. Phases between P and T1 are related crustal layering. It can be seen that the amplitude and timing of the Moho and other reflections vary with back azimuth. For example, the Moho reflection appears earlier than T1 for earthquakes with back azimuths close to 180°. For events to the northwest and northeast, the timing of the Moho reflection is close to that of T1 although the amplitudes for the northeast quadrant are small. Very little is seen on the tangential receiver functions, which is expected for flat layered structures.

Conclusions

Teleseismic receiver functions have been used to model the shear wave velocity structure beneath twenty-one seismograph stations in central and eastern Canada, complementing earlier studies which covered western and Arctic Canada (Cassidy 1995a; Darbyshire, 2003). Stations within the same geological province share many features although those near the boundary with another province may appear to be a hybrid of the two. The relocation of an aftershock sequence in the Lower St. Lawrence provides a clear example of the advantages of using a regional model for earthquake locations rather than a generic continental scale model.

Acknowledgements

Catherine Woodgold provided the aftershock relocations used in the example shown in Figure 17. We thank John Cassidy for his thoughtful and constructive review.

References

Ammon, C. J. (1991). The isolation of receiver effects from teleseismic P waveforms, *Bulletin of the Seismological Society of America*, **81**, 2504-2510.

Ammon, C. J., G. E. Randall and G. Zandt (1990). On the non-uniqueness of receiver function inversions, *Journal of Geophysical Research,* **95**, 15 303-15 318.

Bent, A. L. and H. Kao (2015a). Crustal Structure of the St. Lawrence Corridor from Teleseismic Receiver Functions and a Temporary Broadband Array, accepted for presentation at the 2015 Annual Meeting of the Seismological Society of America.

Bent, A. L. and H. Kao (2015b). Toward a three-dimensional model of the St. Lawrence Corridor, Canada, submitted to the 2015 International Union of Geodesy and Geophysics General Assembly.

Brune, J. and J. Dorman (1963). Seismic waves and earth structure in the Canadian shield, *Bulletin of the Seismological Society of America*, **53**, 167-210.

Cassidy, J. F. (1992). Numerical experiments in broadband receiver function analysis, *Bulletin of the Seismological Society of America*, **82**, 1453-1474.

Cassidy, J. F. (1995a). Review: Receiver function studies of the southern Canadian Cordillera, *Canadian Journal of Earth Sciences*, **32**, 1514-1519.

Cassidy, J. F. (1995b). A comparison of the receiver structure beneath stations of the Canadian National Seismograph Network, *Canadian Journal of Earth Sciences*, **32**, 938-951.

Clayton, R. W. and R. A. Wiggins (1976). Source shape estimation and deconvolution of teleseismic bodywaves, *Geophys. Journal of the Royal Astronomical Society,* **47**, 151-177.

Darbyshire, F. A. (2003). Crustal structure across the Canadian high Arctic from teleseismic receiver function analysis, *Geophysical Journal International*, **152**, 372-391.

Darbyshire, F. A., D. W. Eaton, A. W. Frederiksen and L. Ertolahti (2007). New insights into the lithosphere beneath the Superior Province from Rayleigh wave dispersion and receiver function analysis, *Geophyical Journal International,* **169**, 1043-1068, doi:10.1111/j.1365-246X.2006.03259.x.

Eaton, D. W., S. Dineva and R. Mereu (2006). Crustal thickness and Vp/Vs variations in the Grenville orogen (Ontario, Canada) from analysis of teleseismic receiver functions, *Tectonophysics,* **420**, 223-238, doi:10.1016/j.tecto.2006.01.023.

Helmberger, D. and R. A. Wiggins (1971). Upper mantle structure of the Midwestern United States, *Journal of Geophysical* Research, **76**, 3229-3245.

Kao, H., S.-J. Shan, A. Bent, C. Woodgold, G. Rogers, J. F. Cassidy and J. Ristau (2012). Regional Centroid-Moment-Tensor Analysis for Earthquakes in Canada and Adjacent Regions: An Update, *Seismological Research Letters*, **83**, 505-515, doi:10.1785/gssrl.83.3.505.

Lamontagne, M., A. L. Bent, C. R. D. Woodgold, S. Ma and V. Peci (2004). The 16 March 1999 mN 5.1 Côte-Nord earthquake: The largest earthquake ever recorded in the Lower St. Lawrence Seismic Zone, Canada, *Seismological Research Letters*, **75**, 299-316.

Langston, C. A. (1979). Structure under Mount Rainier, Washington, inferred from teleseismic body waves, *Journal of Geophysical* Research, **84**, 4749-4762.

Li, A., D. W. Forsyth and K. M. Fischer (2003). Shear structure and azimuthal anisotropy beneath eastern North America from Rayleigh wave inversion, *Journal of Geophysical Research*, **108**, 2362-2385, doi:10.1029/2002JB002259.

Motazedian, D., S. Ma and S. Crane (2013). Crustal Shear-wave Velocity Models Retrieved from Rayleigh-wave Dispersion Data in Eastern North America, *Bulletin of the Seismological Society of America*, **103**, 2266-2276, doi:10.1785/0120120187.

National Atlas of Canada (2015). http://www.nrcan.gc.ca/earth-sciences/geography/atlas-canada/selected-thematic-maps/16876, Geological Provinces based on Geological Map of Canada Map D1860A (CD-ROM), 1997, Ottawa; website last accessed on 16 February 2015.

Postlewaite, B., M. G. Bostock, N. I. Christensen and D. B. Snyder (2014). Seismic velocities and composition of the Canadian crust, *Tectonophysics*, **633**, 246-267, doi:10.1016/j.tecto.2014.07.024.

Sambridge, M. (1999). Geophysical inversion with a neighbourhood algorithm- I. Searching a parameter space, *Geophysical Journal International*, **138**, 479-494.

Table 1
Stations Analyzed in Study

Code	Location	Lat. (°N)	Lon. (°W)	Year Installed*	Geological Province
FCC	Fort Churchill MB	58.76	94.09	1993	Hudson Bay
GAC	Glen Almond QC	45.70	75.48	1992	Grenville
GGN	St. George NB	45.12	66.84	2002	Appalachian
ICQ	Islets Caribou QC	49.52	67.27	2001	Grenville
KAPO	Kapuskasing ON	49.45	82.51	1998	Superior
KGNO	Kingston ON	44.23	76.49	1999	St. Lawrence
KILO	Kirkland Lake ON	48.50	79.23	2003	Superior
LMN	Caledonia Mtn. NB	45.85	64.81	1993	Appalachian
LMQ	La Malbaie QC	47.55	70.33	1992	Grenville
MALO	McAlpline Lake ON	50.02	79.76	2003	Superior
MNT	Montreal QC	45.51	73.62	2001	St. Lawrence
MUMO	Musselwhite Mine ON	52.61	90.39	2003	Superior
OTRO	Otter Rapids ON	50.18	81.63	2003	Superior
OTT	Ottawa ON	45.39	75.72	2002	St. Lawrence
SADO	Sadowa ON	44.77	79.14	1994	St. Lawrence
SCHQ	Schefferville QC	54.83	66.83	1994	Churchill
SILO	Sutton Inlier ON	54.48	84.91	2003	Hudson Bay
SUNO	Sudbury Onaping ON	46.64	81.34	2003	Southern
ULM	Lac du Bonnet MB	50.25	95.88	1994	Interior
VIMO	Victor Mine ON	52.82	83.75	2003	Hudson Bay
VLDQ	Val-D'Or QC	48.11	77.45	2002	Superior

* year 3-component broadband instrument installed; some sites previously hosted other instruments

Figures

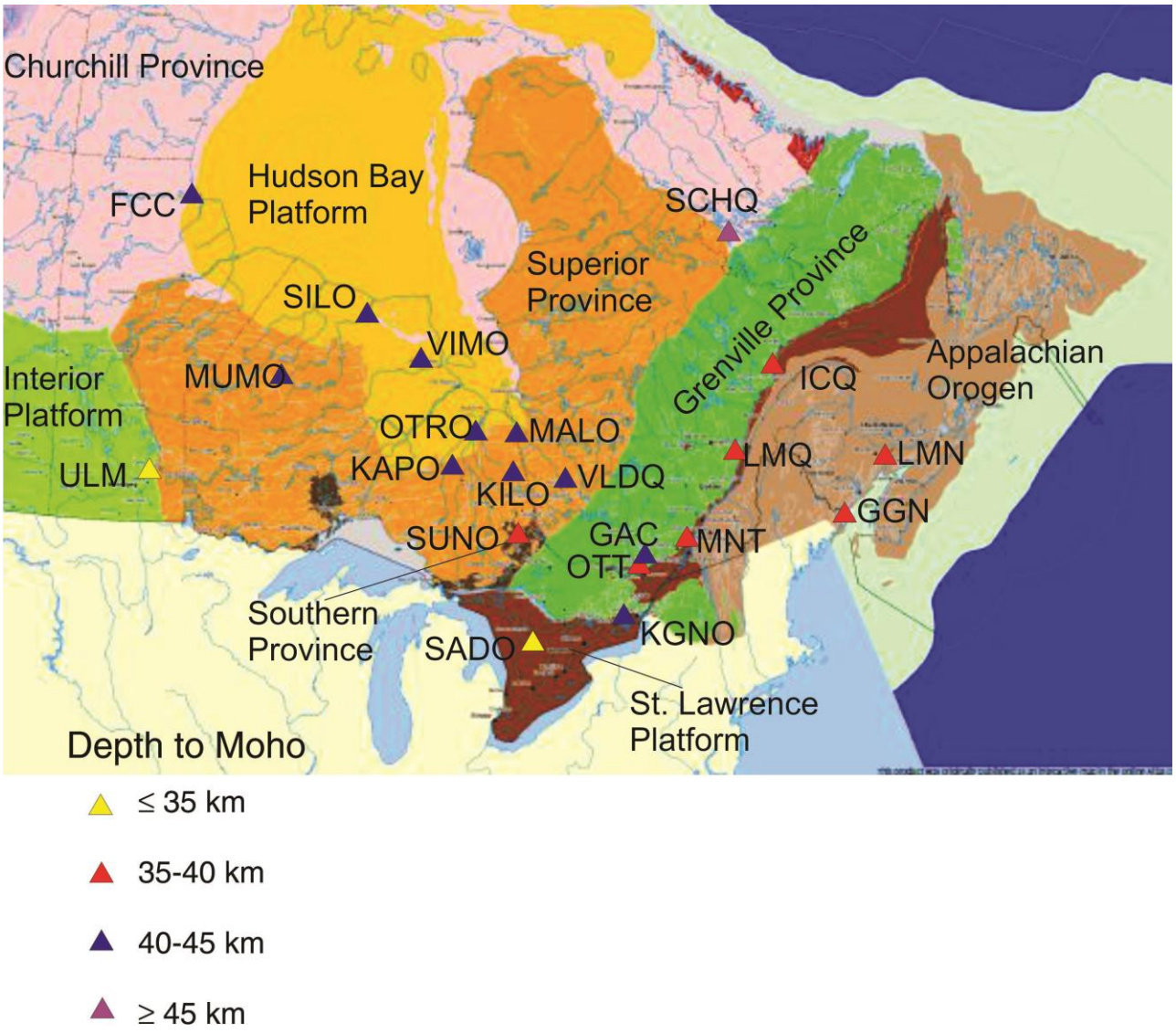

Figure 1: Map showing stations (triangles) analyzed in this study. The colors indicate the best estimate of Moho depth from the NA inversion. More details about each station may be found in Table 1. The background showing the geological provinces is from the National Atlas of Canada (2015).

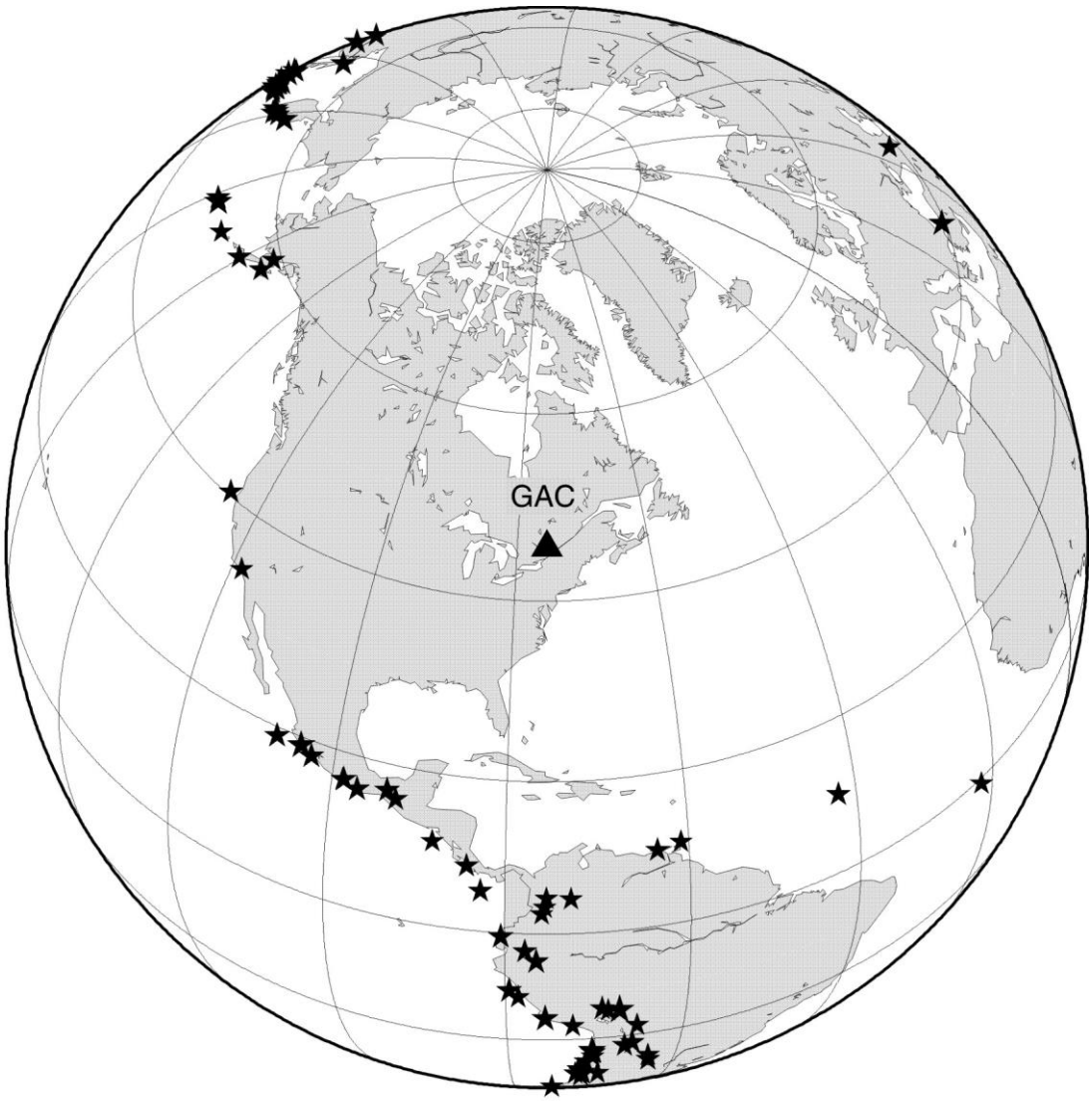

Figure 2

Figure 2: Earthquakes (black stars) used to make receiver functions for station GAC (black triangle). The event distribution is typical of most of the other stations shown in Figure 1.

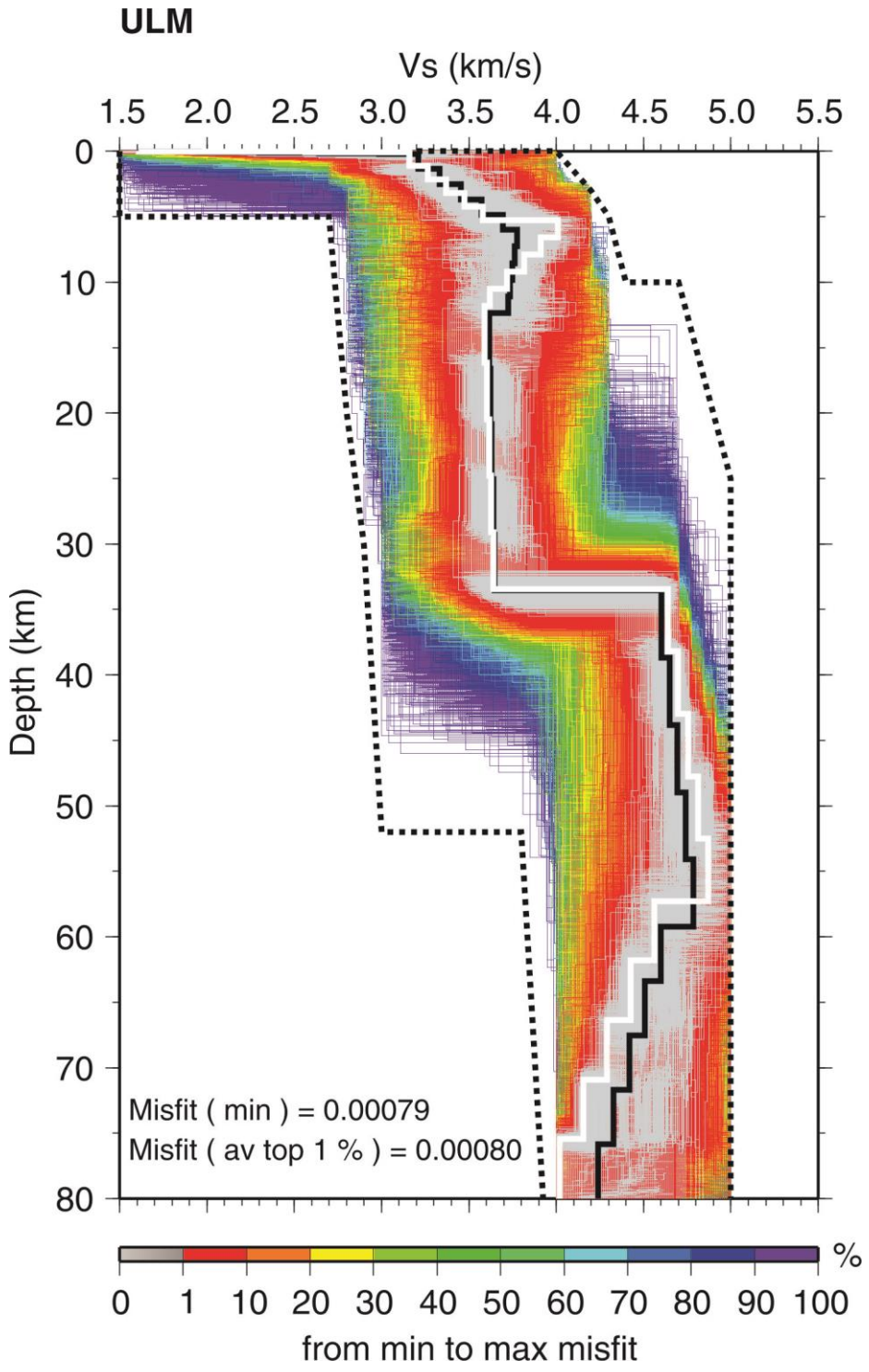
ULM
Vs (km/s)
1.5 2.0 2.5 3.0 3.5 4.0 4.5 5.0 5.5
Depth (km)
0 10 20 30 40 50 60 70 80
Misfit (min) = 0.00079
Misfit (av top 1 %) = 0.00080
%
0 1 10 20 30 40 50 60 70 80 90 100
from min to max misfit

Figure 3-i

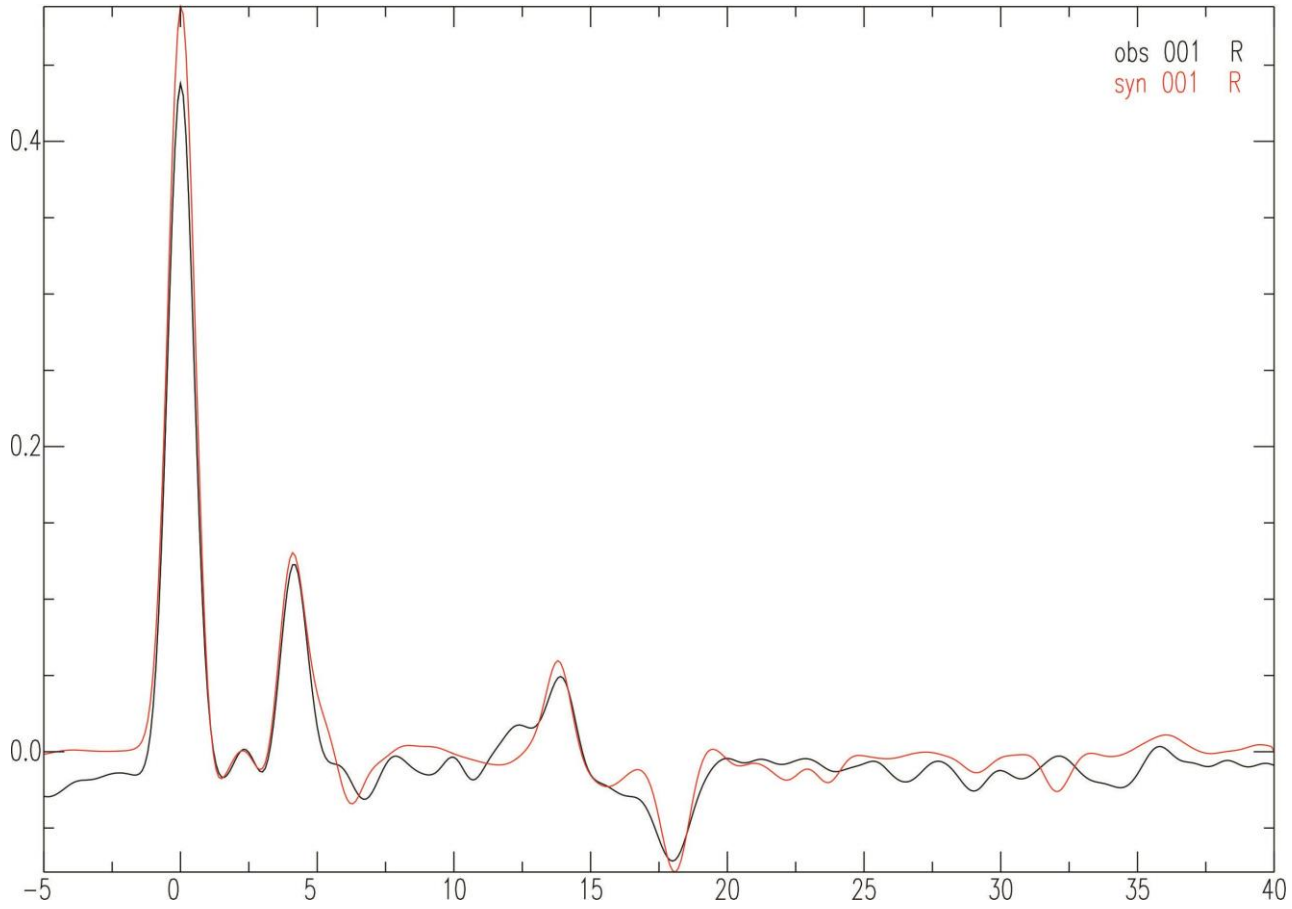

Figure 3-ii

Figure 3: Full Neighborhood Algorithm results for station ULM in the Interior Platform. The dashed lines show the range of models searched, the white line the best fitting model and the black line the average of the top 1% of the models. The other models tested are color coded based on their fit (see scale bar). The waveform part of the figure shows the receiver function used to generate the model in black and the synthetic receiver function based on the model in red. The horizontal axis shows the time in seconds with the direct P arrival at 0. The vertical axis indicates the amplitude.

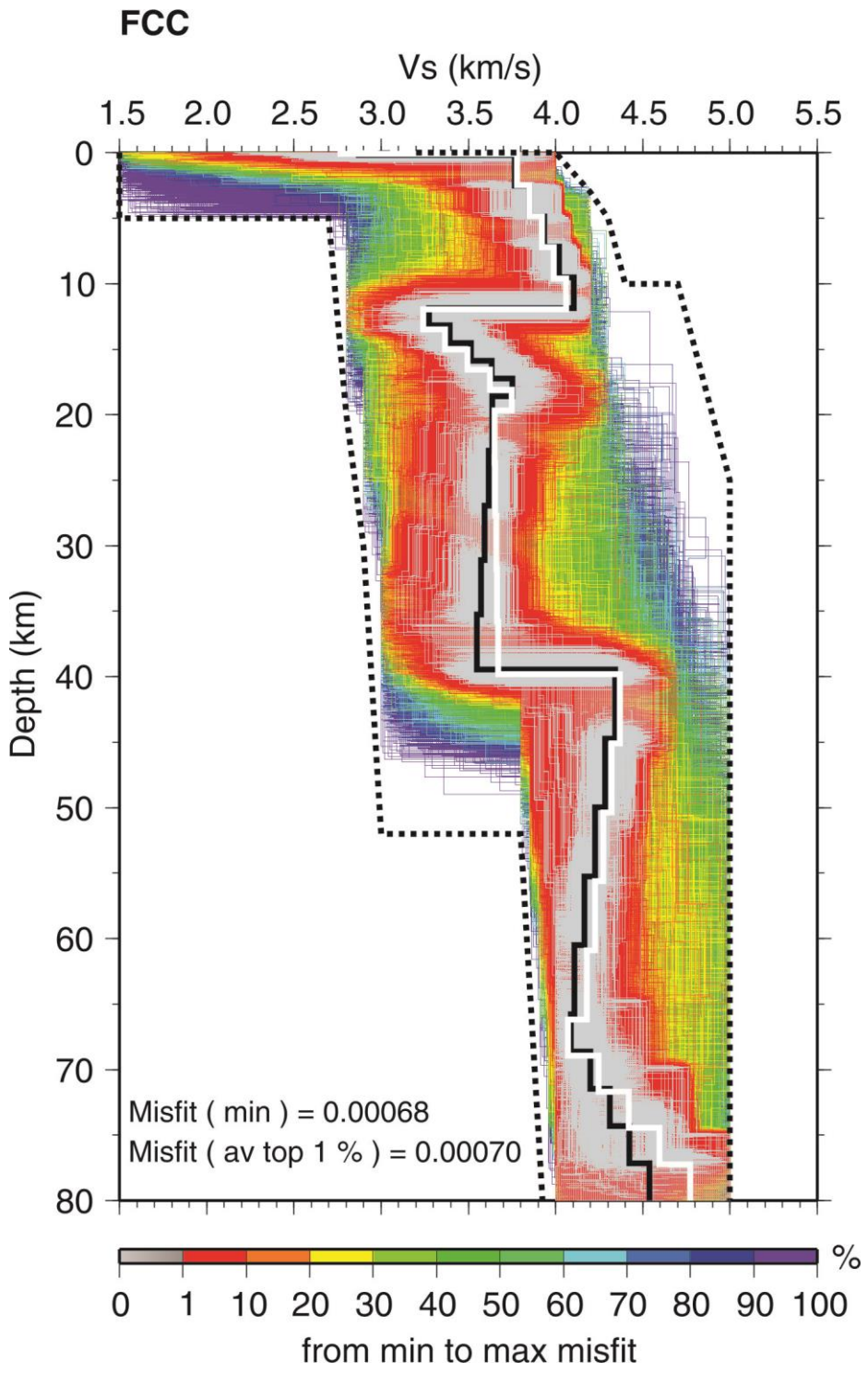
FCC
Vs (km/s)
1.5 2.0 2.5 3.0 3.5 4.0 4.5 5.0 5.5
Depth (km)
0 10 20 30 40 50 60 70 80
Misfit (min) = 0.00068
Misfit (av top 1 %) = 0.00070
%
0 1 10 20 30 40 50 60 70 80 90 100
from min to max misfit

Figure 4a-i

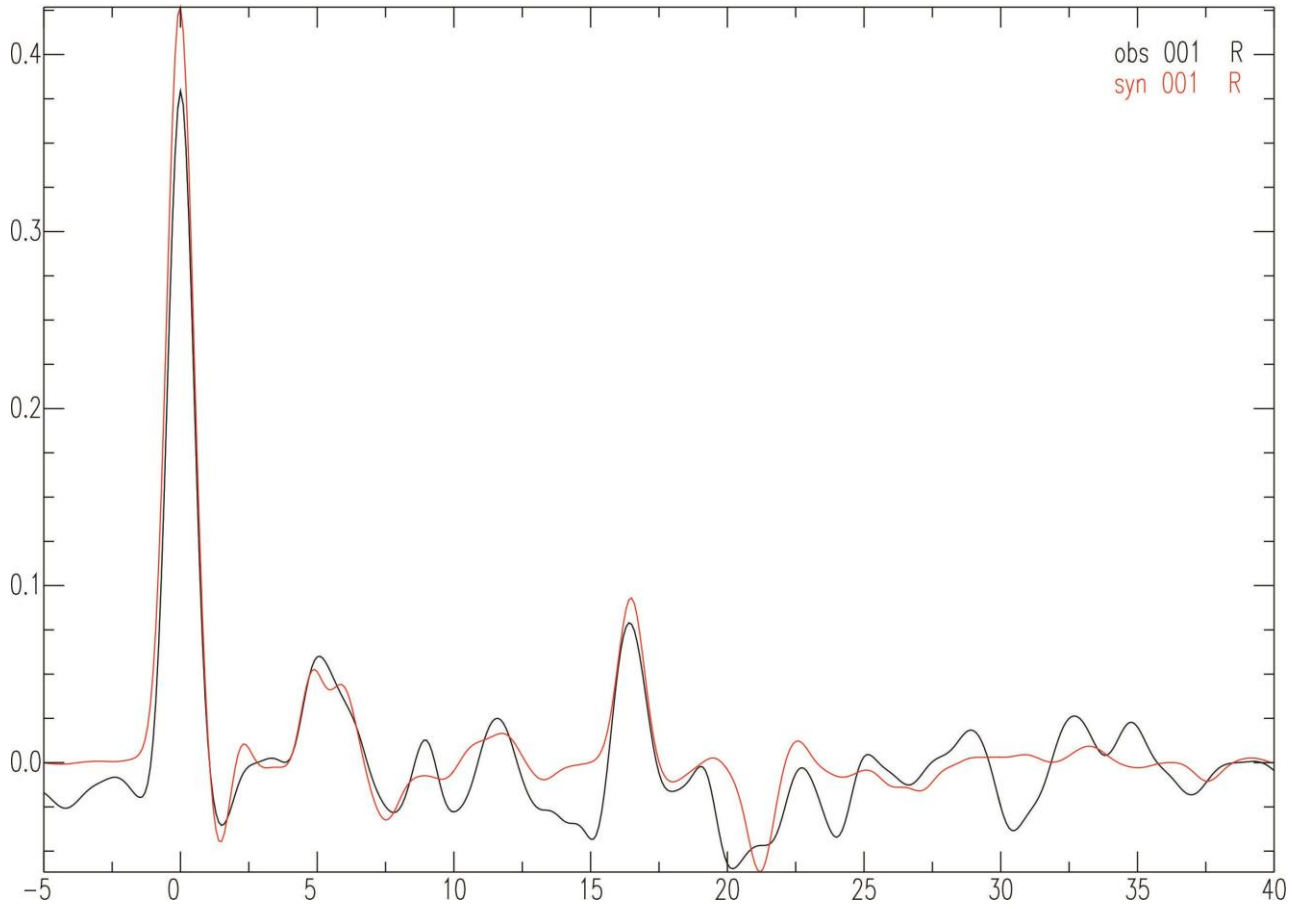

Figure 4a-ii (FCC)

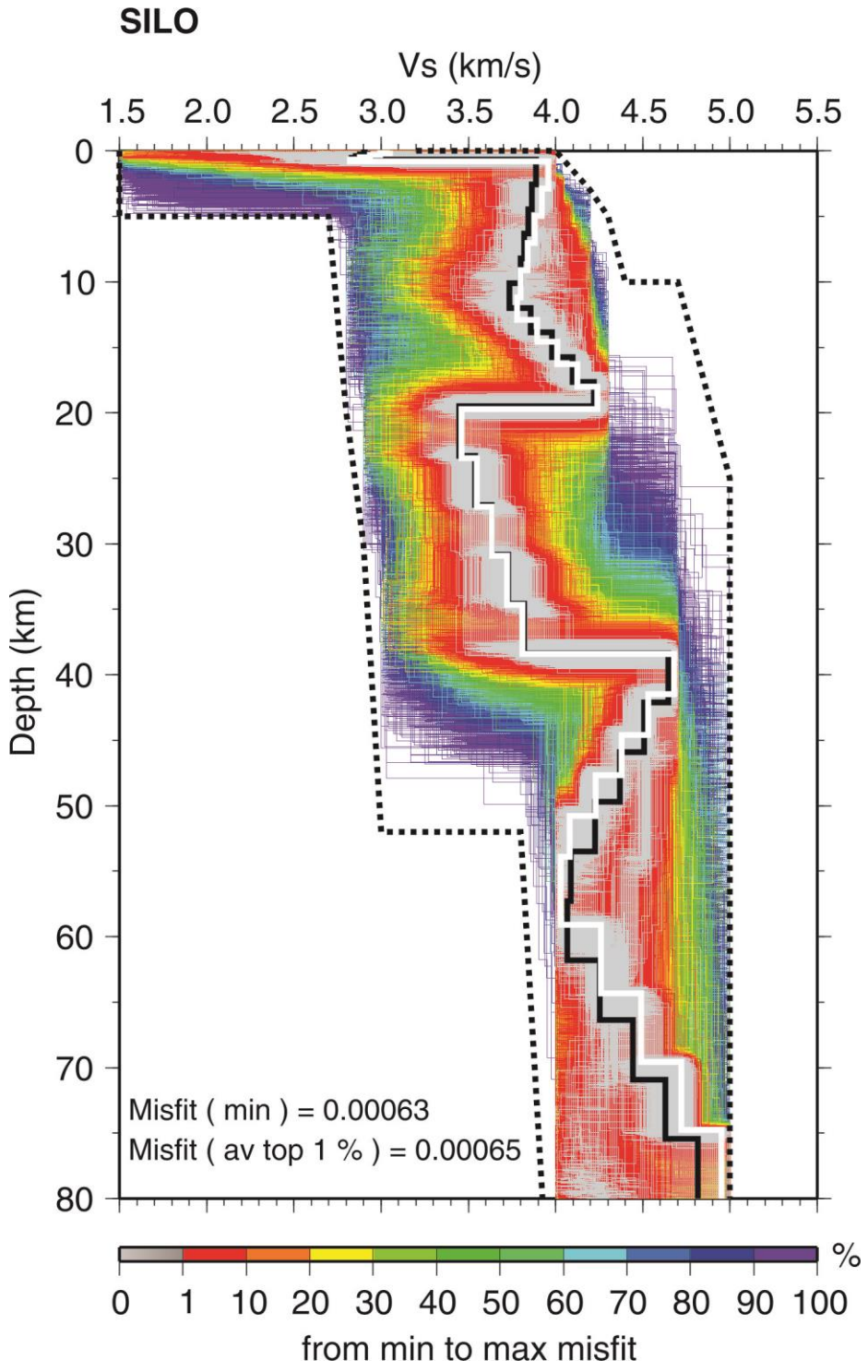
SILO
Vs (km/s)
1.5 2.0 2.5 3.0 3.5 4.0 4.5 5.0 5.5
Depth (km)
0 10 20 30 40 50 60 70 80
Misfit (min) = 0.00063
Misfit (av top 1 %) = 0.00065
%
0 1 10 20 30 40 50 60 70 80 90 100
from min to max misfit

Figure 4b-i

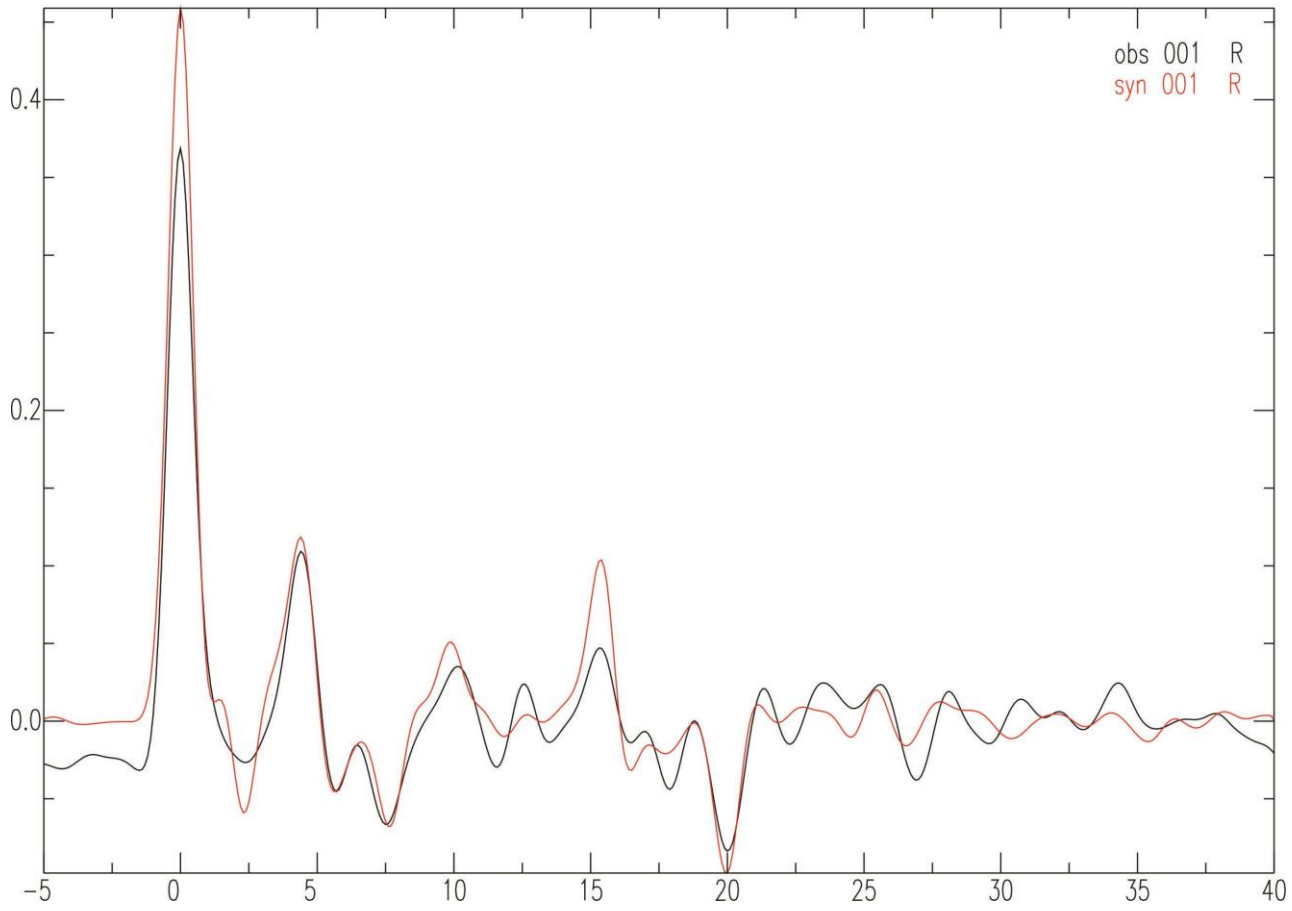

Figure 4b-ii (SILO)

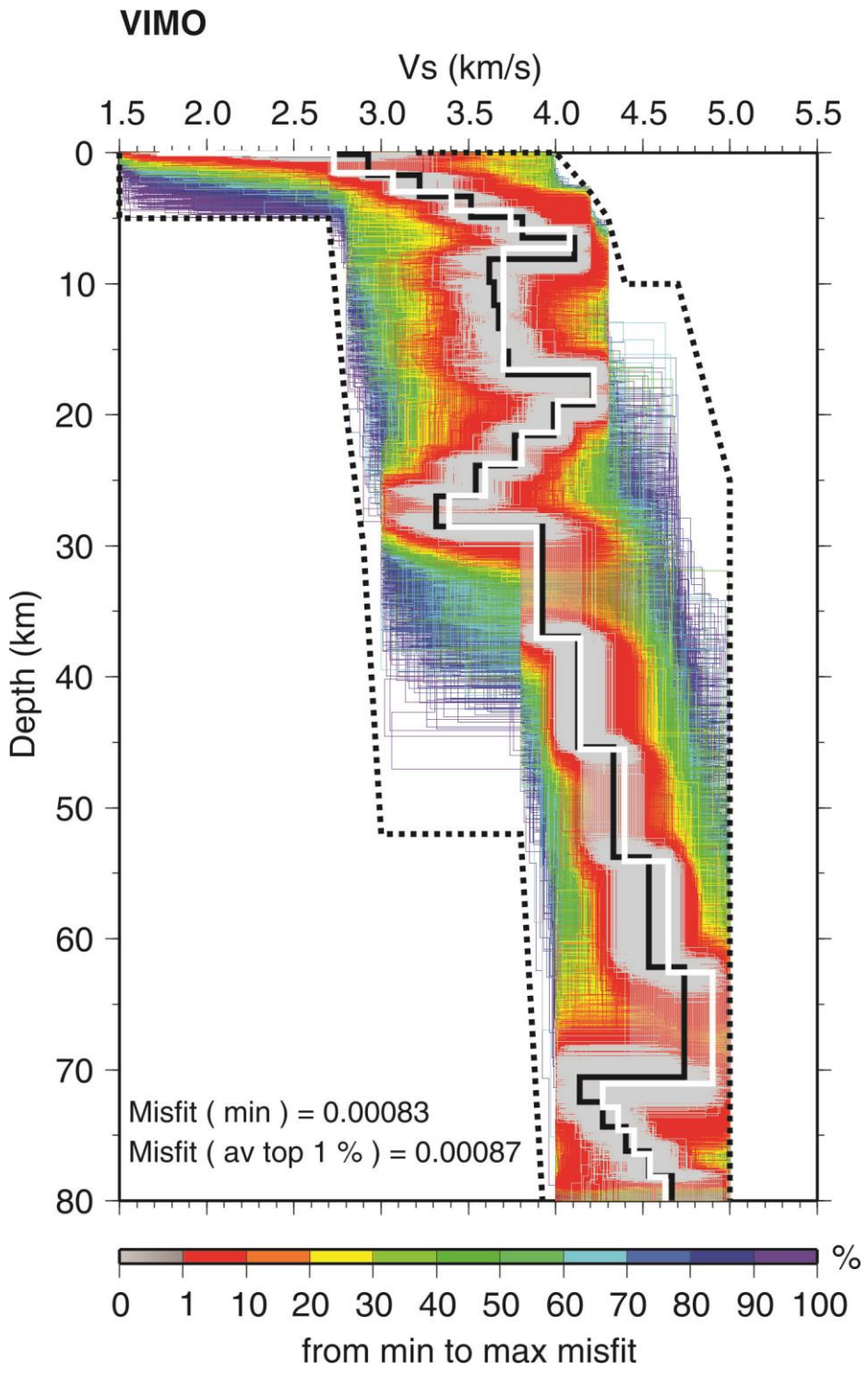
VIMO
Vs (km/s)
1.5 2.0 2.5 3.0 3.5 4.0 4.5 5.0 5.5
Depth (km)
0 10 20 30 40 50 60 70 80
Misfit (min) = 0.00083
Misfit (av top 1 %) = 0.00087
%
0 1 10 20 30 40 50 60 70 80 90 100
from min to max misfit

Figure 4c-i

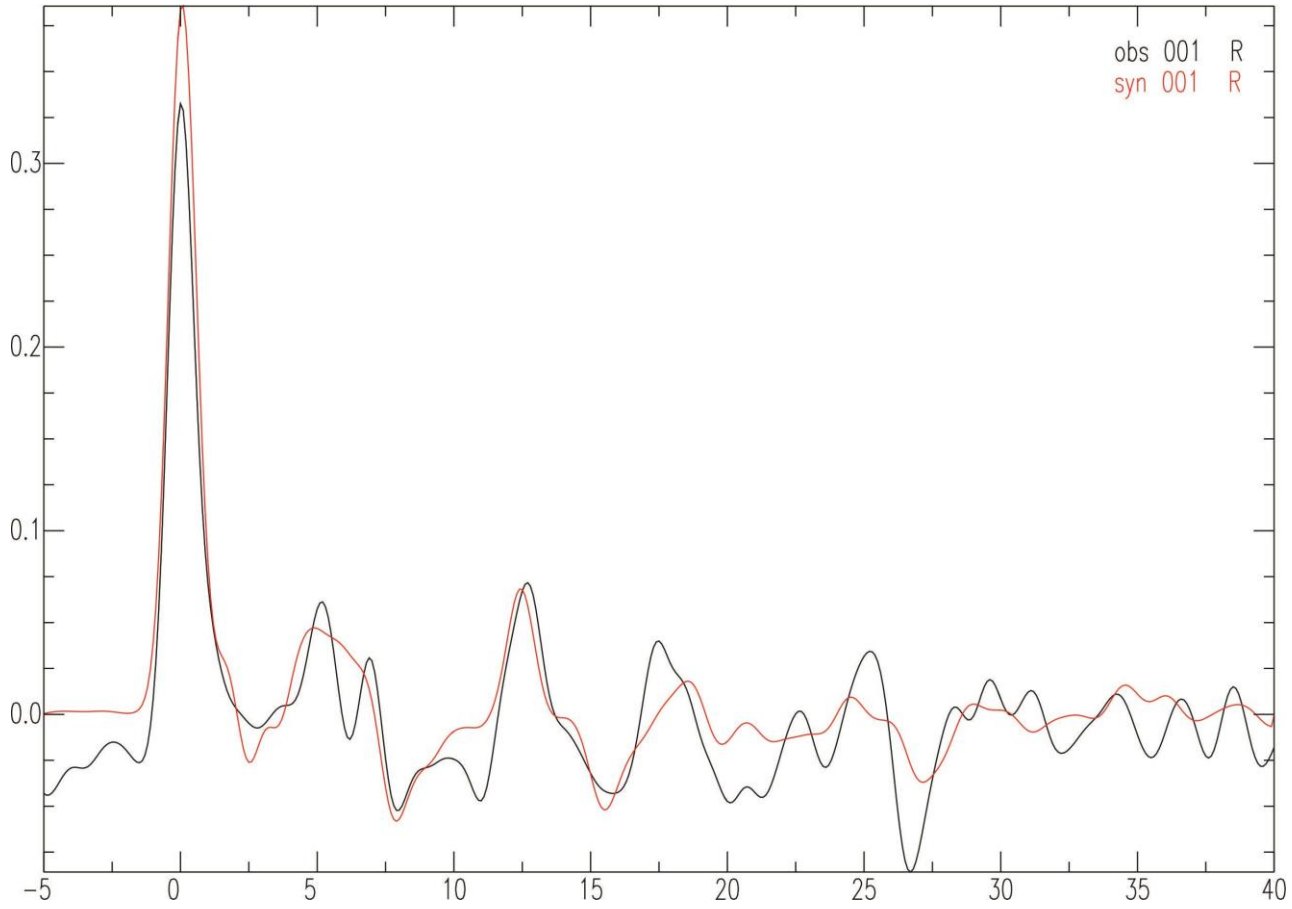

Figure 4c-ii (VIMO)

Figure 4. Structural models and receiver functions for stations in the Hudson Bay Platform: a) FCC, b) SILO and c) VIMO. Format the same as for Figure 3.

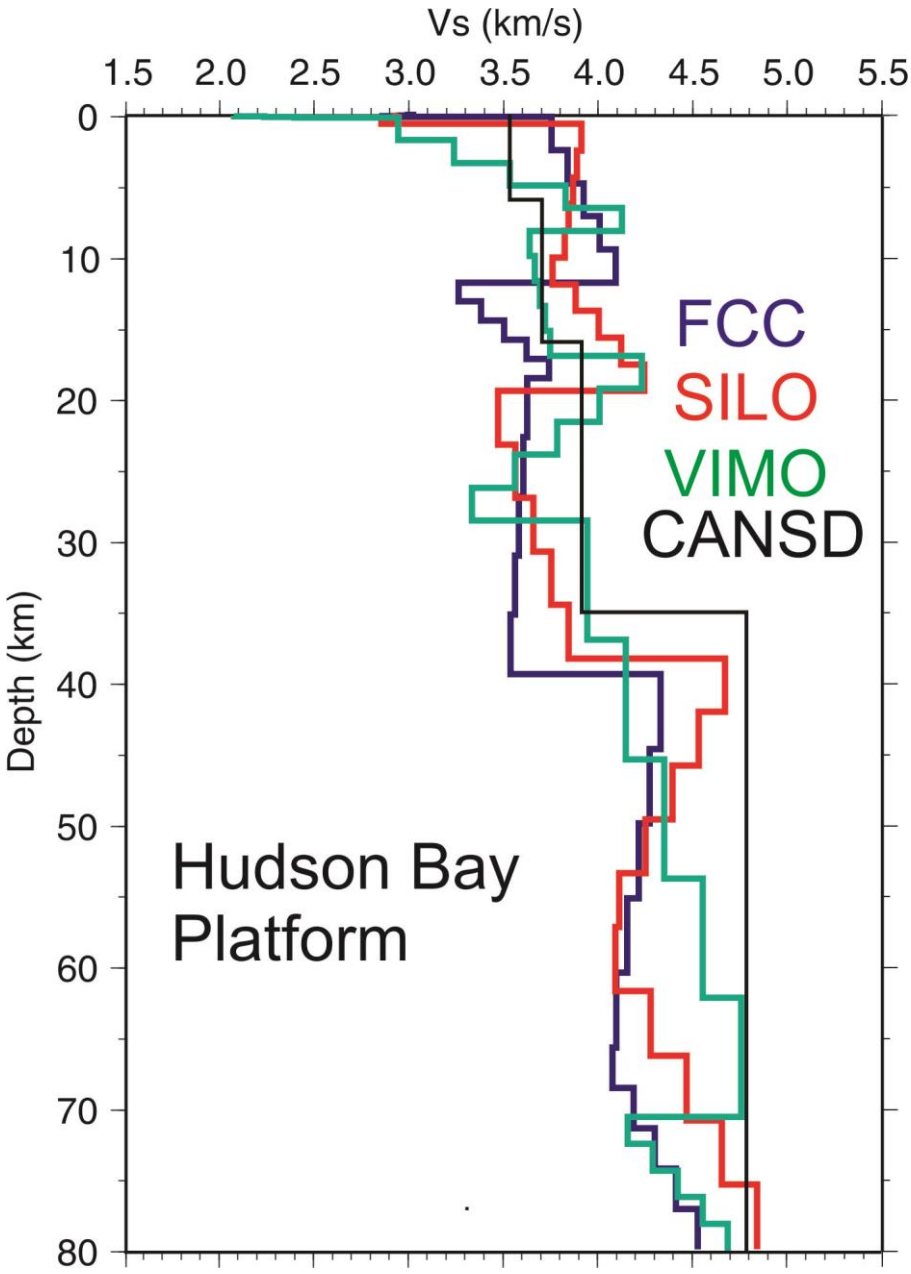

Figure 5. Preferred shear wave velocity models for stations in the Hudson Bay Platform. In this and subsequent, similar figures, CANSD refers to the shield model of Brune and Dorman (1963), which serves as a generic velocity model for eastern Canada.

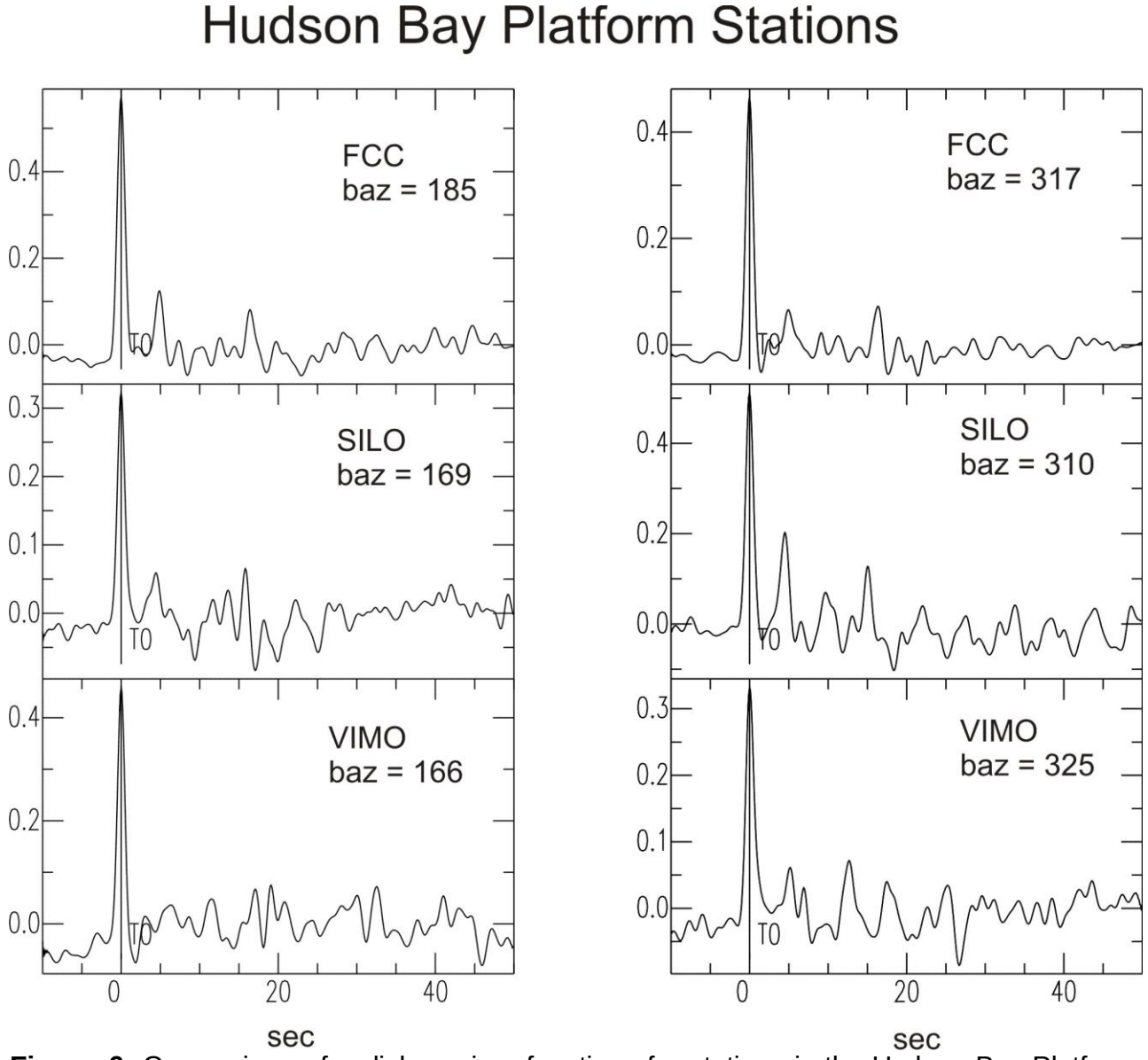

Figure 6. Comparison of radial receiver functions for stations in the Hudson Bay Platform. The receiver functions on the left are for events occurring to the south and on the right for events from the northwest. T0 indicates the direct P wave.

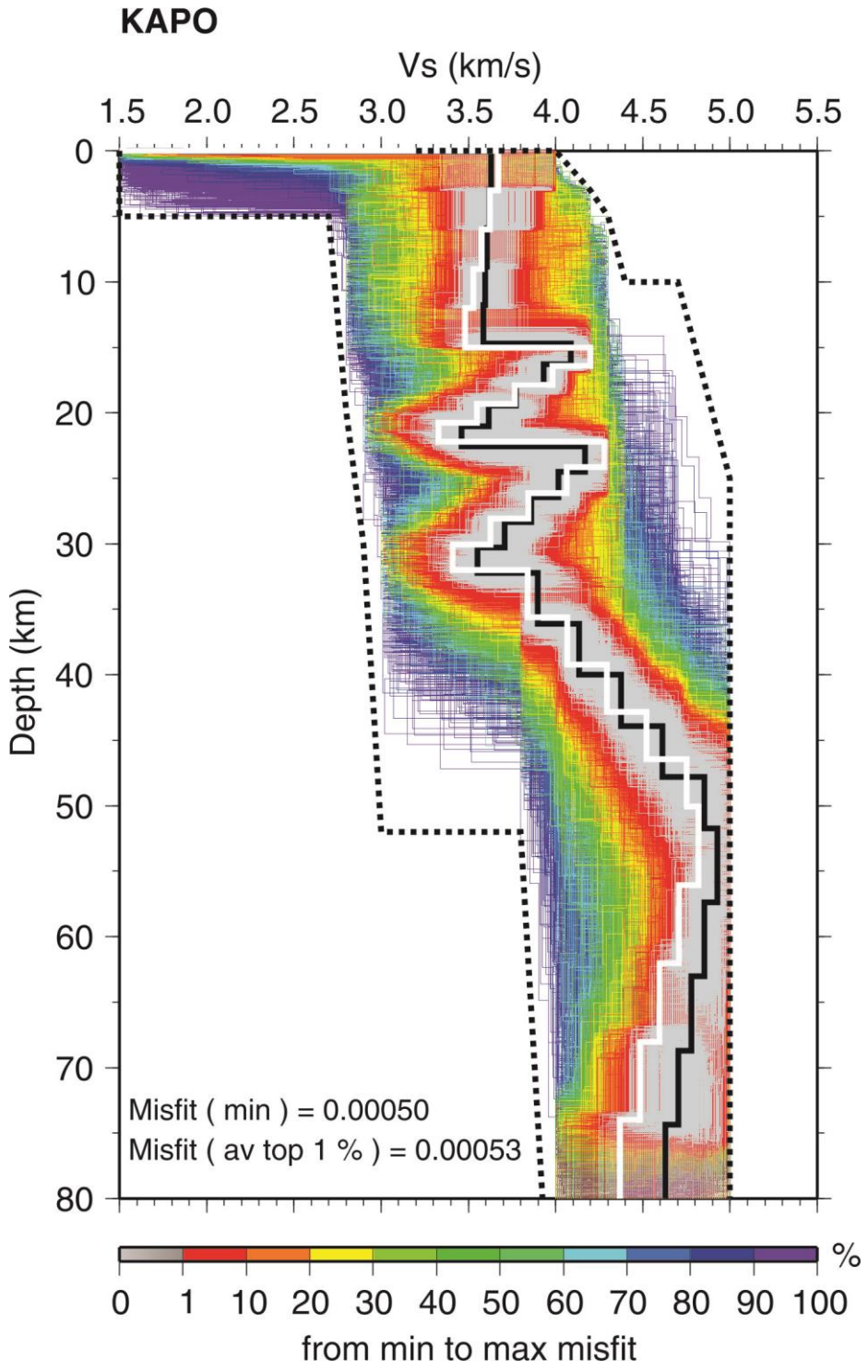
KAPO
Vs (km/s)
1.5 2.0 2.5 3.0 3.5 4.0 4.5 5.0 5.5
Depth (km)
0 10 20 30 40 50 60 70 80
Misfit (min) = 0.00050
Misfit (av top 1 %) = 0.00053
%
0 1 10 20 30 40 50 60 70 80 90 100
from min to max misfit

Figure 7a-i

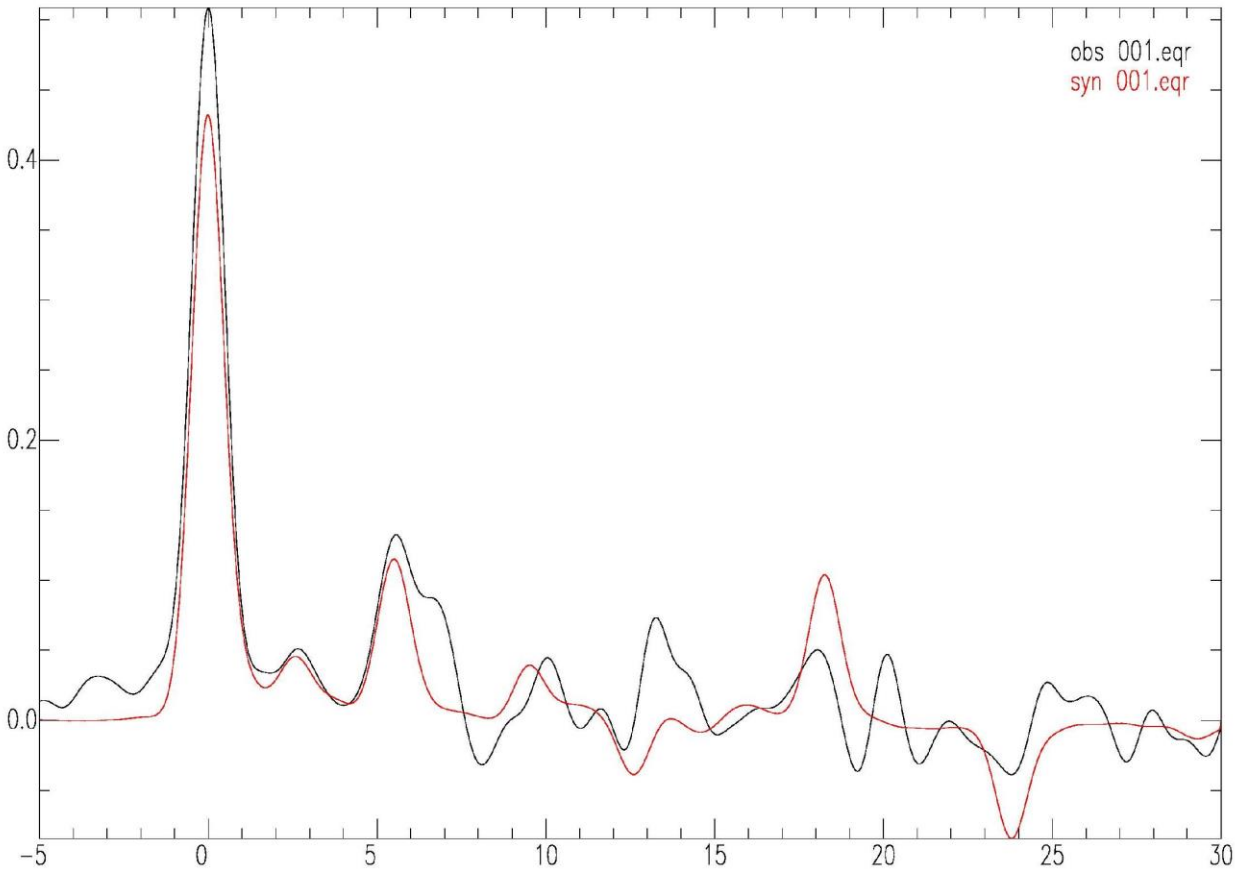

Figure 7a-ii (KAPO)

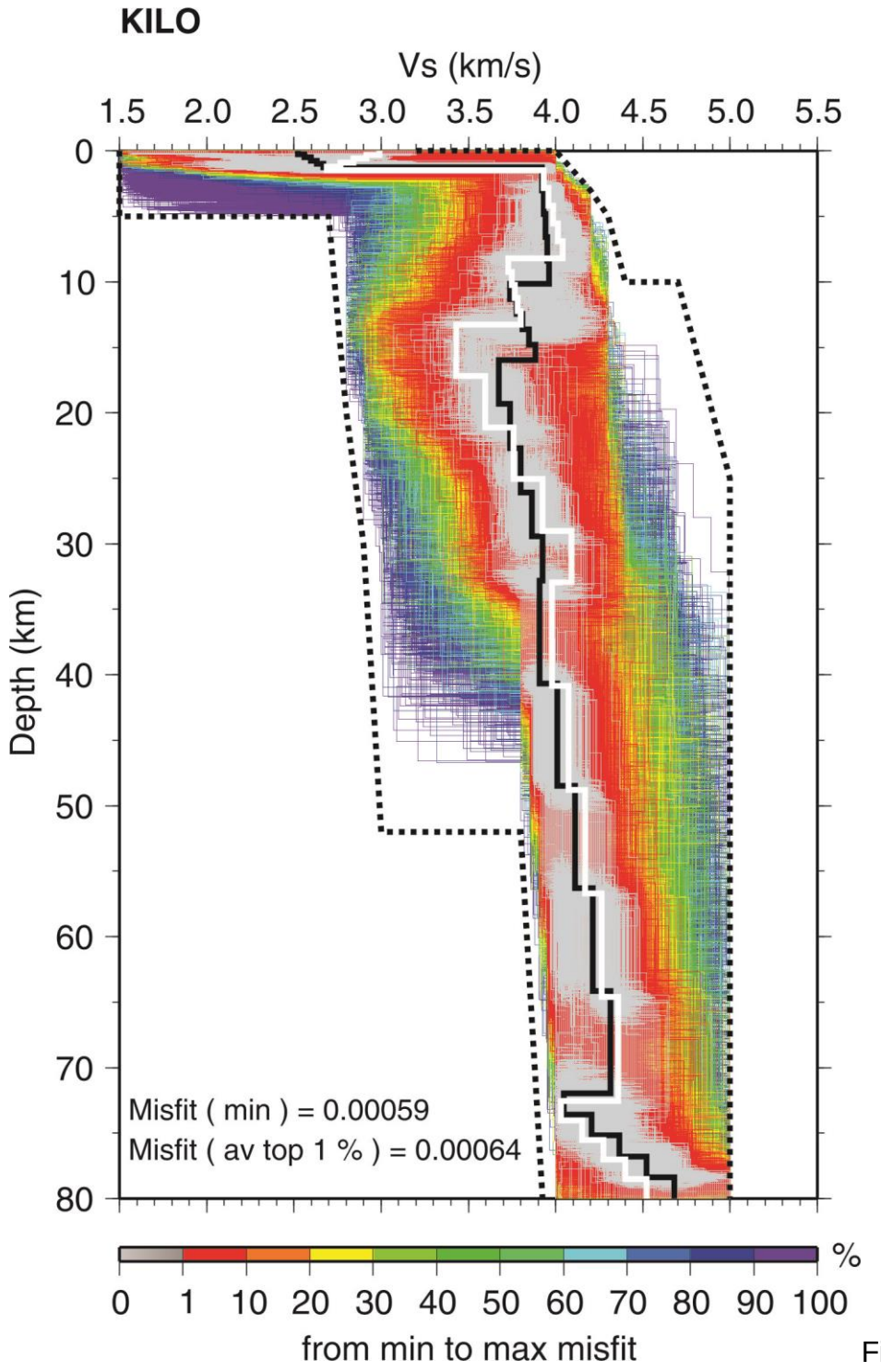
KILO
Vs (km/s)
1.5 2.0 2.5 3.0 3.5 4.0 4.5 5.0 5.5
Depth (km)
0 10 20 30 40 50 60 70 80
Misfit (min) = 0.00059
Misfit (av top 1 %) = 0.00064
%
0 1 10 20 30 40 50 60 70 80 90 100
from min to max misfit

Figure 7b-i

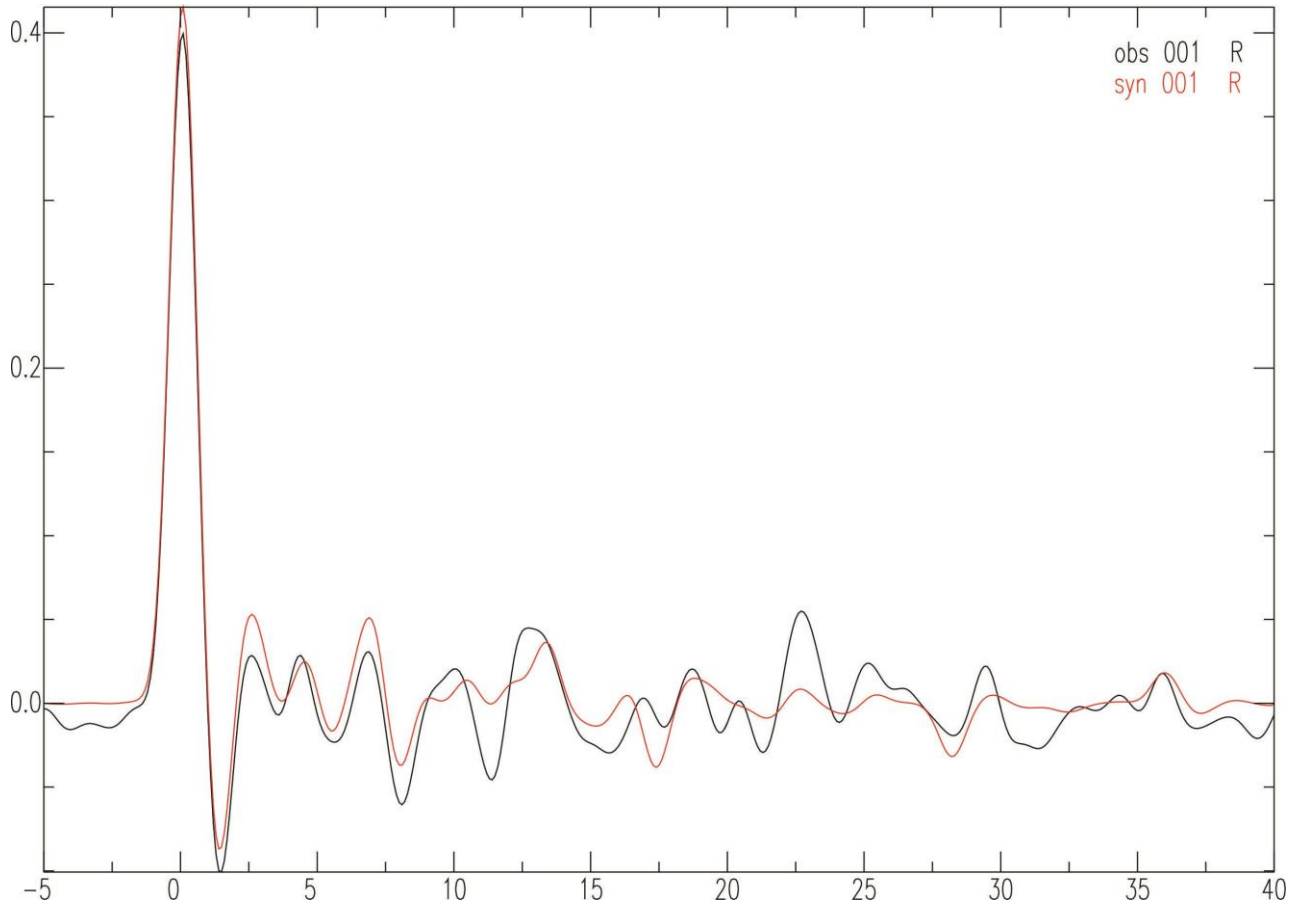

Figure 7b-ii (KILO)

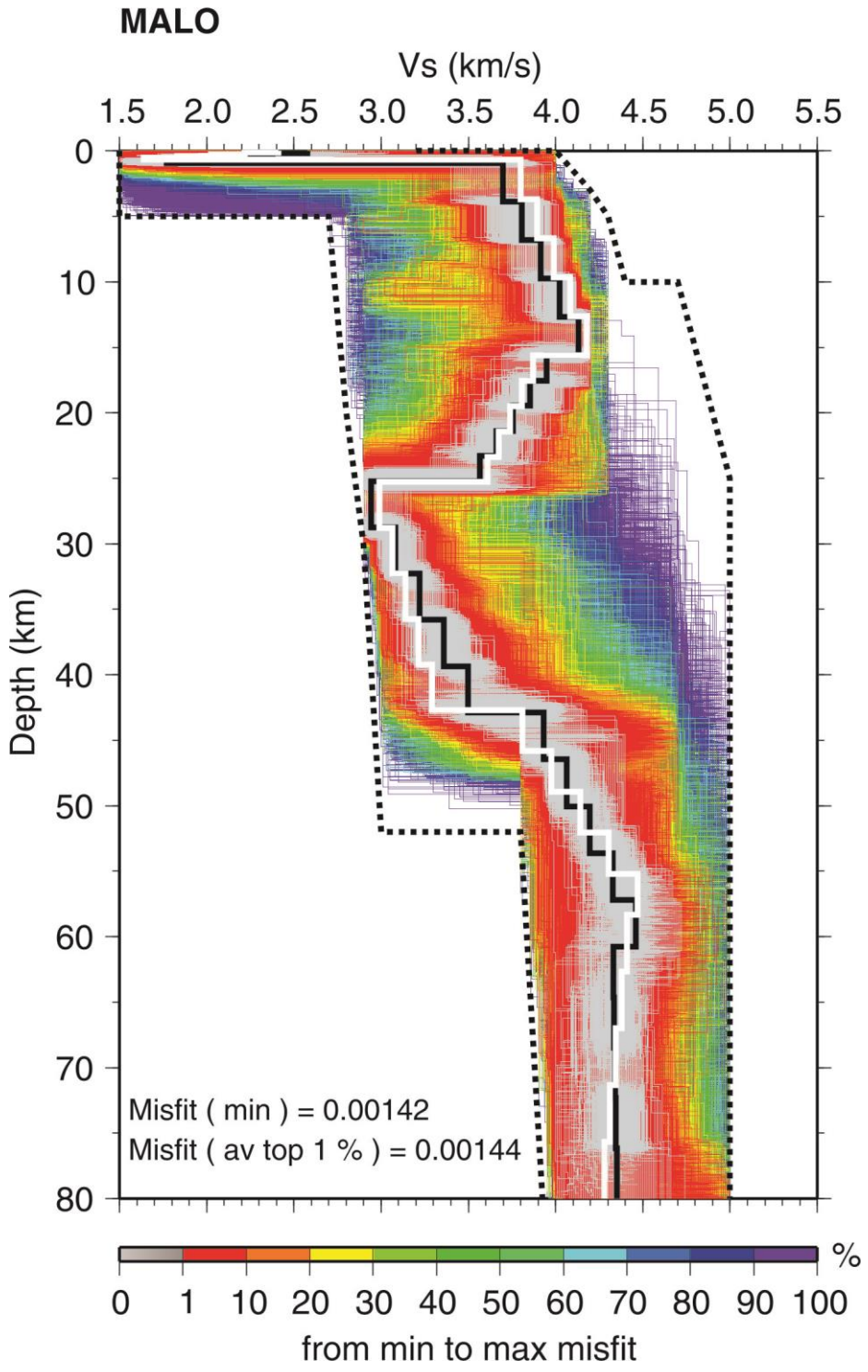
MALO
Vs (km/s)
1.5 2.0 2.5 3.0 3.5 4.0 4.5 5.0 5.5
Depth (km)
0 10 20 30 40 50 60 70 80
Misfit (min) = 0.00142
Misfit (av top 1 %) = 0.00144
%
0 1 10 20 30 40 50 60 70 80 90 100
from min to max misfit

Figure 7c-i

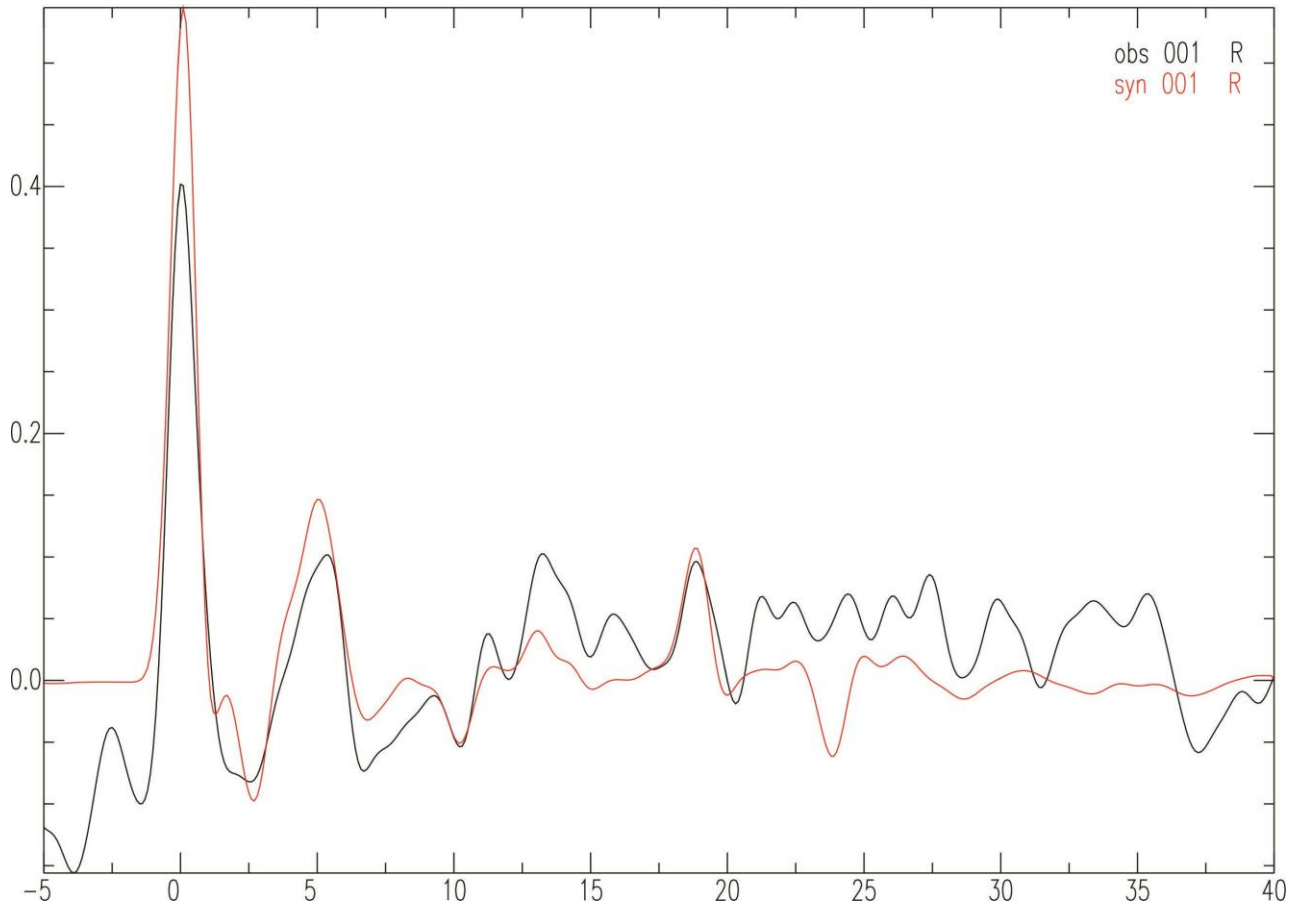

Figure 7c-ii (MALO)

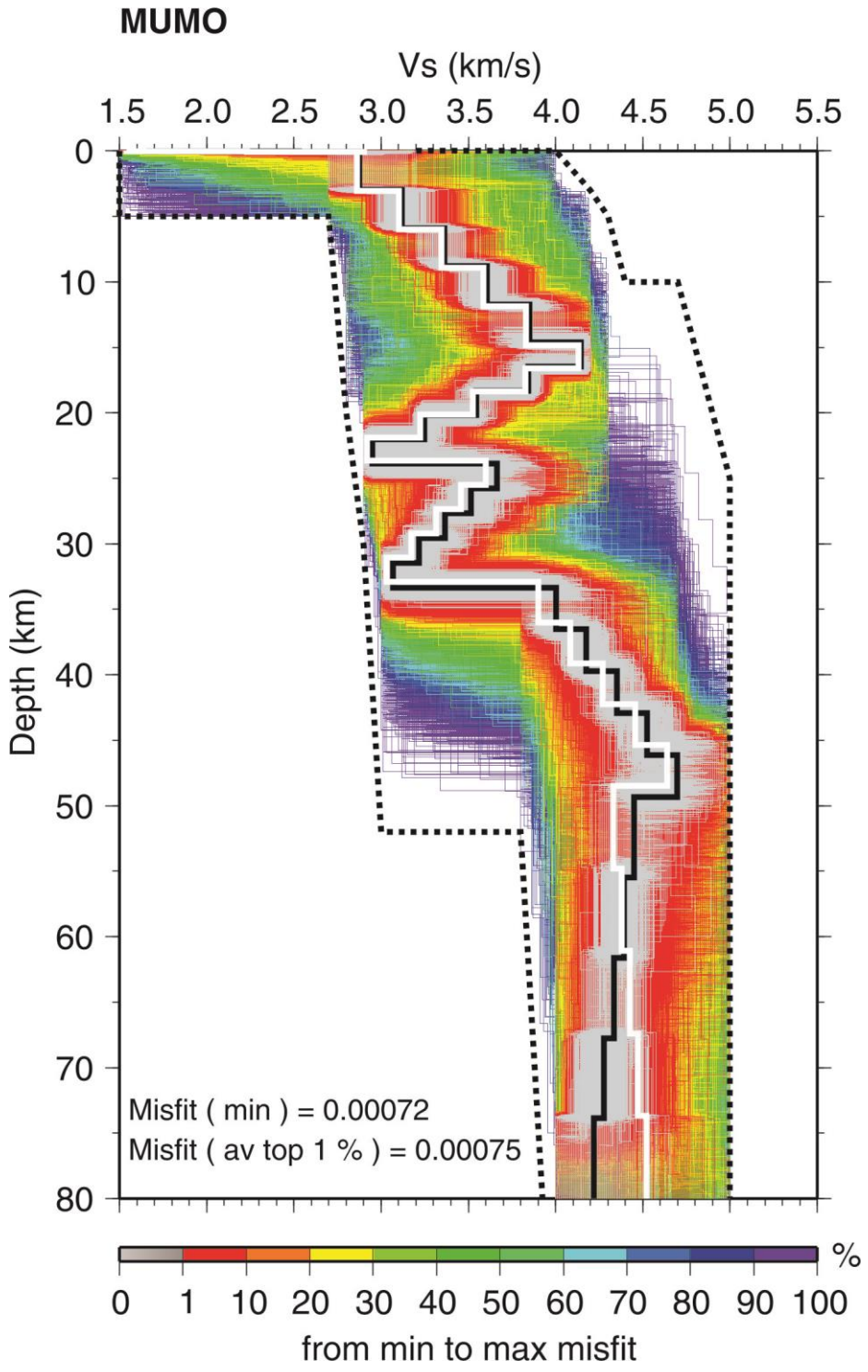
MUMO
Vs (km/s)
1.5 2.0 2.5 3.0 3.5 4.0 4.5 5.0 5.5
Depth (km)
0 10 20 30 40 50 60 70 80
Misfit (min) = 0.00072
Misfit (av top 1 %) = 0.00075
%
0 1 10 20 30 40 50 60 70 80 90 100
from min to max misfit

Figure 7d-i

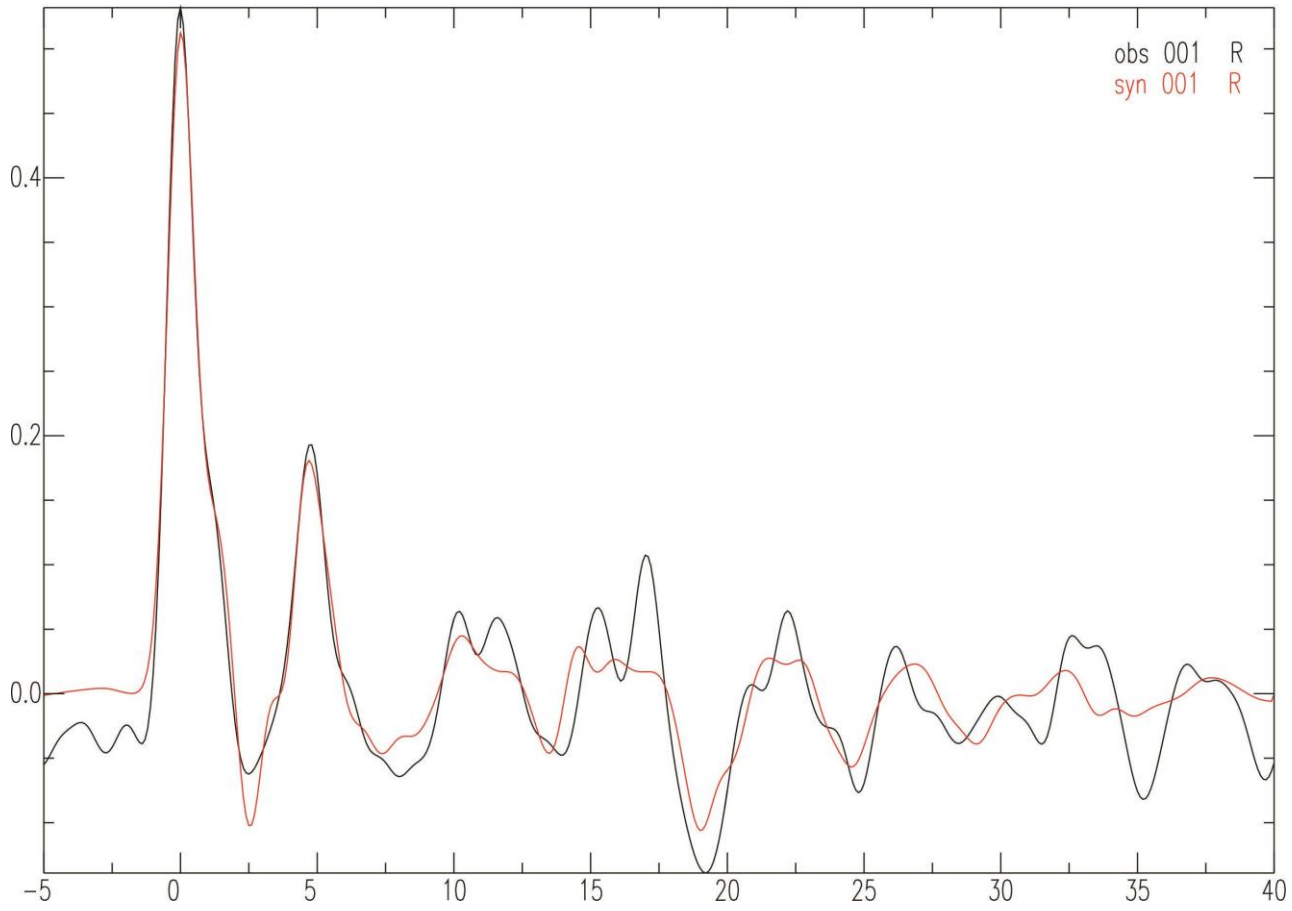

Figure 7d-ii (MUMO)

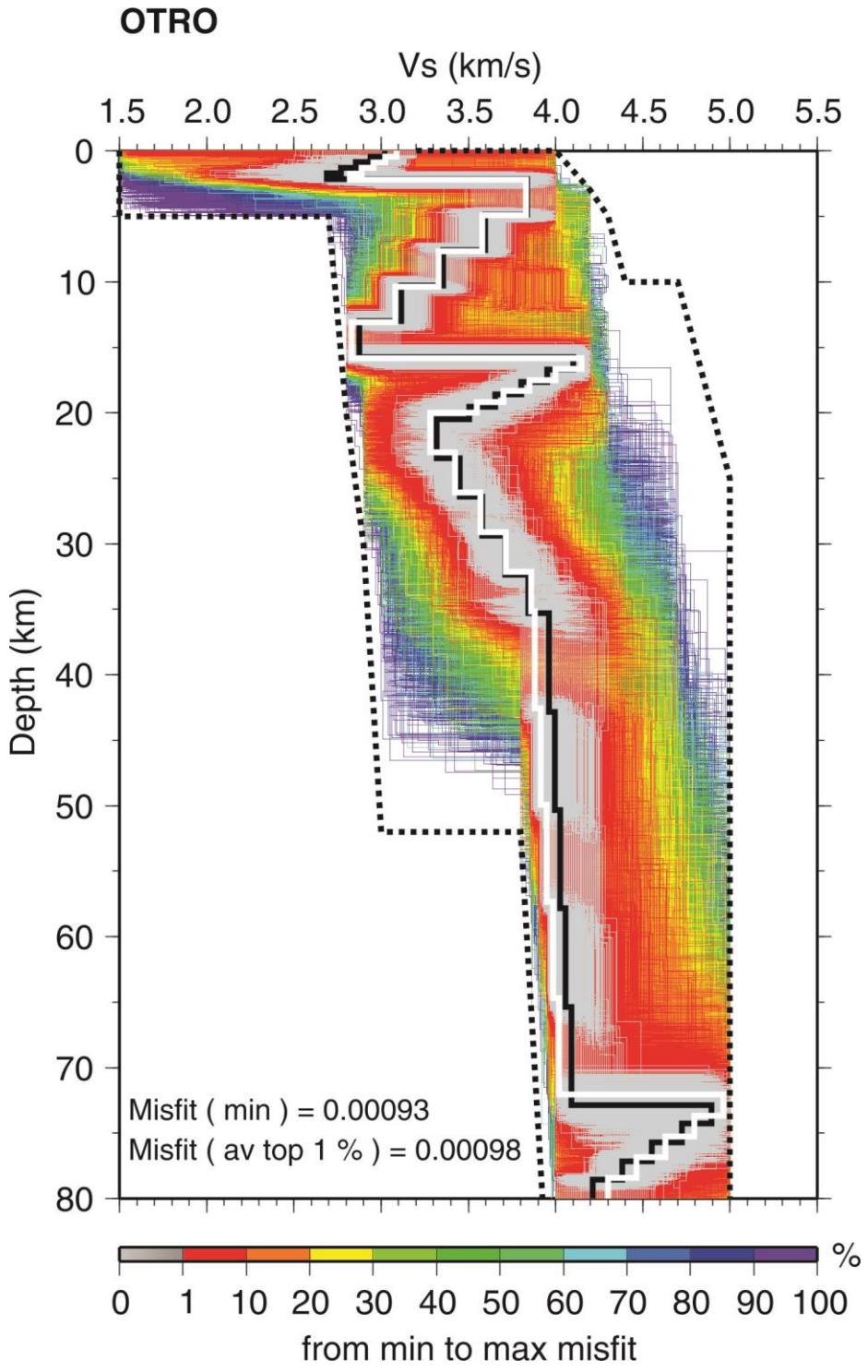
OTRO
Vs (km/s)
1.5 2.0 2.5 3.0 3.5 4.0 4.5 5.0 5.5
Depth (km)
0 10 20 30 40 50 60 70 80
Misfit (min) = 0.00093
Misfit (av top 1 %) = 0.00098
%
0 1 10 20 30 40 50 60 70 80 90 100
from min to max misfit

Figure 7e-i

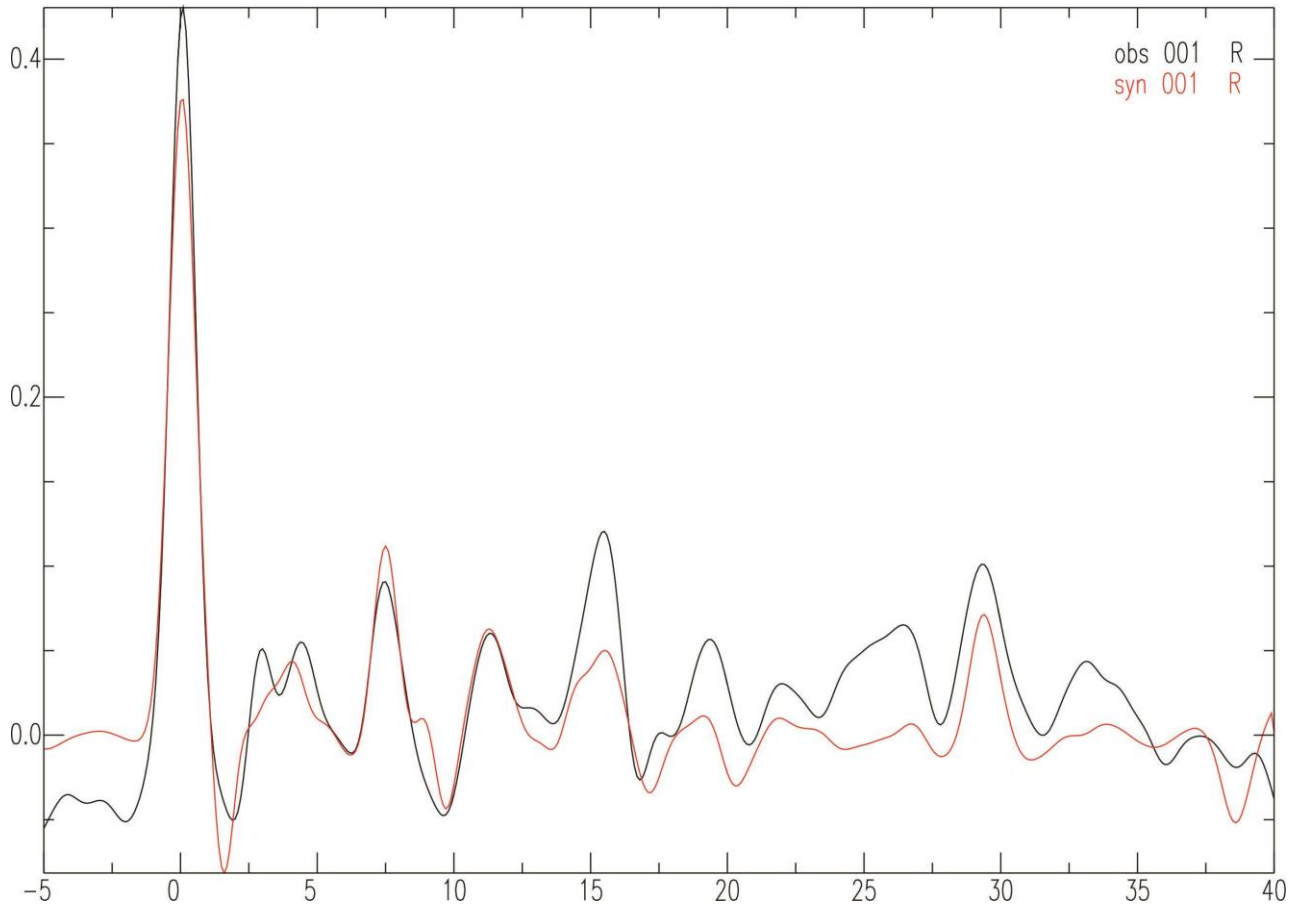

Figure 7e-ii (OTRO)

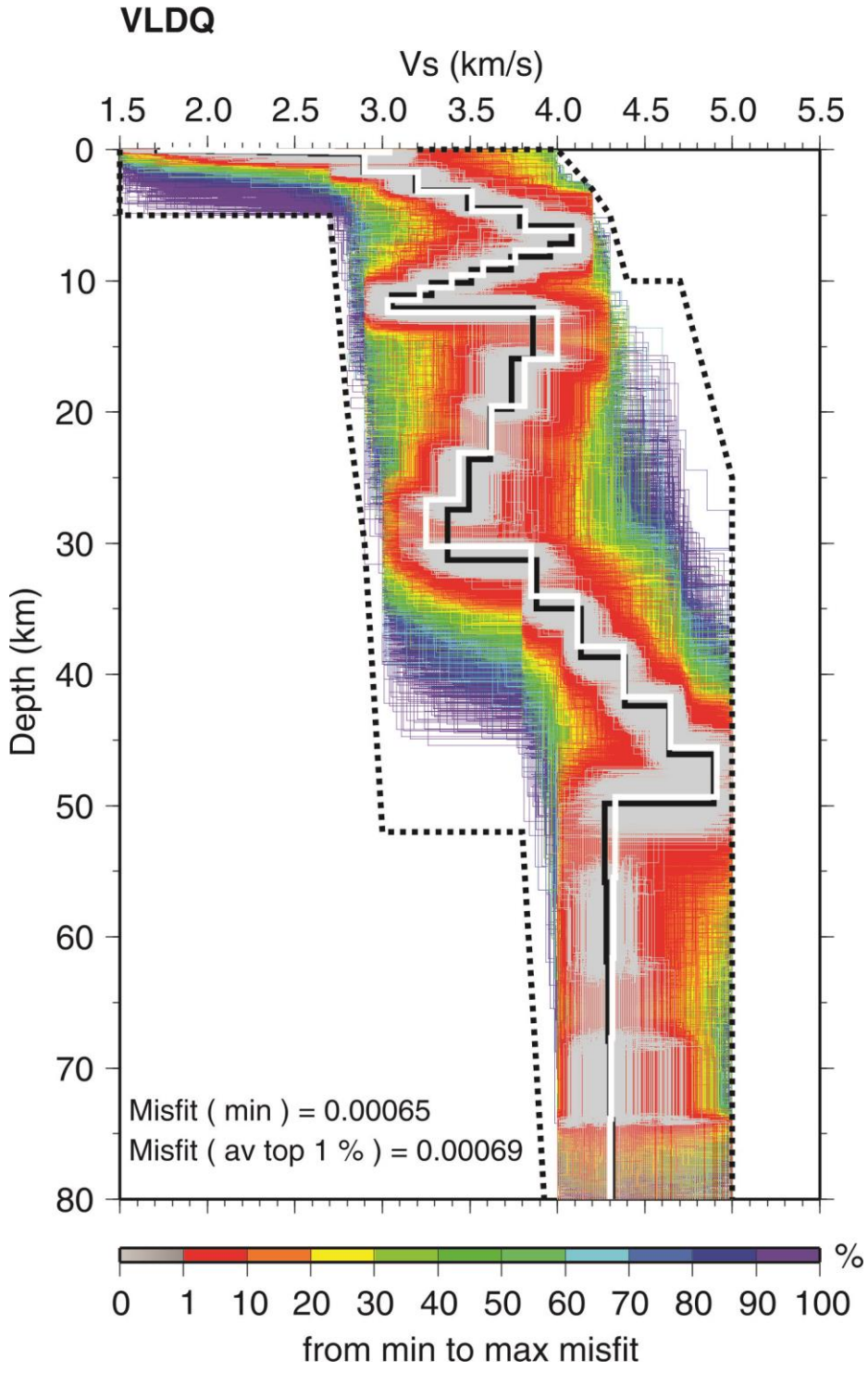
VLDQ
Vs (km/s)
1.5 2.0 2.5 3.0 3.5 4.0 4.5 5.0 5.5
Depth (km)
0 10 20 30 40 50 60 70 80
Misfit (min) = 0.00065
Misfit (av top 1 %) = 0.00069
%
0 1 10 20 30 40 50 60 70 80 90 100
from min to max misfit

Figure 7f-i

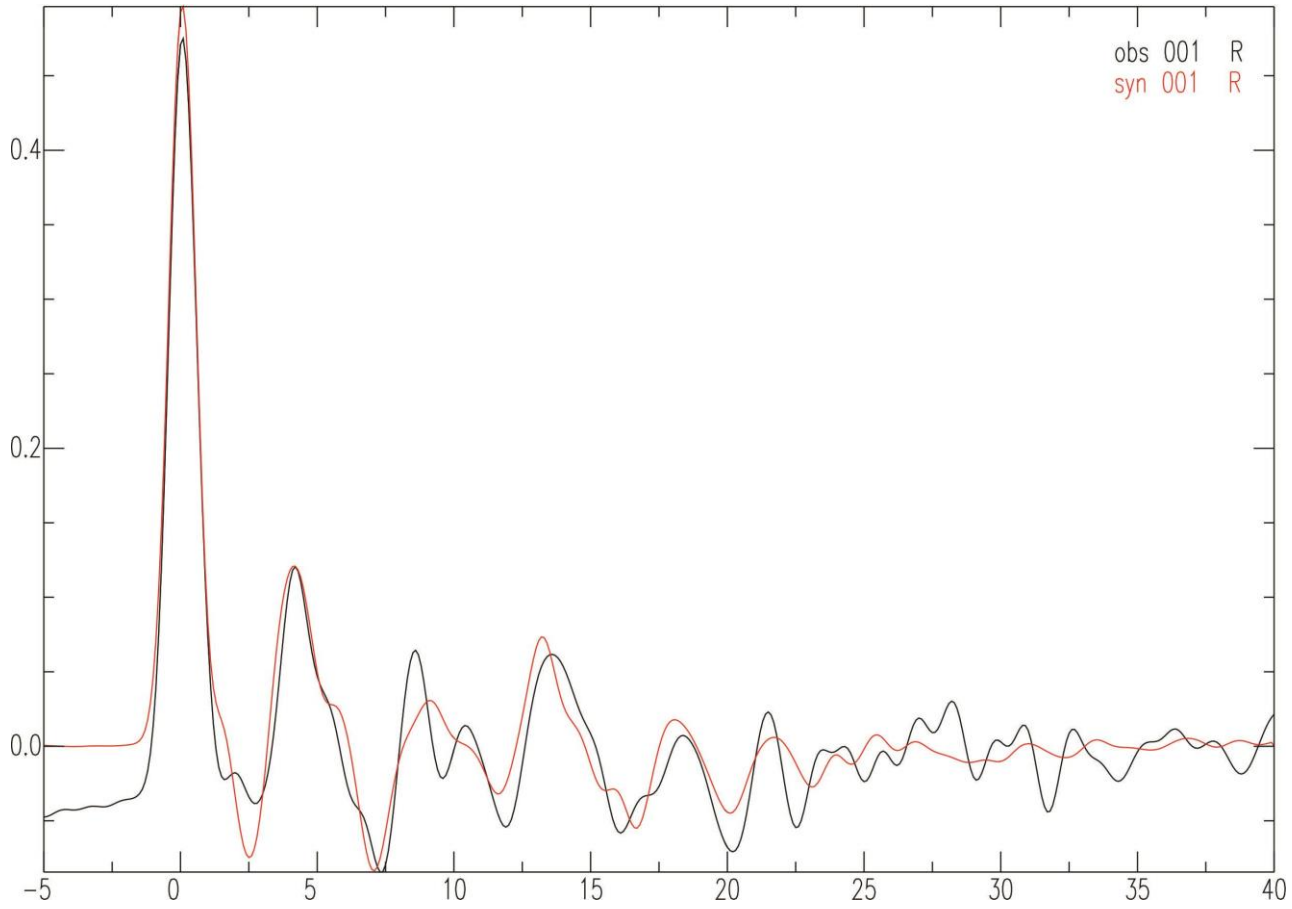

Figure 7f-ii (VLDQ)

Figure 7. Structural models and receiver functions for stations in the Superior Province: a) KAPO, b) KILO, c) MALO, d) MUMO, e) OTRO and f) VLDQ. Format the same as for Figure 3.

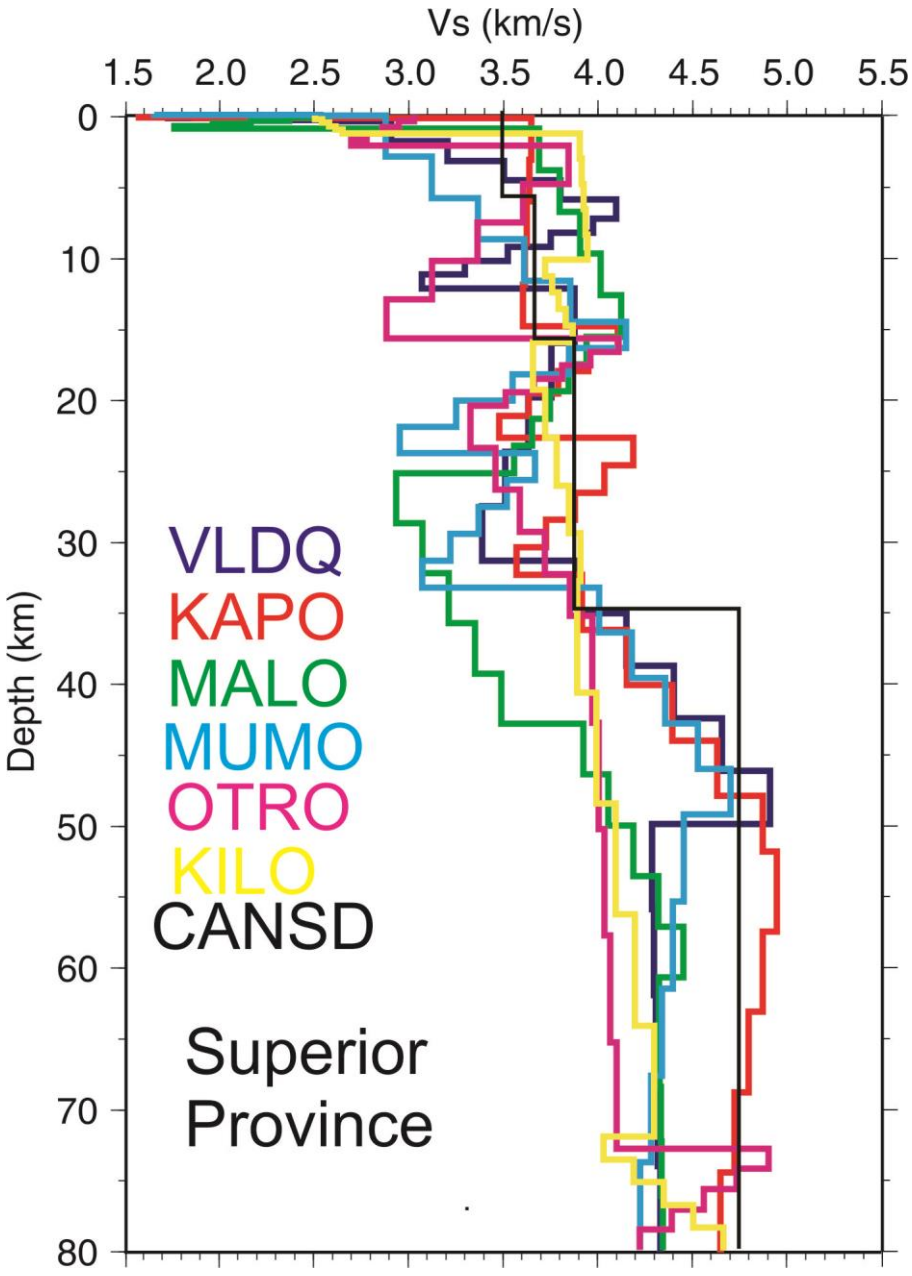

Figure 8: Preferred shear wave velocity models for stations in the Superior Province.

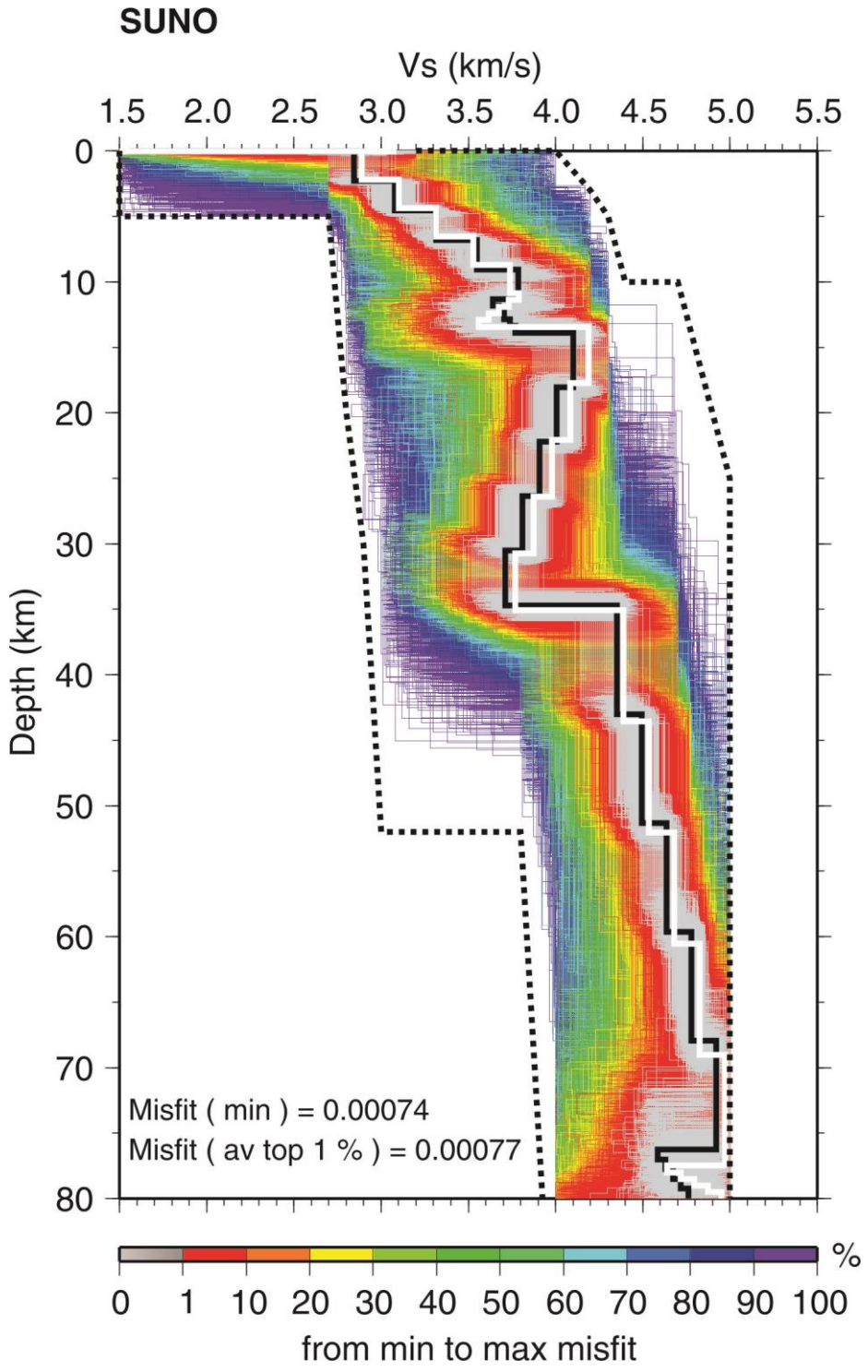
SUNO
Vs (km/s)
1.5 2.0 2.5 3.0 3.5 4.0 4.5 5.0 5.5
Depth (km)
0 10 20 30 40 50 60 70 80
Misfit (min) = 0.00074
Misfit (av top 1 %) = 0.00077
%
0 1 10 20 30 40 50 60 70 80 90 100
from min to max misfit

Figure 9-i

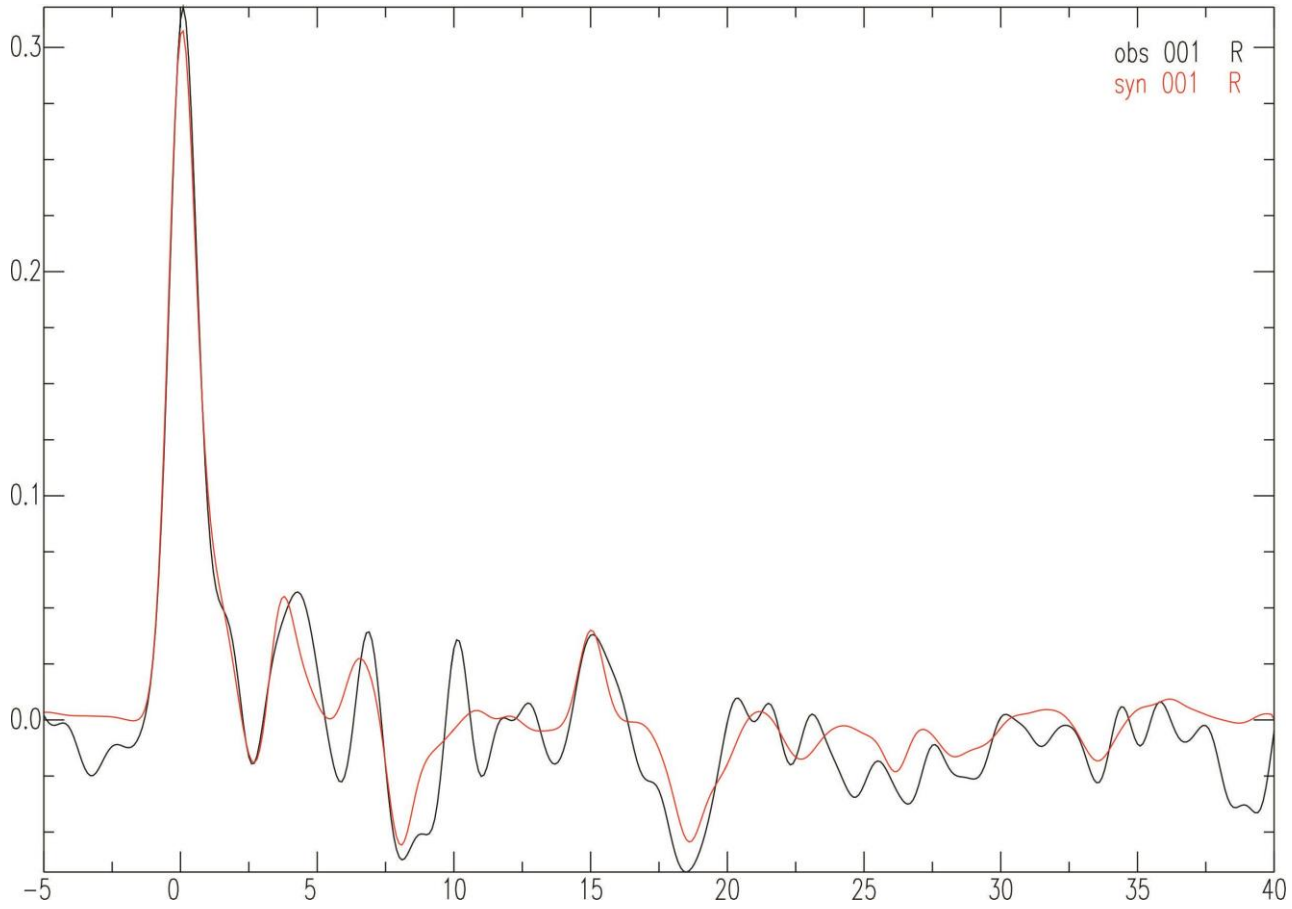

Figure 9-ii

Figure 9. Structural models and receiver function for station SUNO in the Southern Province. Format the same as for Figure 3.

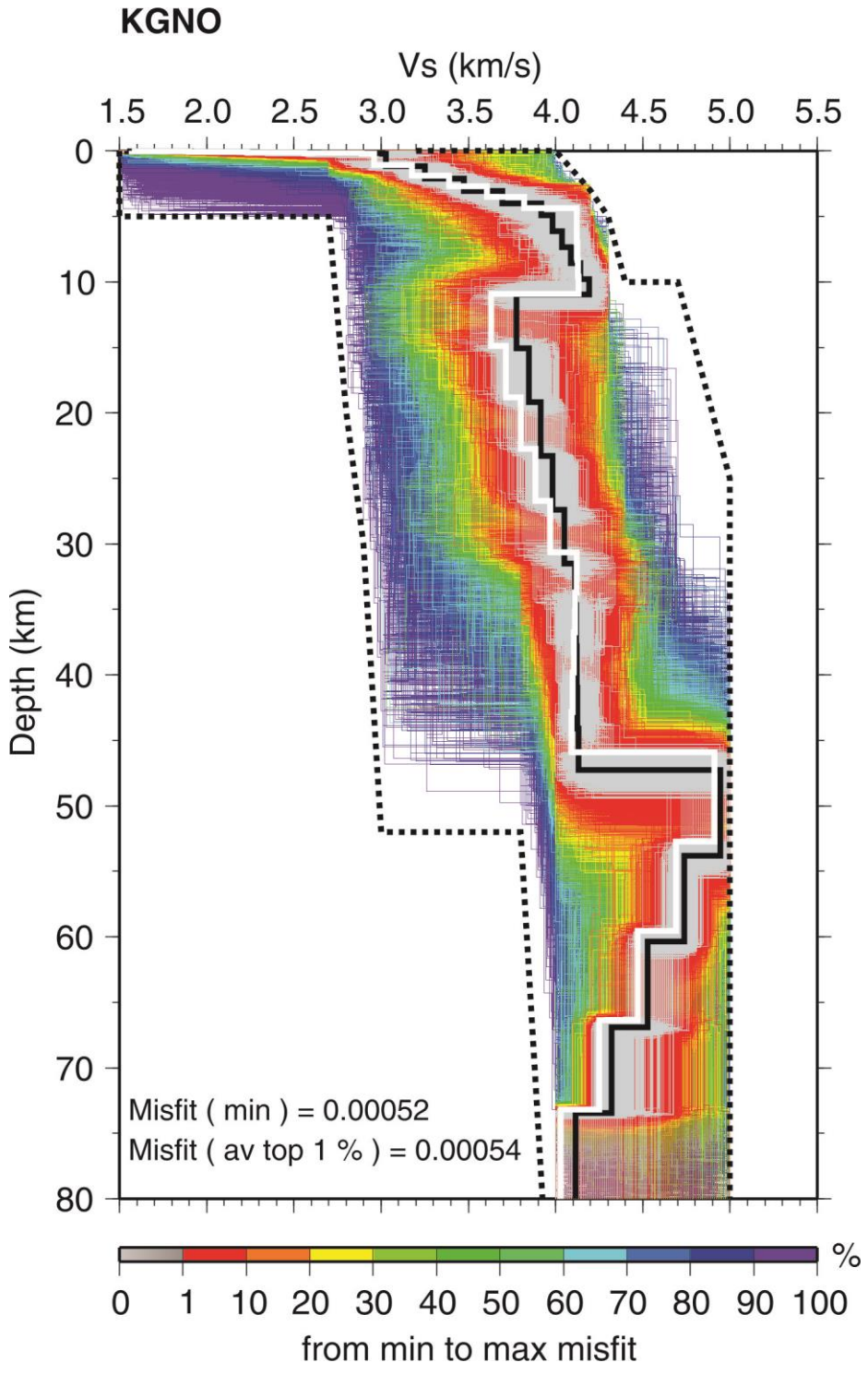
KGNO
Vs (km/s)
1.5 2.0 2.5 3.0 3.5 4.0 4.5 5.0 5.5
Depth (km)
0 10 20 30 40 50 60 70 80
Misfit (min) = 0.00052
Misfit (av top 1 %) = 0.00054
%
0 1 10 20 30 40 50 60 70 80 90 100
from min to max misfit

Figure10a-i

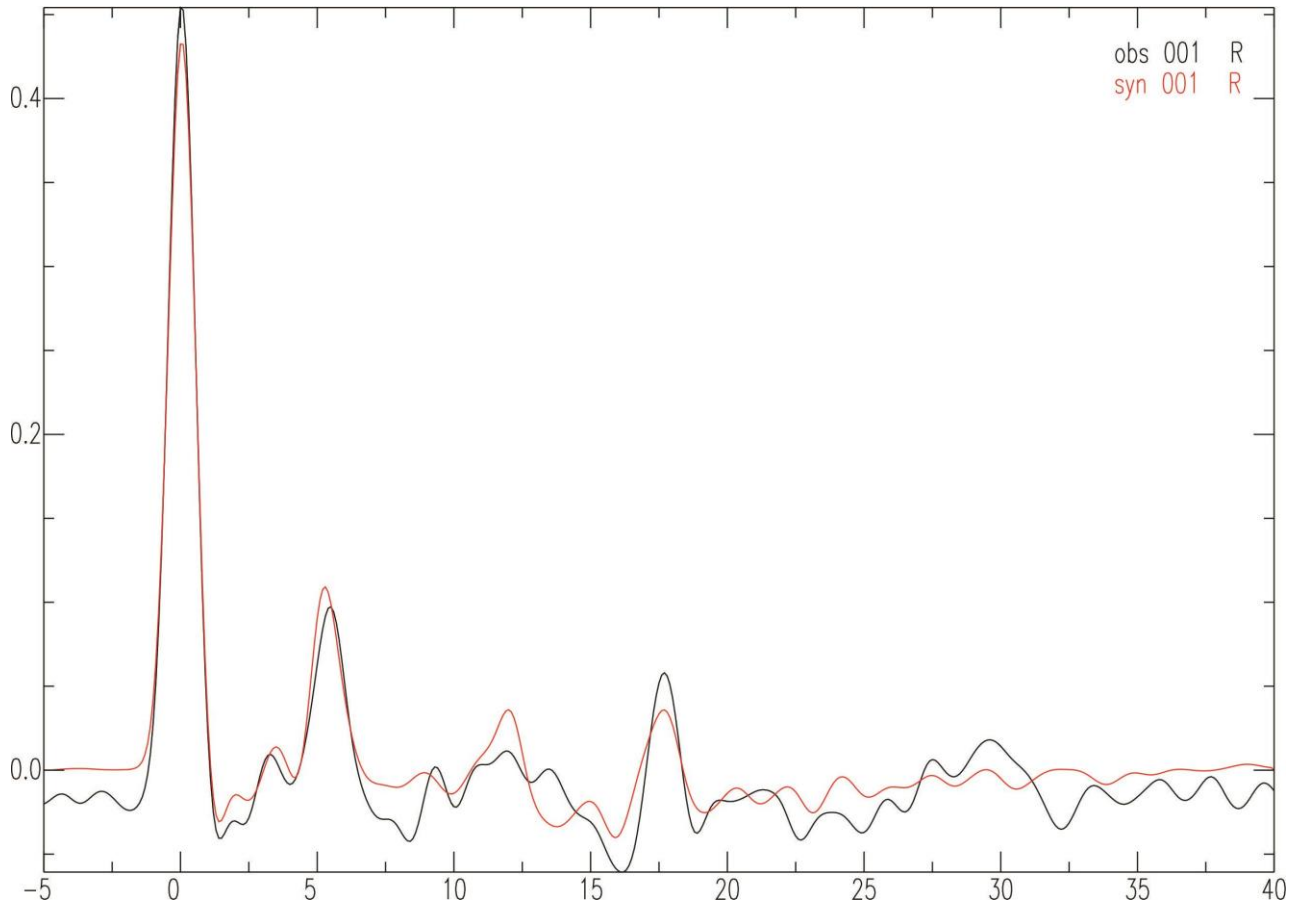

Figure 10a-ii (KGNO)

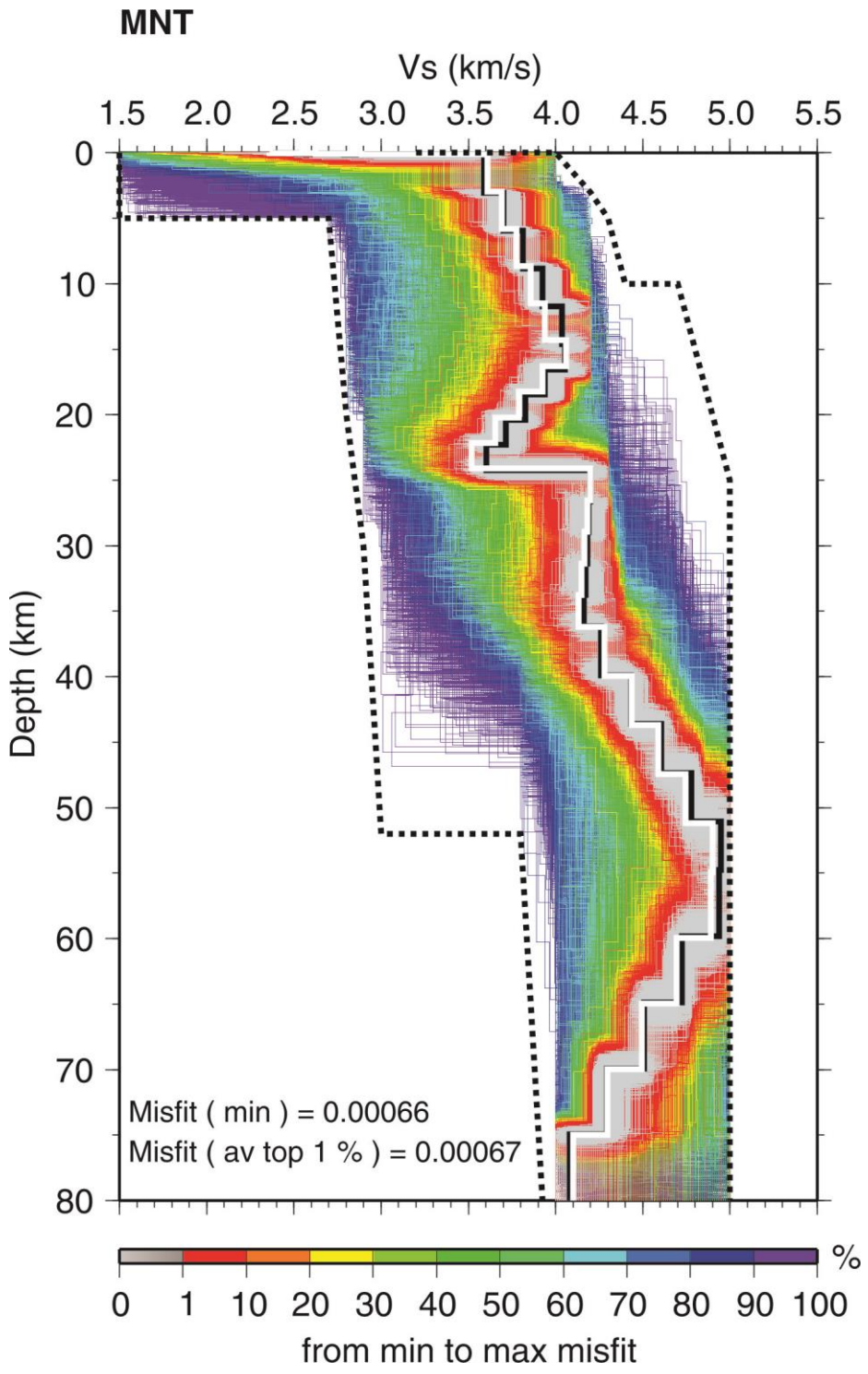
MNT
Vs (km/s)
1.5 2.0 2.5 3.0 3.5 4.0 4.5 5.0 5.5
Depth (km)
0 10 20 30 40 50 60 70 80
Misfit (min) = 0.00066
Misfit (av top 1 %) = 0.00067
%
0 1 10 20 30 40 50 60 70 80 90 100
from min to max misfit

Figure 10b-i

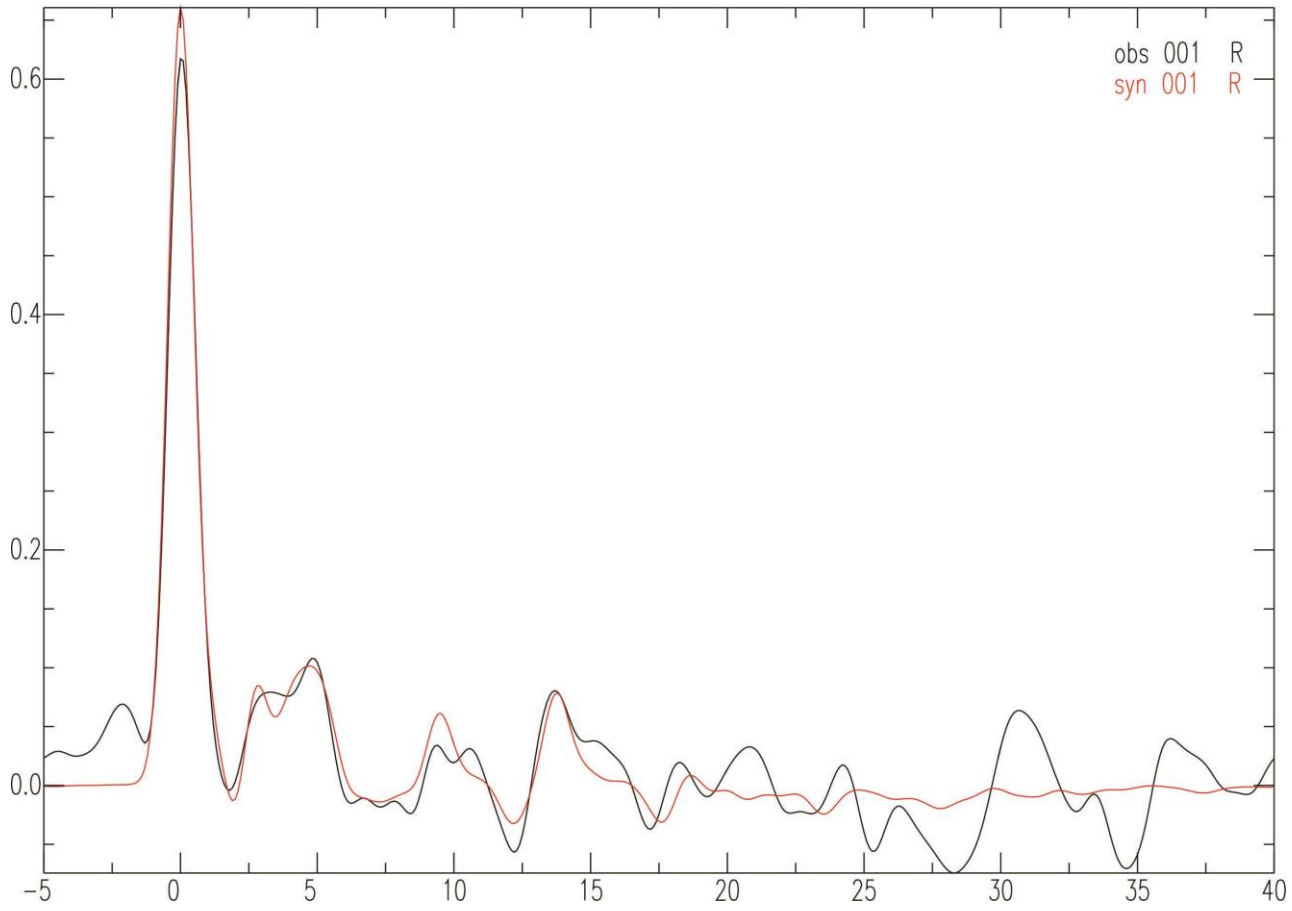

Figure 10b-ii (MNT)

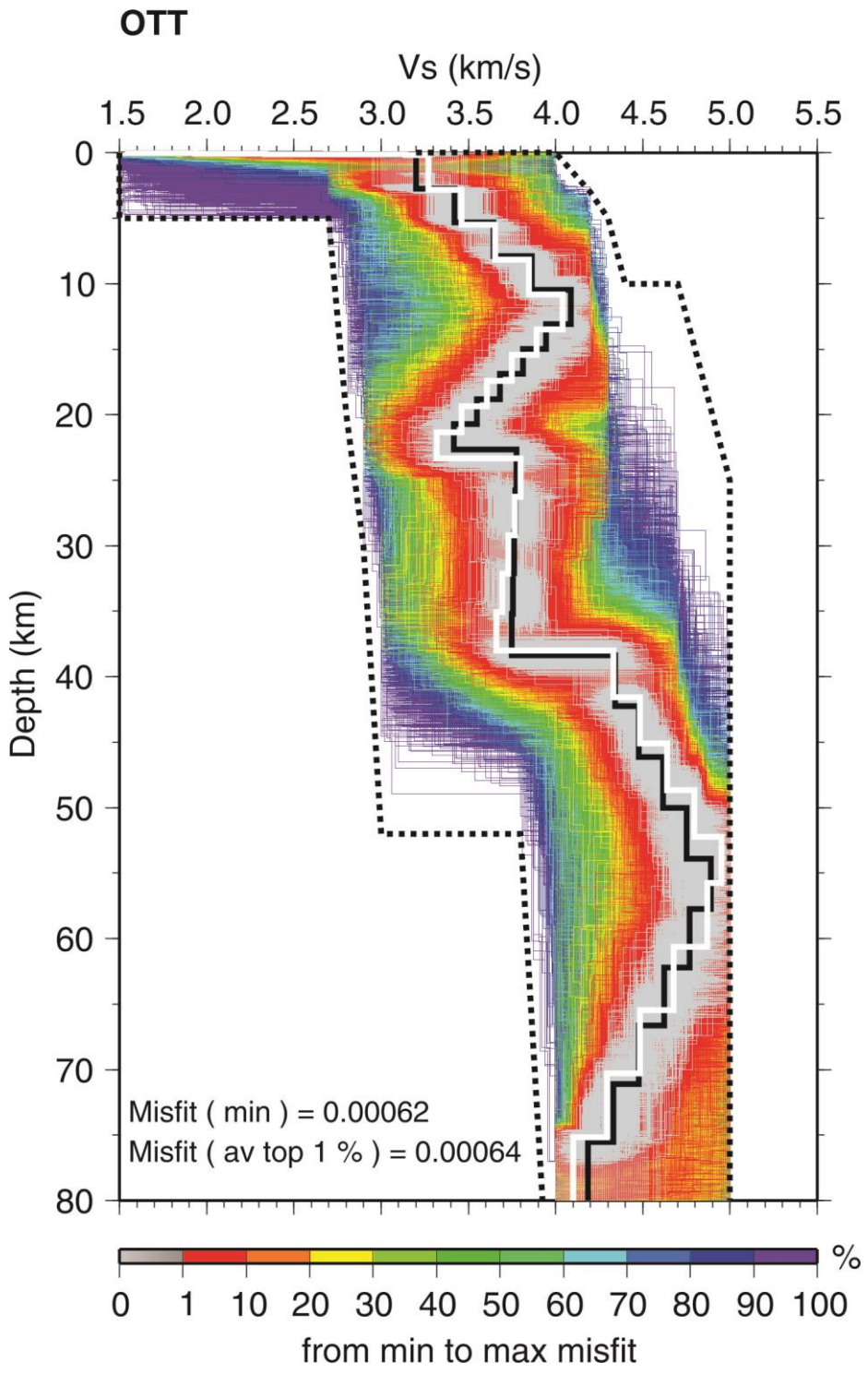
OTT
Vs (km/s)
1.5 2.0 2.5 3.0 3.5 4.0 4.5 5.0 5.5
Depth (km)
0 10 20 30 40 50 60 70 80
Misfit (min) = 0.00062
Misfit (av top 1 %) = 0.00064
%
0 1 10 20 30 40 50 60 70 80 90 100
from min to max misfit

Figure 10c-i

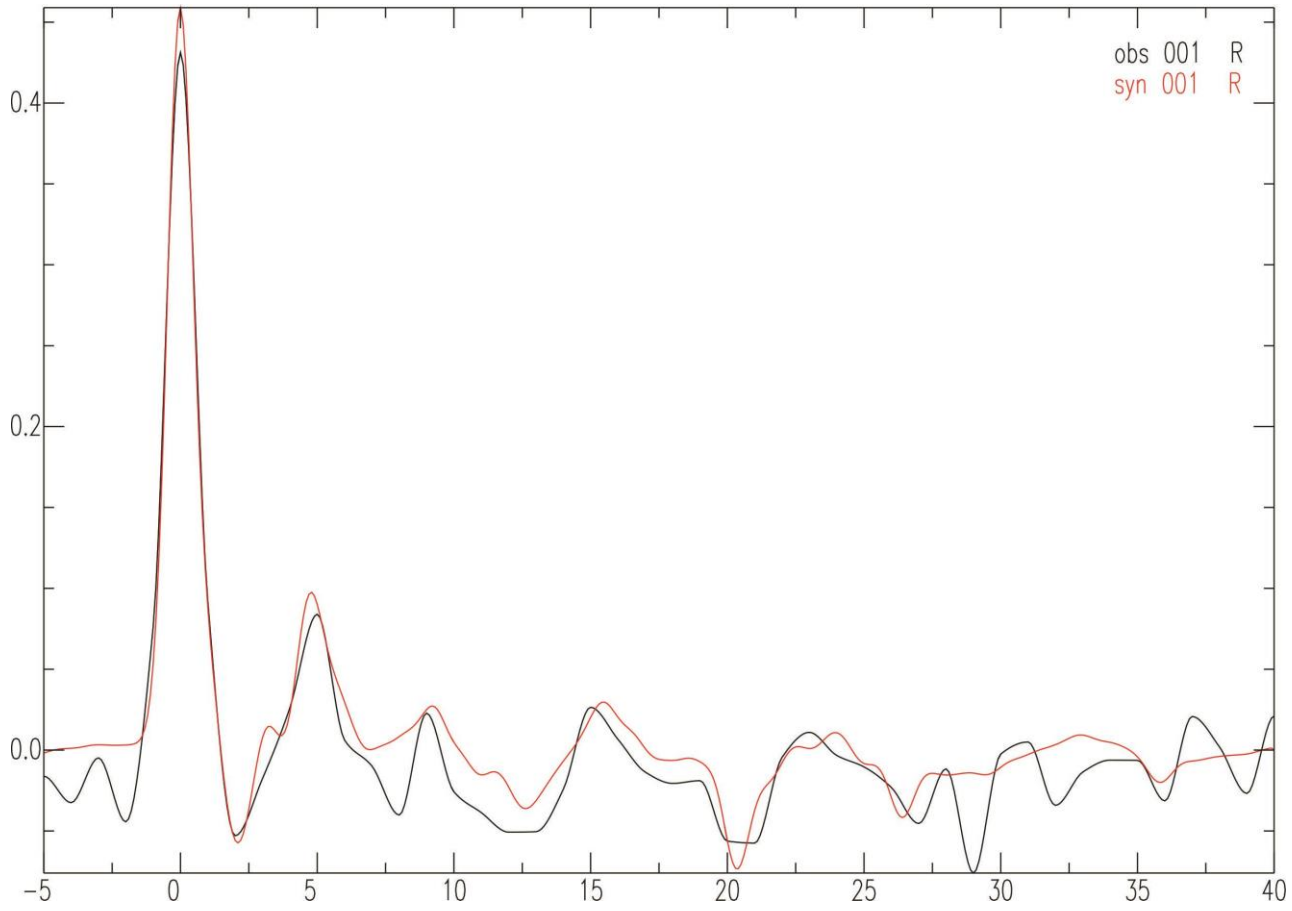

Figure 10c-ii (OTT)

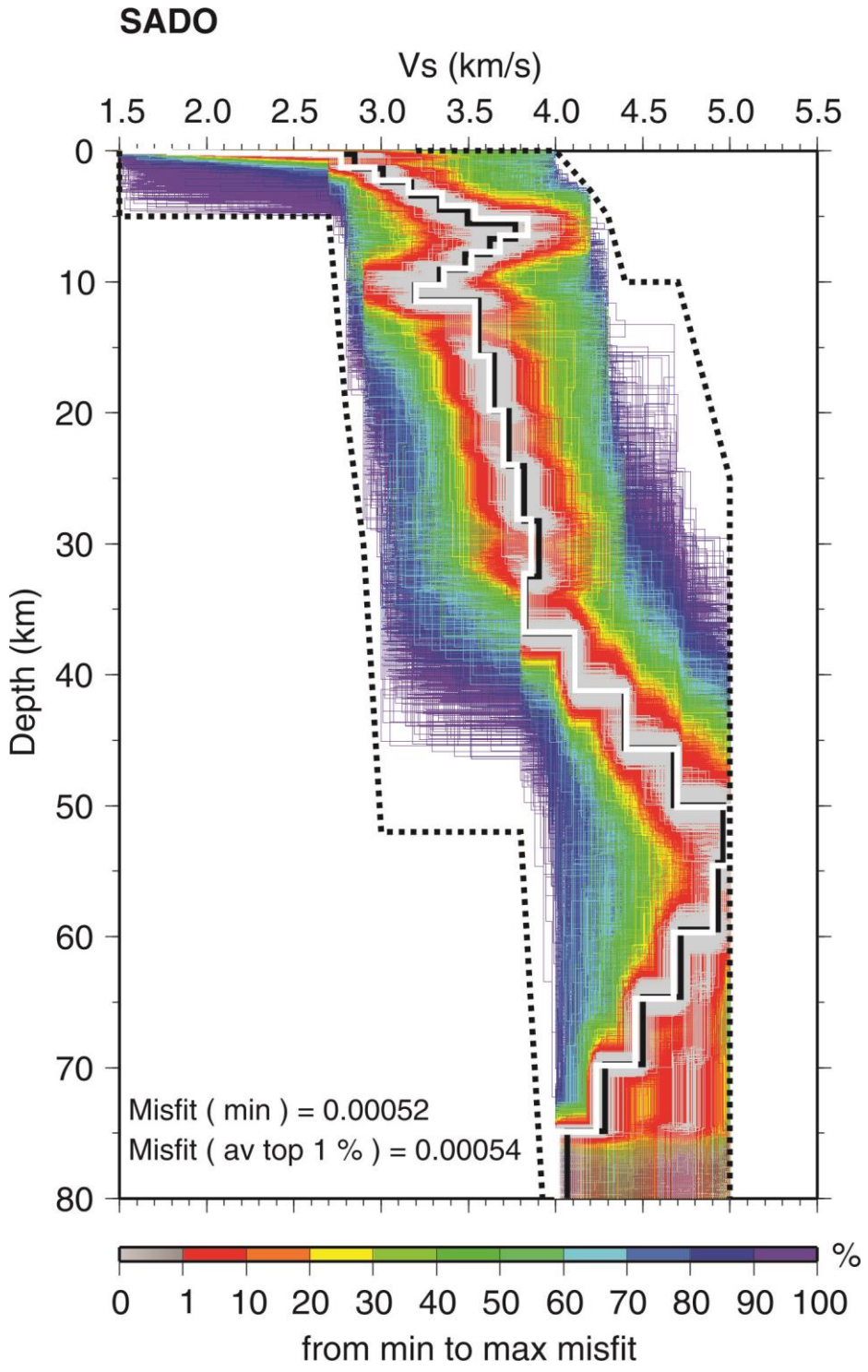
SADO
Vs (km/s)
1.5 2.0 2.5 3.0 3.5 4.0 4.5 5.0 5.5
Depth (km)
0 10 20 30 40 50 60 70 80
Misfit (min) = 0.00052
Misfit (av top 1 %) = 0.00054
%
0 1 10 20 30 40 50 60 70 80 90 100
from min to max misfit

Figure 10d-i

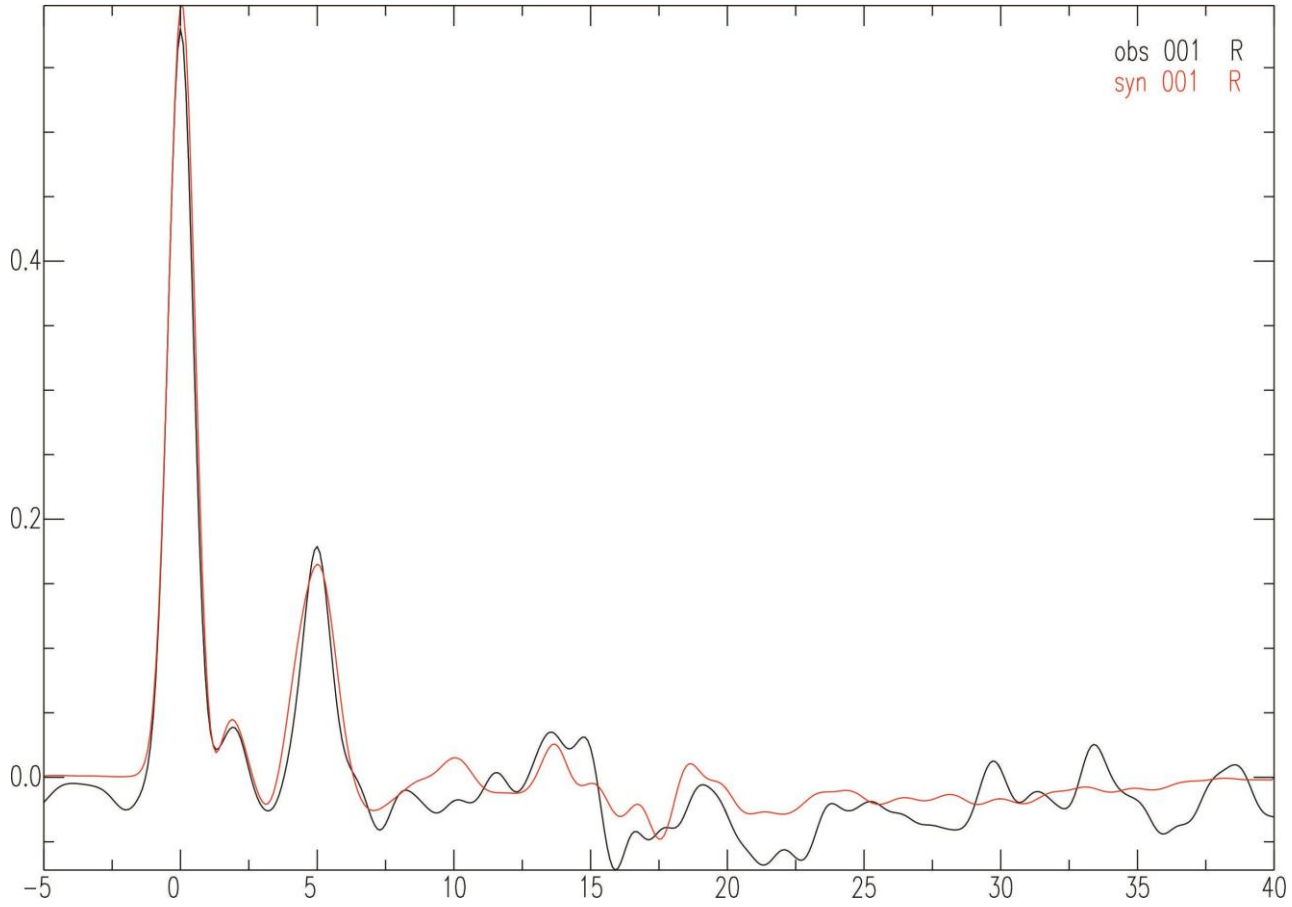

Figure 10d-ii (SADO)

Figure 10. Structural models and receiver functions for stations in the St. Lawrence Platform: a) KGNO, b) MNT, c) OTT and d) SADO. Format the same as for Figure 3.

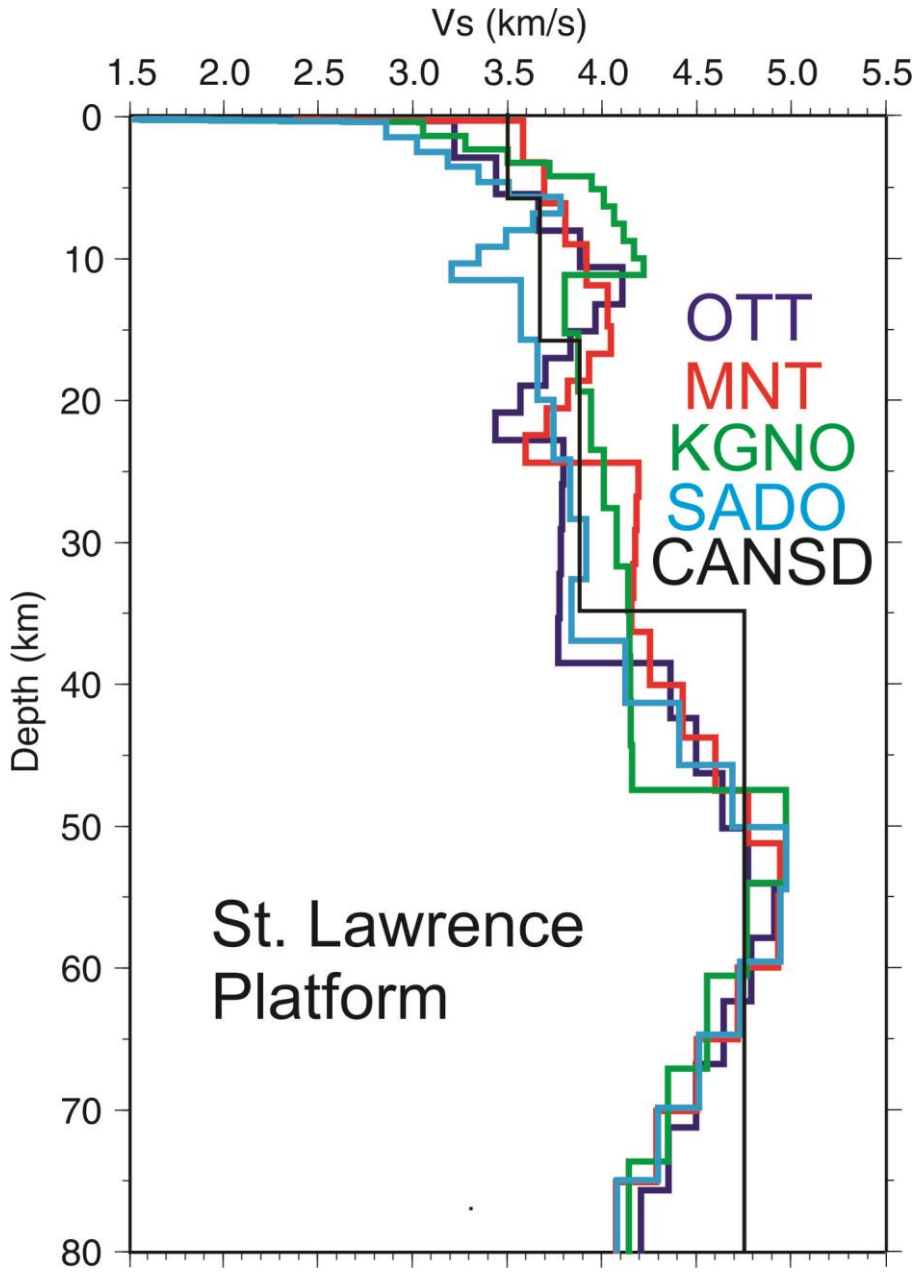

Figure 11. Preferred shear wave velocity models for stations in the St. Lawrence Platform.

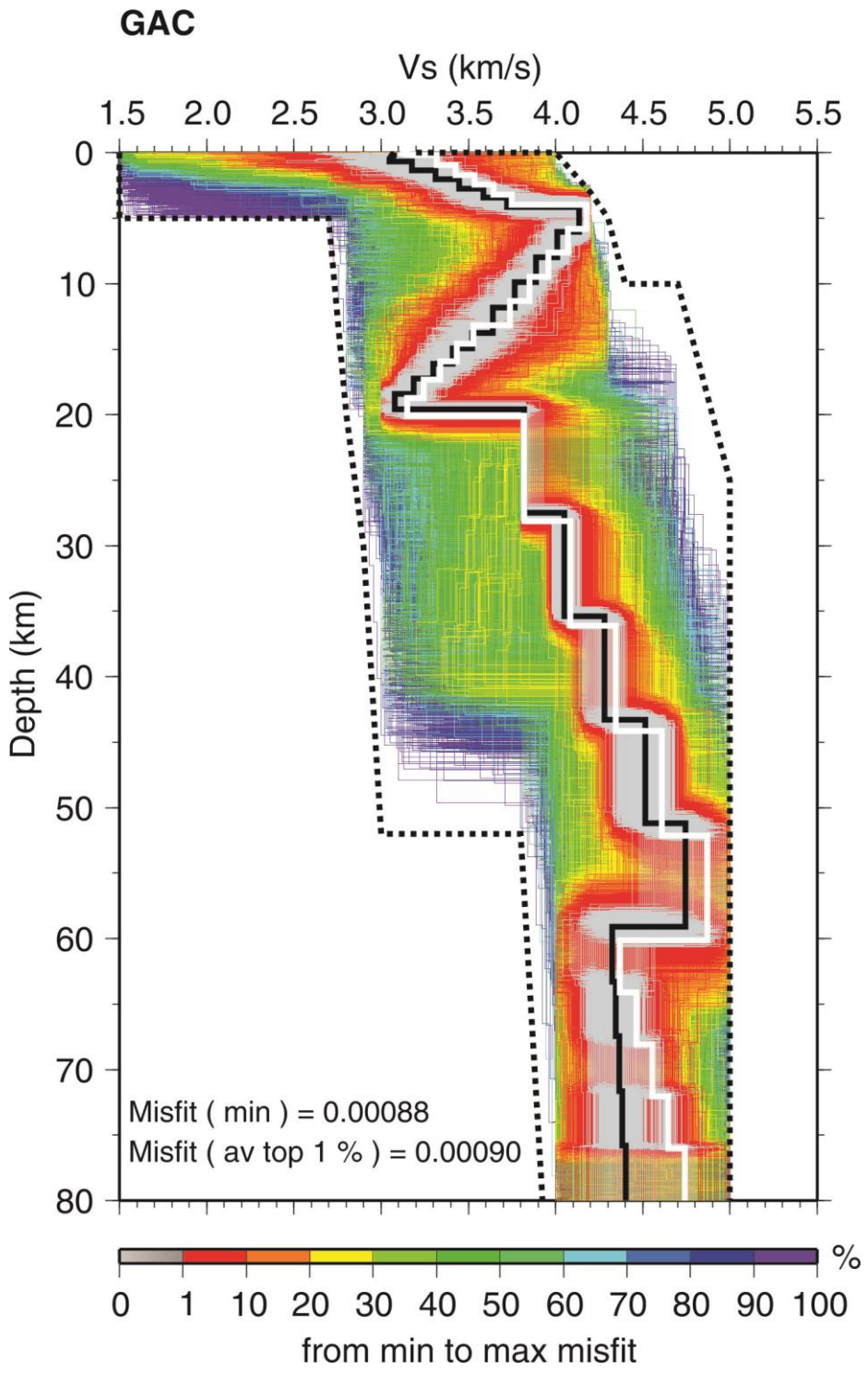
GAC
Vs (km/s)
1.5 2.0 2.5 3.0 3.5 4.0 4.5 5.0 5.5
Depth (km)
0 10 20 30 40 50 60 70 80
Misfit (min) = 0.00088
Misfit (av top 1 %) = 0.00090
%
0 1 10 20 30 40 50 60 70 80 90 100
from min to max misfit

Figure 12a-i

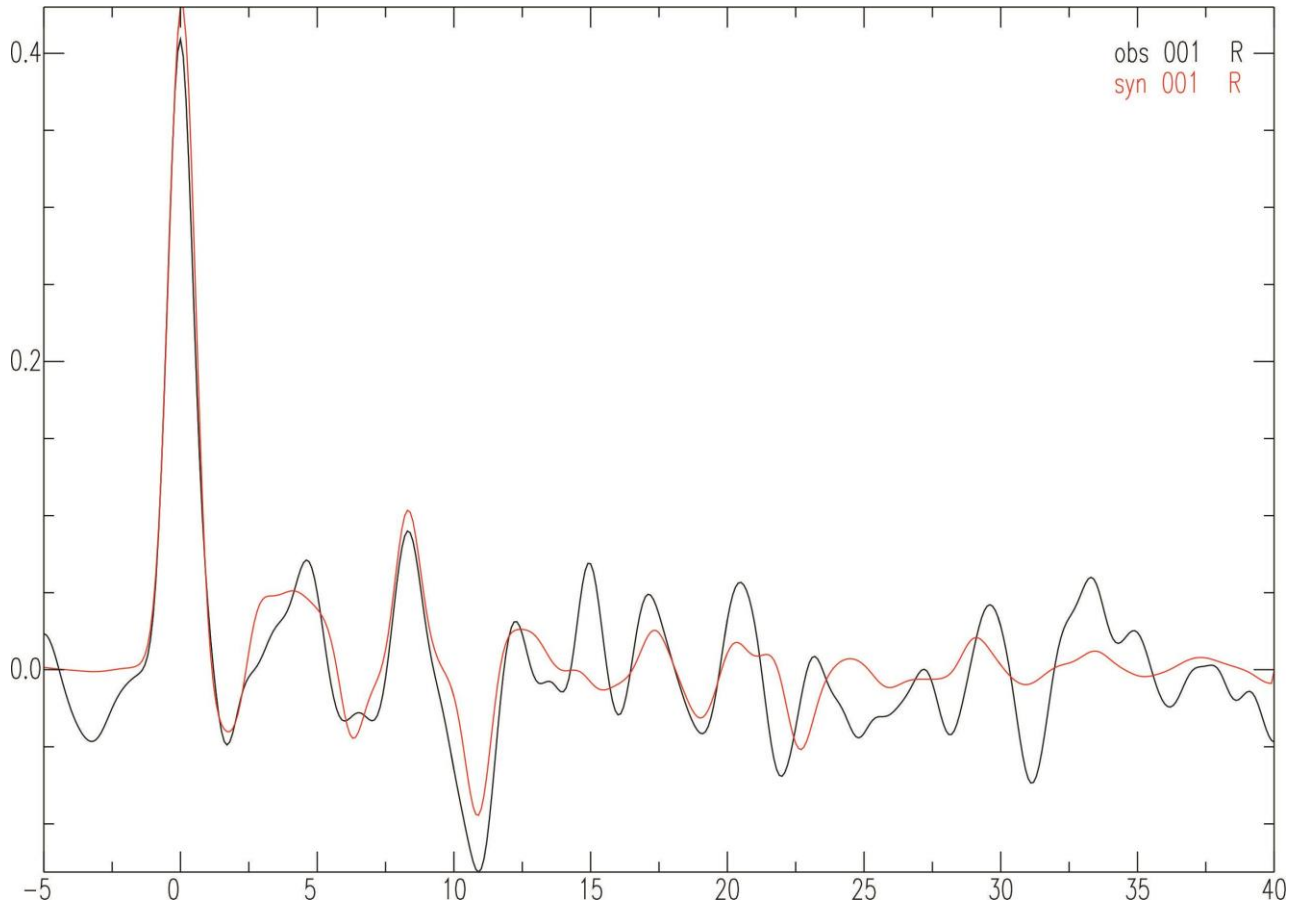

Figure 12a-ii (GAC)

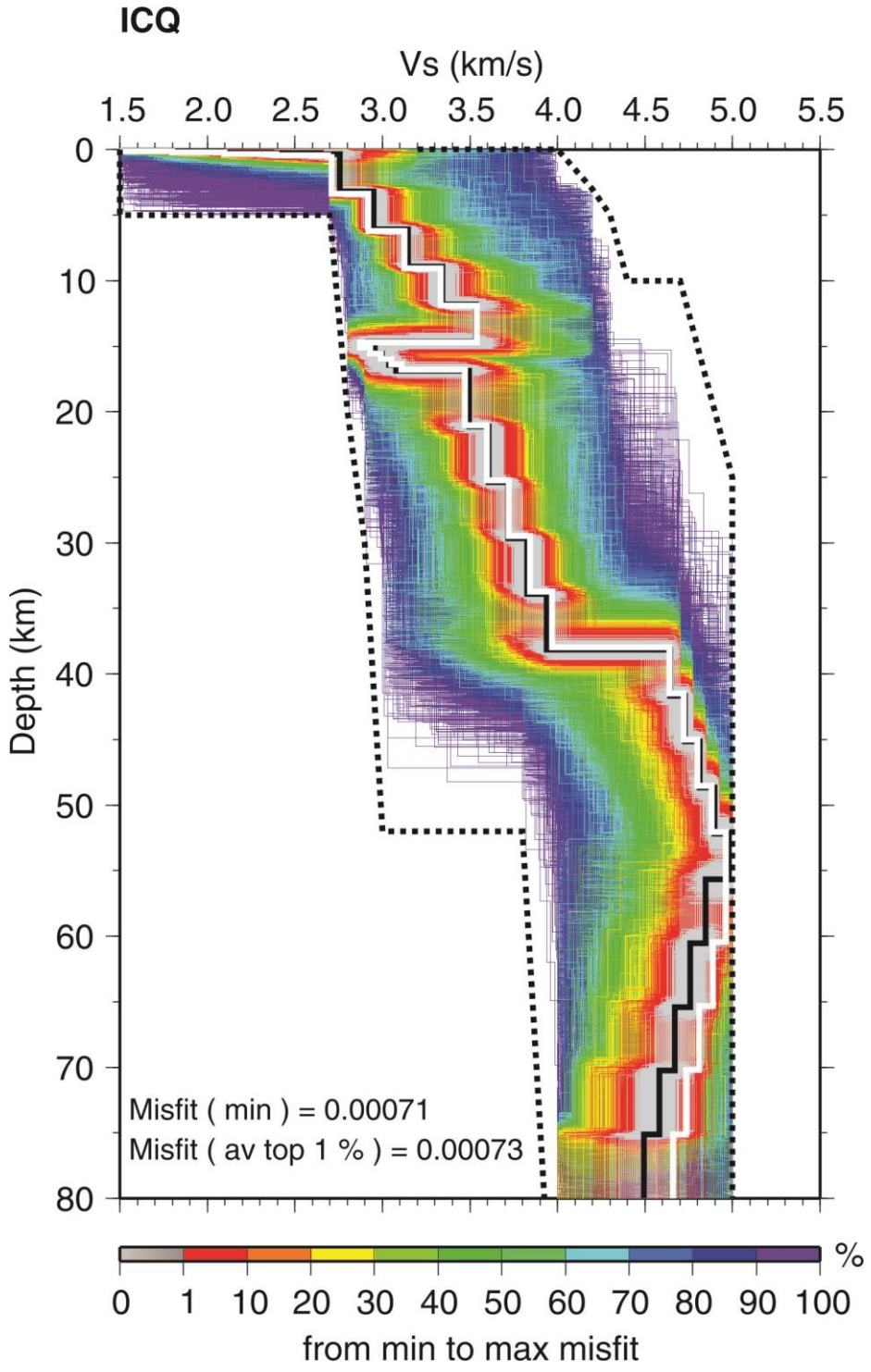
ICQ
Vs (km/s)
1.5 2.0 2.5 3.0 3.5 4.0 4.5 5.0 5.5
Depth (km)
0 10 20 30 40 50 60 70 80
Misfit (min) = 0.00071
Misfit (av top 1 %) = 0.00073
%
0 1 10 20 30 40 50 60 70 80 90 100
from min to max misfit

Figure 12b-i

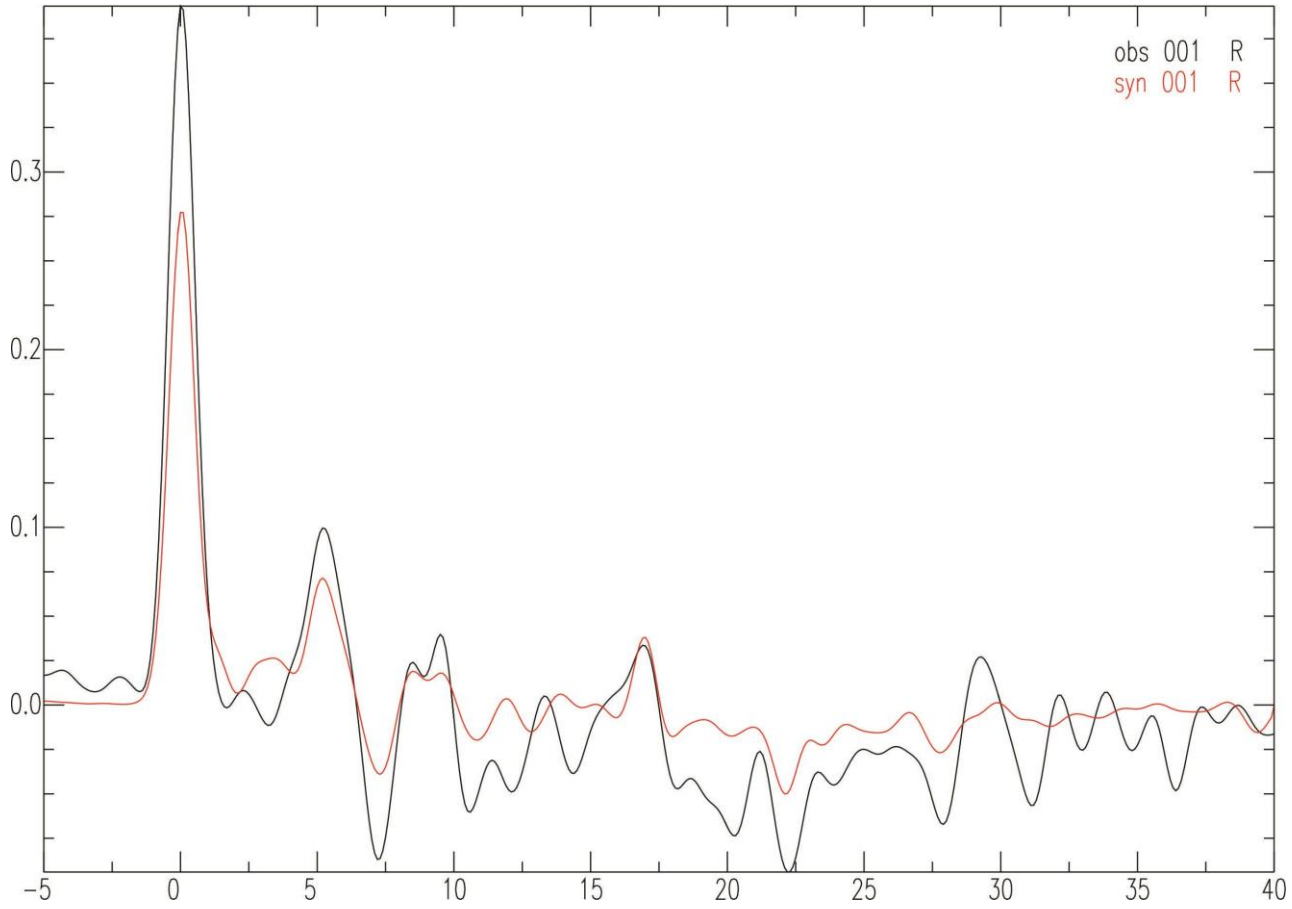

Figure 12b-ii (ICQ)

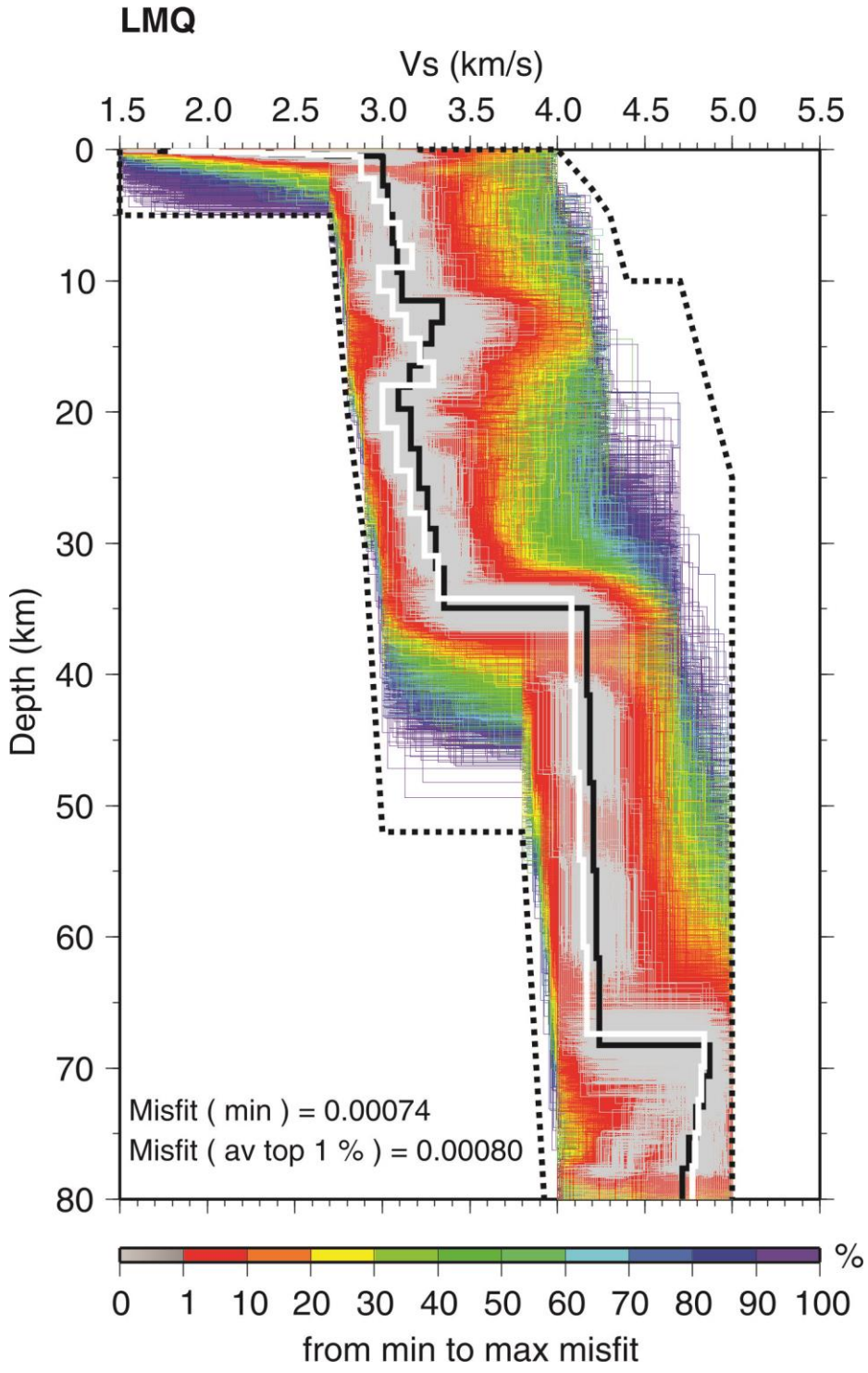
LMQ
Vs (km/s)
1.5 2.0 2.5 3.0 3.5 4.0 4.5 5.0 5.5
Depth (km)
0 10 20 30 40 50 60 70 80
Misfit (min) = 0.00074
Misfit (av top 1 %) = 0.00080
%
0 1 10 20 30 40 50 60 70 80 90 100
from min to max misfit

Figure 12c-i

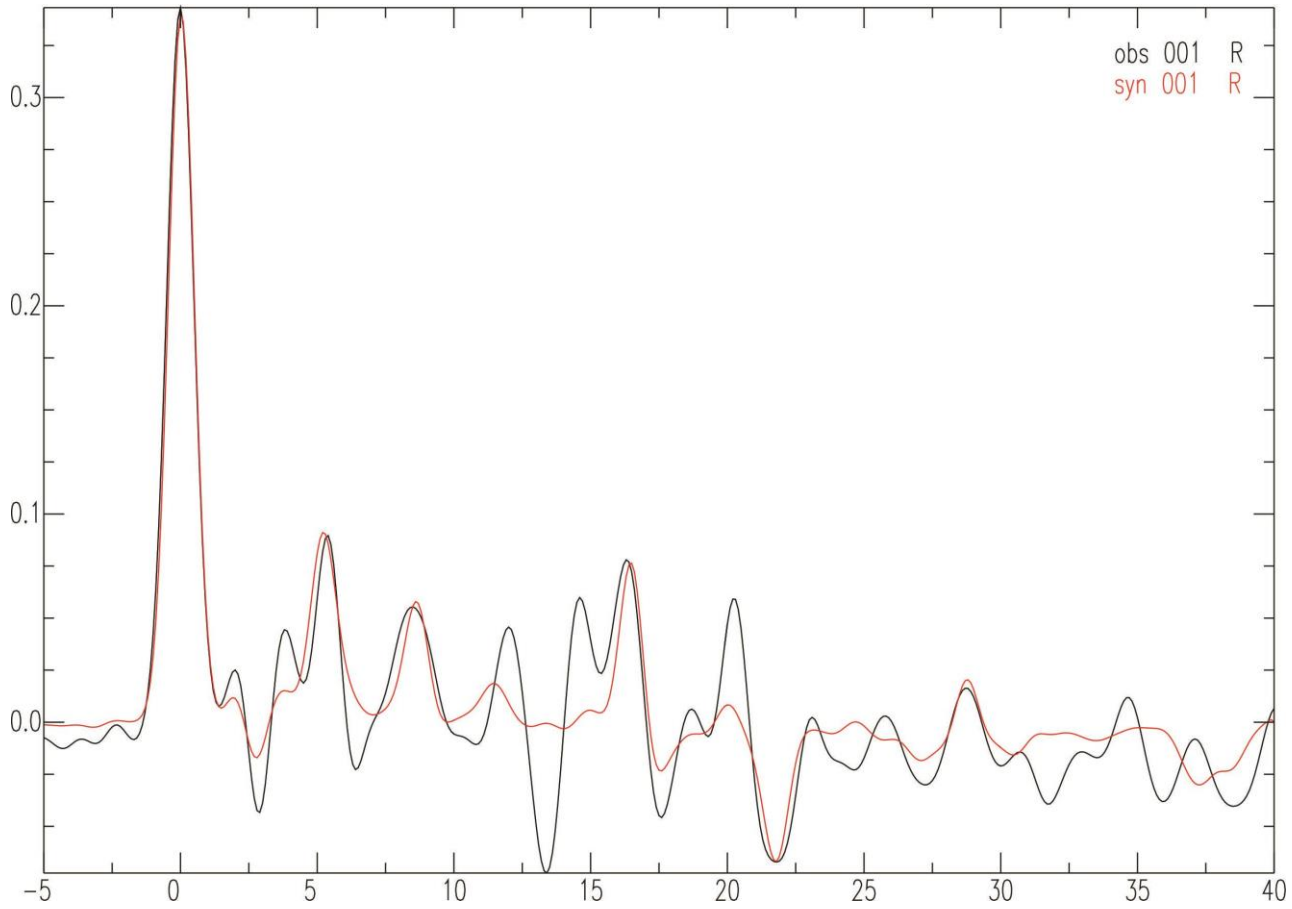

Figure 12c-ii (LMQ)

Figure 12. Structural models and receiver functions for stations in the Grenville Province: a) GAC. b) ICQ and c) LMQ. Format the same as for Figure 3.

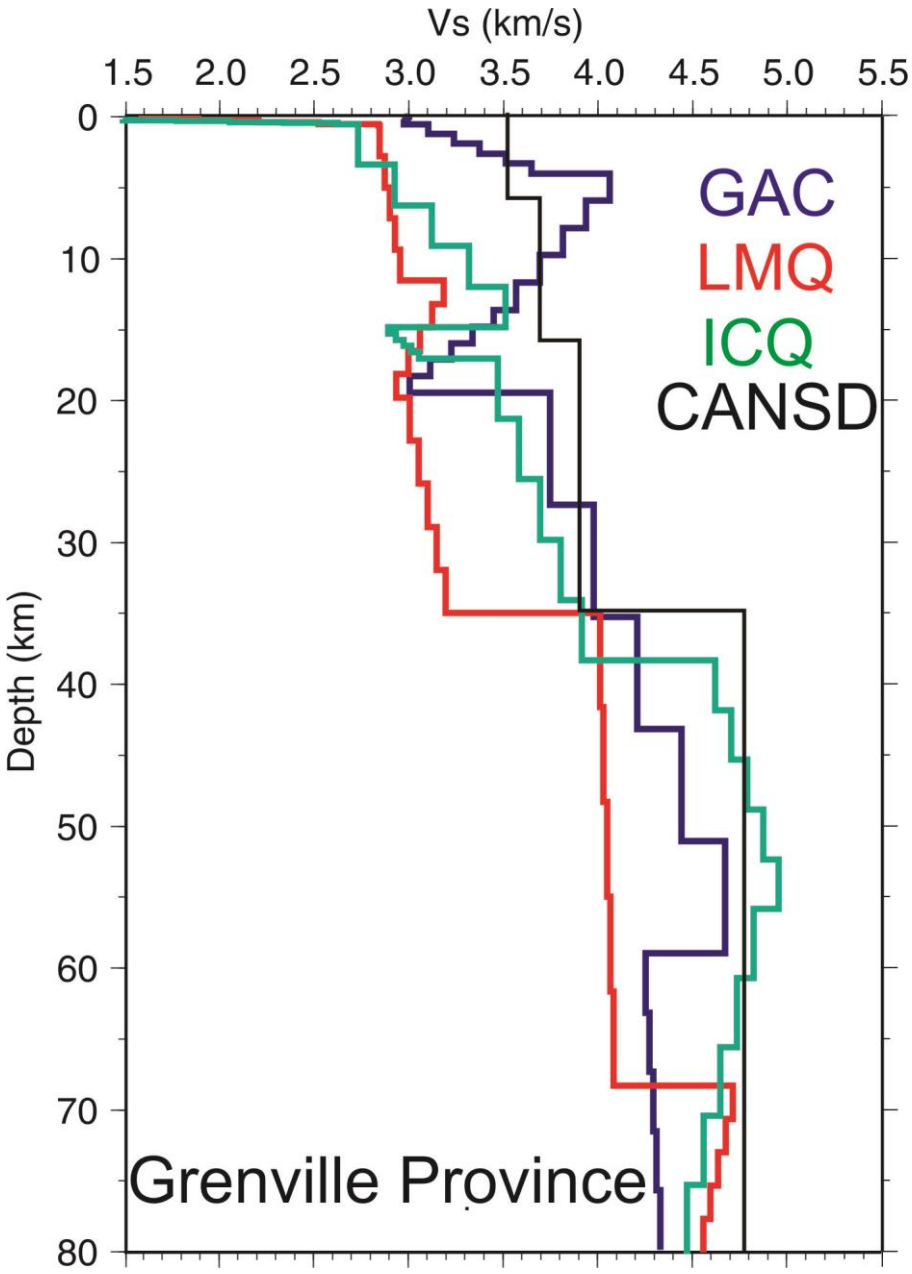

Figure 13. Preferred shear wave velocity model for stations in the Grenville Province.

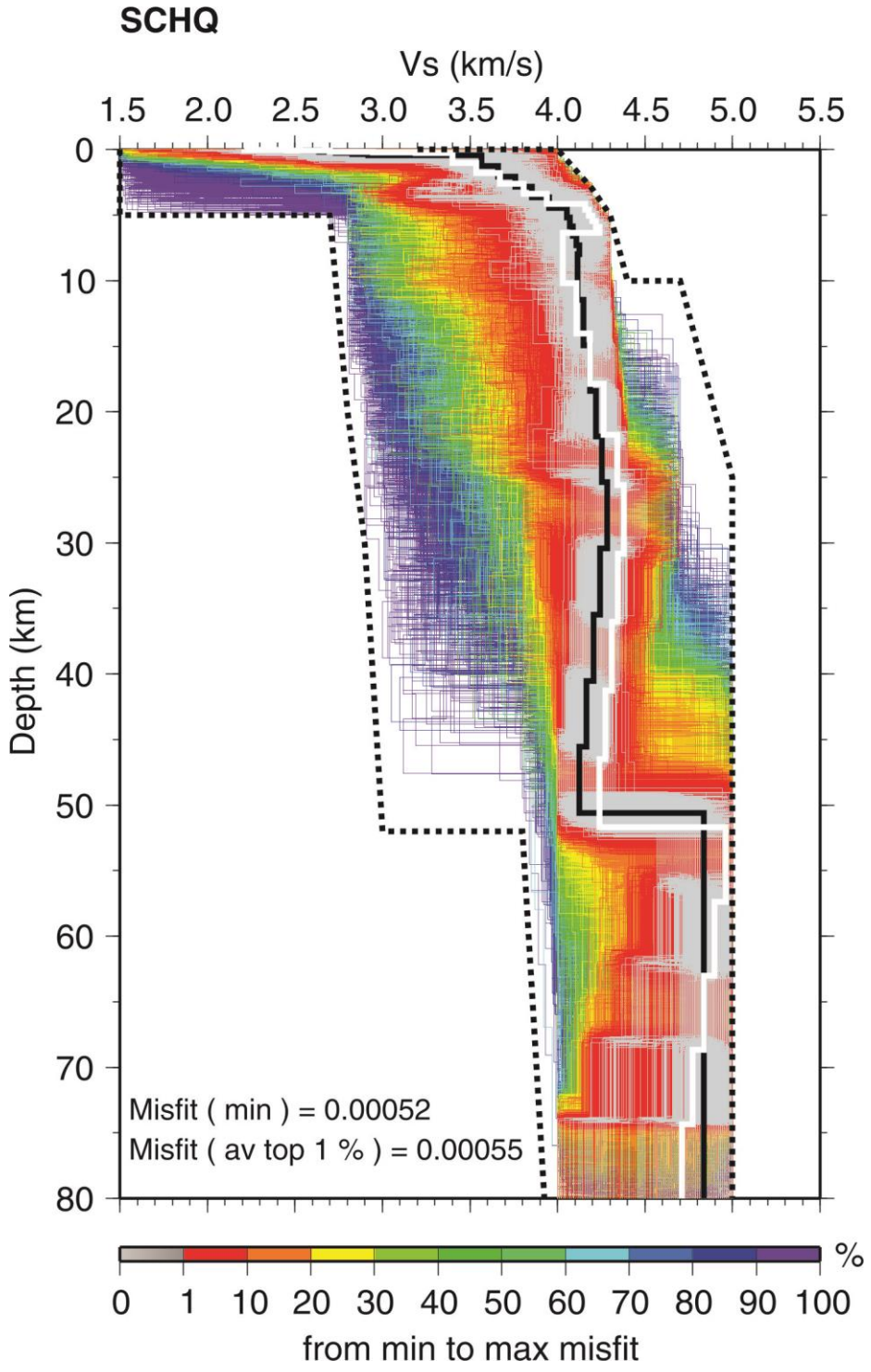
SCHQ
Vs (km/s)
1.5 2.0 2.5 3.0 3.5 4.0 4.5 5.0 5.5
Depth (km)
0 10 20 30 40 50 60 70 80
Misfit (min) = 0.00052
Misfit (av top 1 %) = 0.00055
%
0 1 10 20 30 40 50 60 70 80 90 100
from min to max misfit

Figure 14-i

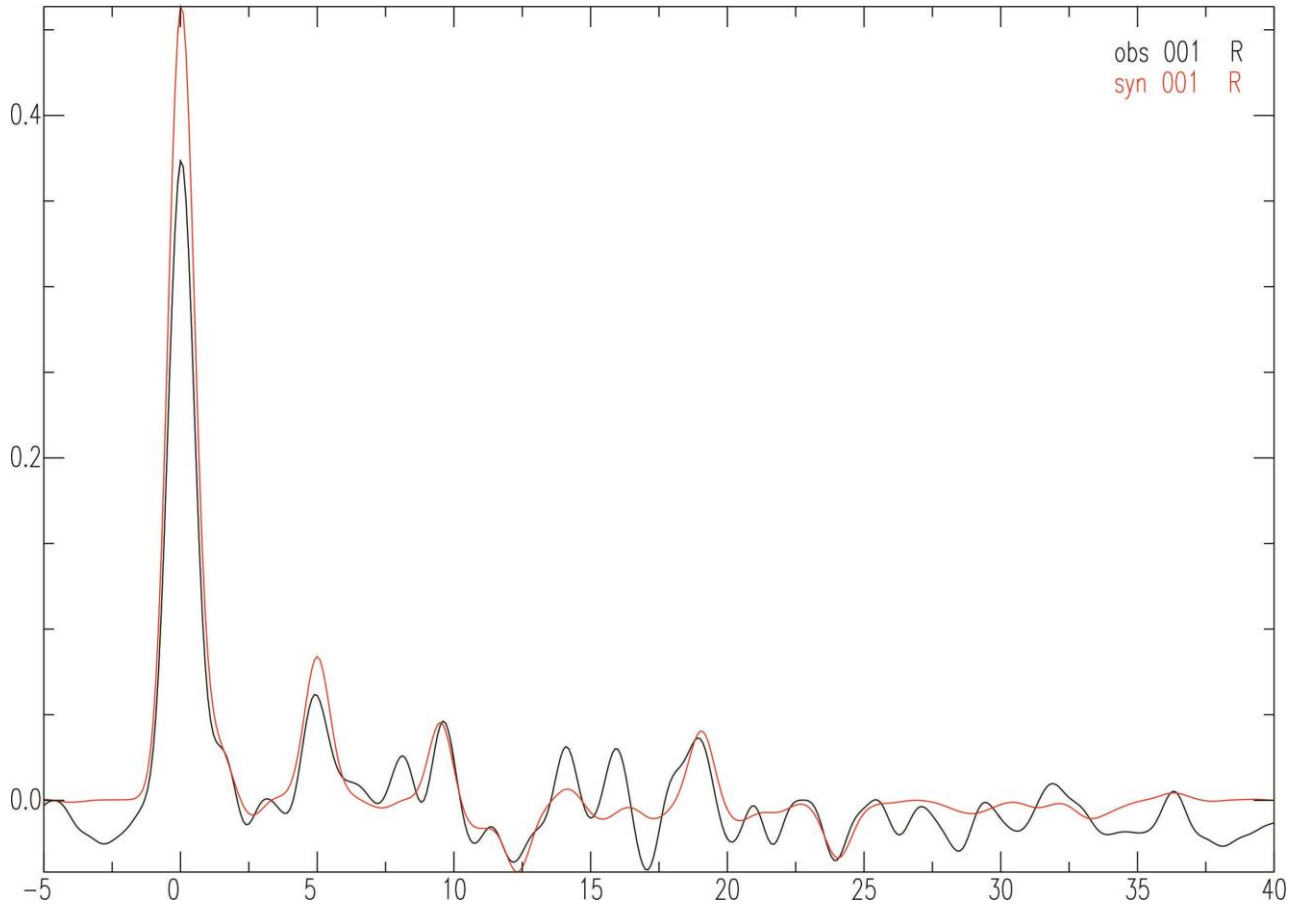

Figure 14-ii

Figure 14. Structural model and receiver function for station SCHQ in the Churchill Province. Format the same as for Figure 3.

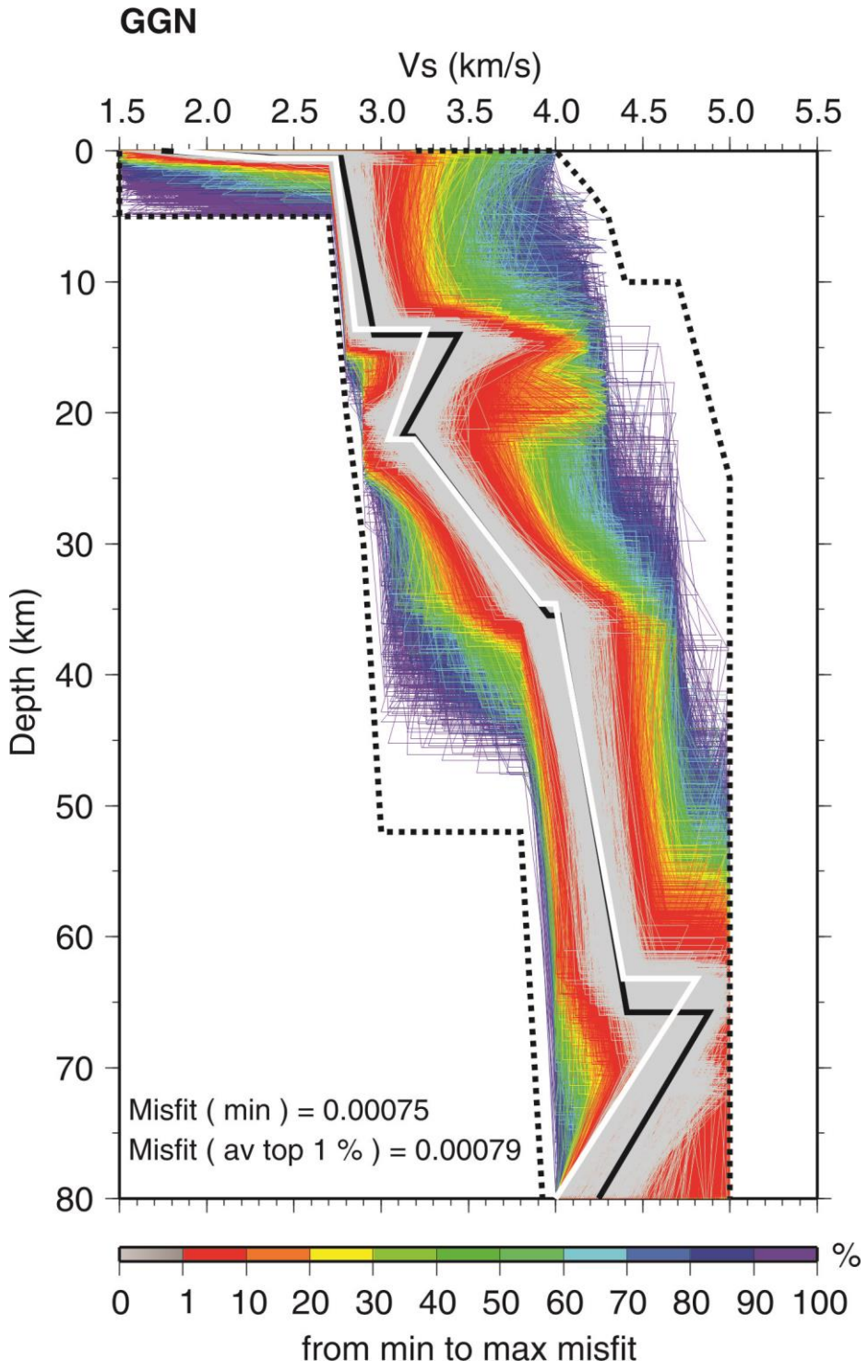
GGN
Vs (km/s)
1.5 2.0 2.5 3.0 3.5 4.0 4.5 5.0 5.5
Depth (km)
0 10 20 30 40 50 60 70 80
Misfit (min) = 0.00075
Misfit (av top 1 %) = 0.00079
%
0 1 10 20 30 40 50 60 70 80 90 100
from min to max misfit

Figure 15a-i

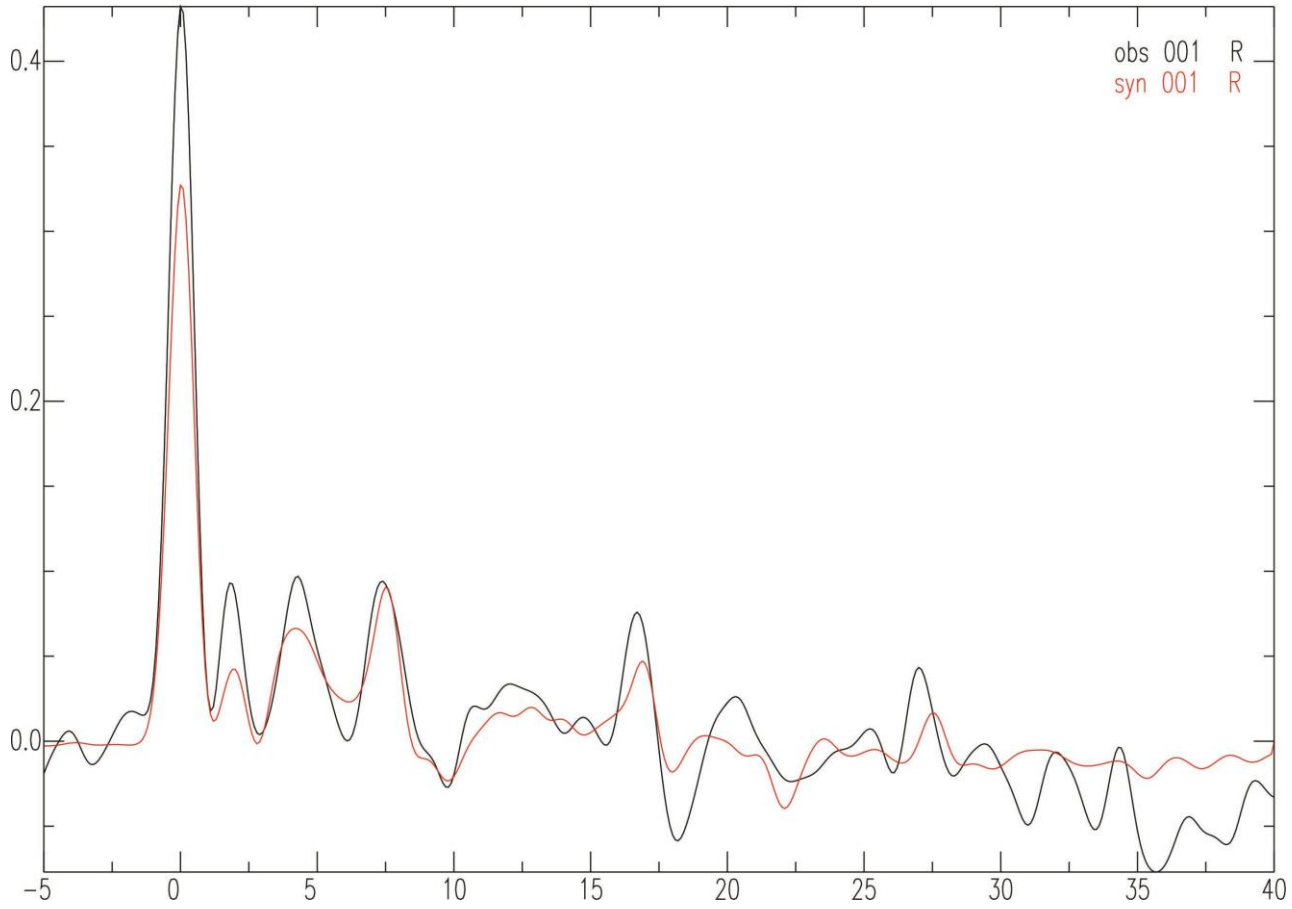

Figure 15a-ii (GGN)

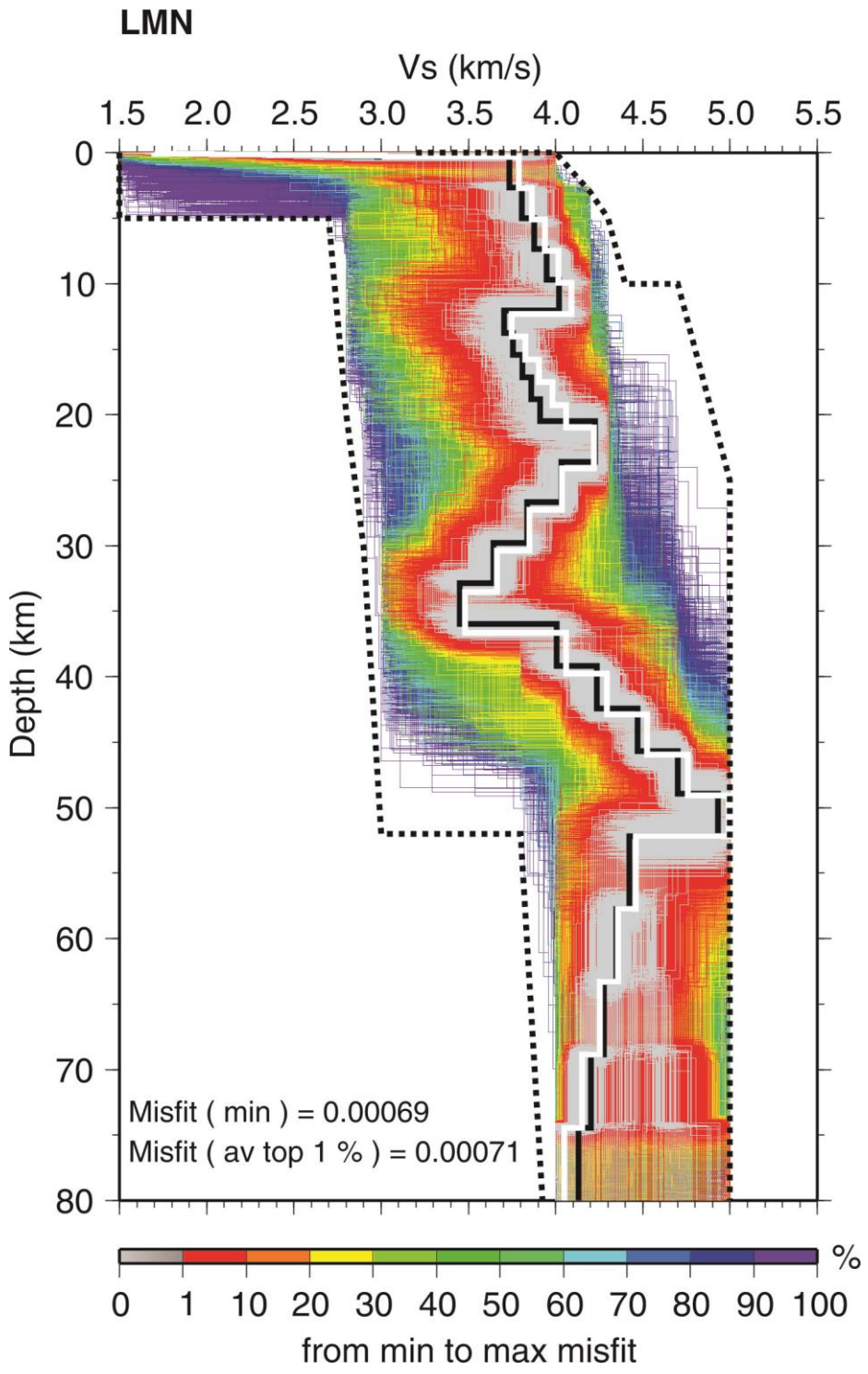
LMN
Vs (km/s)
1.5 2.0 2.5 3.0 3.5 4.0 4.5 5.0 5.5
Depth (km)
0 10 20 30 40 50 60 70 80
Misfit (min) = 0.00069
Misfit (av top 1 %) = 0.00071
%
0 1 10 20 30 40 50 60 70 80 90 100
from min to max misfit

Figure 15b-i

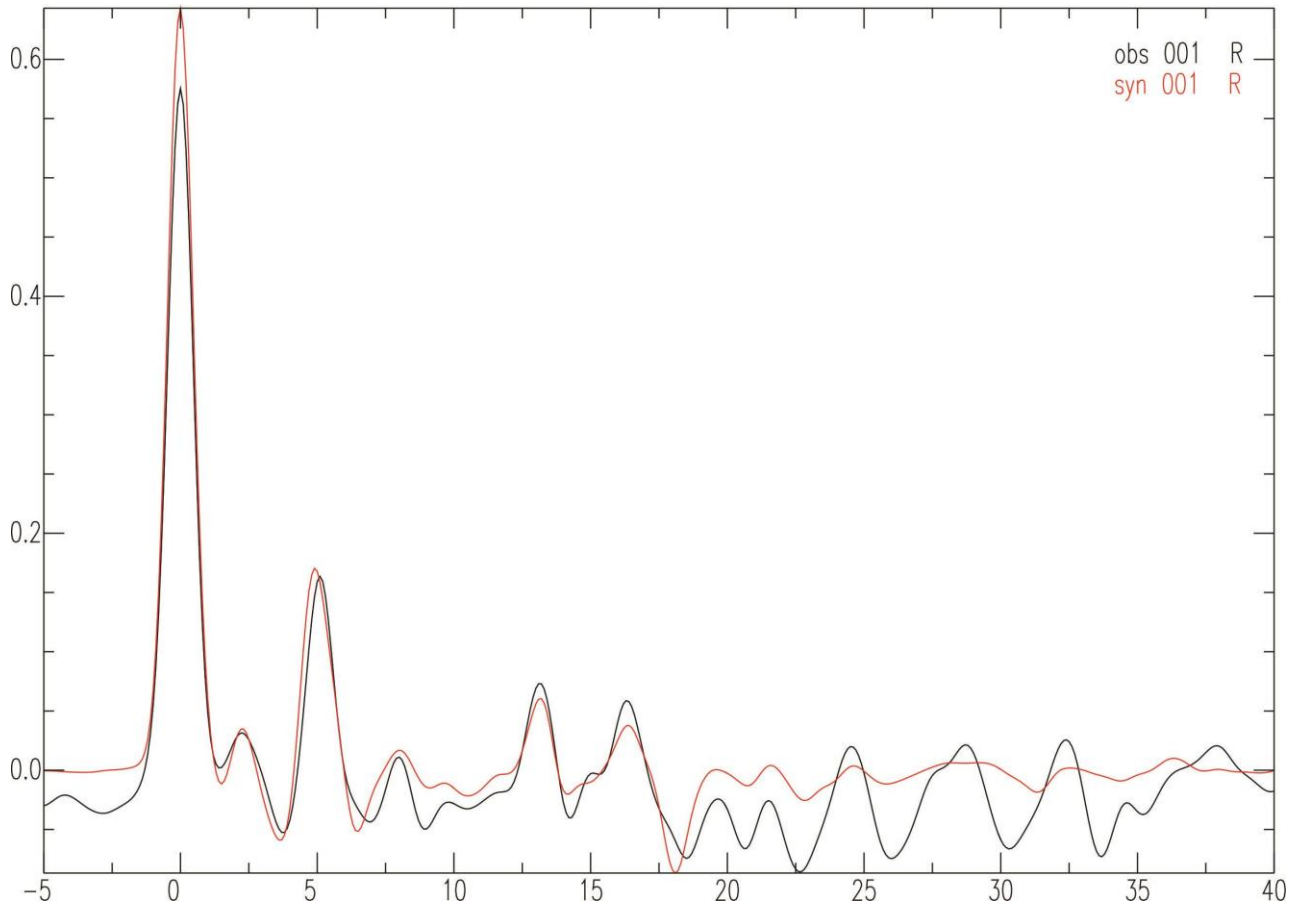

Figure 15b-ii (LMN)

Figure 15. Structural models and receiver functions for stations in the Appalachian Orogen: a) GGN and b) LMN. Format the same as for Figure 3.

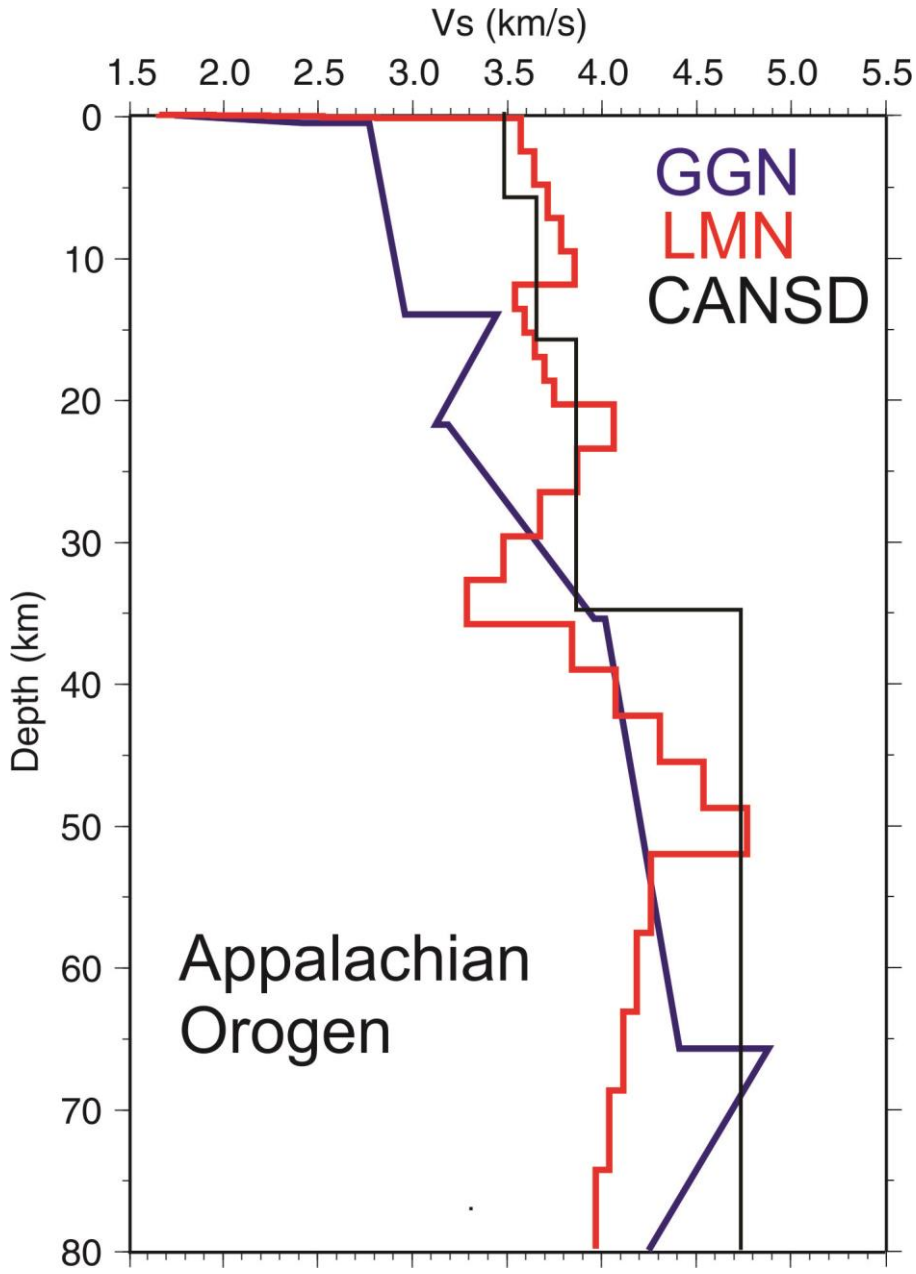

Figure 16. Preferred shear wave velocity models for stations in the Appalachian Orogen.

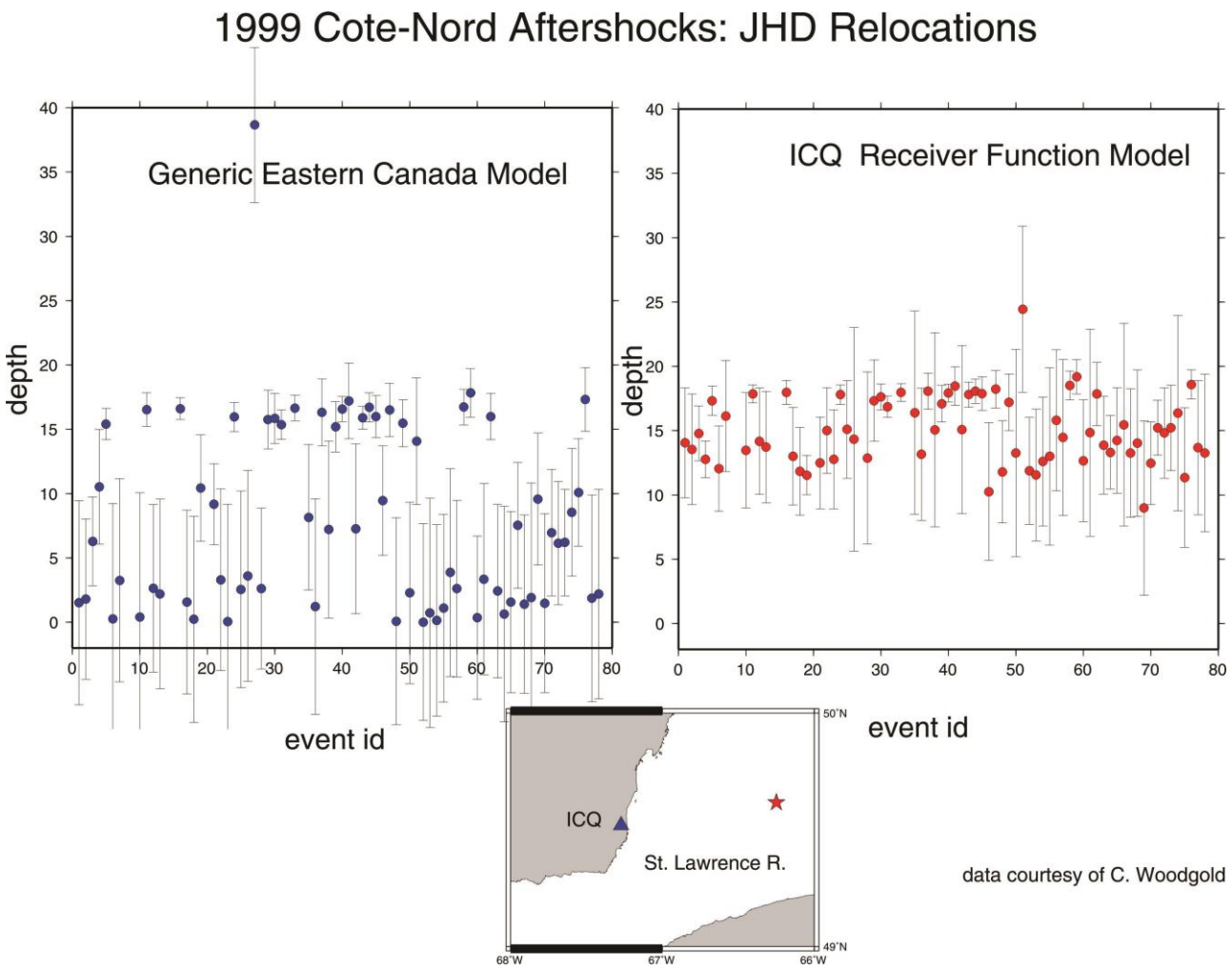

Figure 17. Depths of aftershocks of the 1999 Côte-Nord earthquakes determined using the standard eastern Canadian (CANSD) velocity model (left) and that derived for station ICQ in this study (right). The "event id" is the order in which an aftershock occurred in the sequence. The inset shows the location of the mainshock relative to station ICQ. The uncertainties in the depths are indicated by the error bars. Both velocity models are shown in Figure 13.

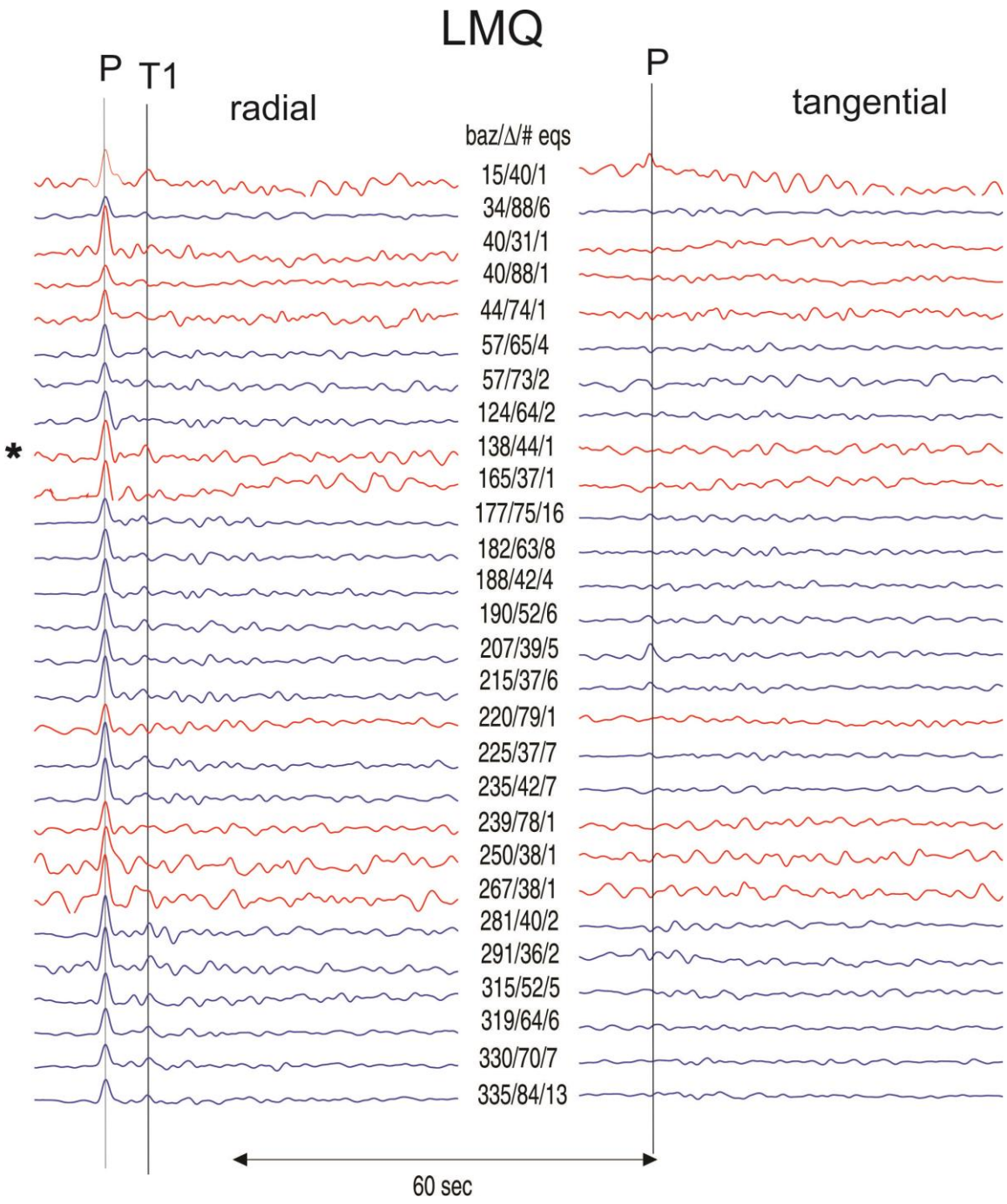

Figure 18. Radial (left) and tangential (right) receiver functions for station LMQ plotted by back azimuth. Red lines are receiver functions for individual earthquakes and blue lines are receiver functions for stacked data. The numbers between the radial and tangential receiver functions indicate back azimuth, distance in degrees and number of earthquakes. For stacked data the back azimuth and distance are mean values. The direct P wave is noted. Marker T1 denotes what is presumed to be the Moho reflection for the event indicated by a star (*).